学位論文

Self-Assembly of Conical Fullerene Amphiphiles and Their Behavior at Air-, Oil-, and Solid-Water Interfaces

（両親媒性コニカルフラーレンの自己集合とその気液，液液，
および固液界面における挙動）

平成 26 年 12 月博士（理学）申請

東京大学大学院理学系研究科
化学専攻

新田　寛久

Abstract

Surfactants lower the interfacial tensions between air, liquid and solid, and form micelles in water. They are used as detergent, foaming and wetting agent, dispersion agent, etc. Suppression or enhancement of one function over others is often necessary but difficult for conventional alkyl surfactants.

Chapter 1 describes the general properties of conventional alkyl surfactants and synthetic surfactants with more complex backbone structures. The amphiphilic molecules behave similarly in water, but the specific characteristics can be enhanced by modulating backbones of surfactant molecules. Among them, amphiphilic fullerenes are promising material for enhancing a specific function of surfactants.

Chapter 2 describes the synthesis of a cationic conical fullerene amphiphile (CFA) and its application to DNA compaction. The CFA was synthesized by modular assembly of a pentaorganofullerene and hydrophilic groups via click cycloaddition chemistry. The cationic CFA forms a stable micelle in water and in a buffer at low critical micelle concentration, CMC. The efficient DNA compaction at a small ration of the CFA to DNA is expected to render this new aminofullerene a transfection agent with minimum side effects.

Chapter 3 describes the influence of molecular geometry of CFA on interfacial activity at air-water interface and micelle formation. Surfactant properties of regioisomers on nonionic CFAs with different hydrophobes were investigated. CMC could be lowered than the concentration where interfacial tension drops by introducing an appropriate CFA framework.

Chapter 4 describes the non-interfacial activity of ionic CFAs at air-water and oil-water interfaces and application to dispersion of solid nanoparticles. The ionic groups inhibit the interfacial activity, retaining the micellization ability. The CFAs function as effective dispersion agents for nanoparticles at lower concentration than conventional alkyl surfactants.

Finally, chapter 5 summarizes the present thesis and shows perspective of the fullerene amphiphiles.

Acknowledgement

The work presented in this Ph.D. thesis was performed under the direction of Professor Eiichi Nakamura at the Department of Chemistry, Graduate School of Science, the University of Tokyo, from April 2012 to March 2015.

I am greatly indebted to Professor Eiichi Nakamura for his support and advice. His clear insights and highly educational guidance for research have always been inspiring.

I would like to show my sincere appreciation to Assistant Professor Koji Harano, whose daily advice, fruitful discussion, and support made it possible for us to brush up this work. I am grateful for the inspiring discussions and advices from Associate Professor Hayato Tsuji, Associate Professor Laurean Ilies, Assistant Professor Hideyuki Tanaka, and Assistant Professor Shunsuke Furukawa.

I would also like to thank our secretary Ms. Akemi Maruyama and all the members in Harano group, Dr. Chao Liu, Mr. Satoshi Okada, Mr. Junya Yamada, Mr. Kei Matsumoto, Mr. Junfei Xing, Mr. Takuya Tsubota, as well as the former members, Dr. Li-Fu Hugang, Dr. Yonggang Zhen, Ms. Eri Nishiyama, Mr. Shin-ichiro Mizuno, Ms. Kaori Kubo, Mr. Takakazu Seki, and Ms. Mami Nakatake.

I am especially grateful to Mr. Ricardo Mizoguchi Gorgoll and Mr. Tsuyoshi Suzuki, and Ms. Utako Takeda for their support and appropriate advice. I would also like to thank all the members of Nakamura group for their warm support in everyday life in the laboratory.

I am thankful to Professor Mitsuhiko Shionoya and Assistant Professor Shouhei Tashiro for MS measurement, Ms. Mayuko Isomura for the synthesis and characterization of **_m_-HEO**, and Dr. Akihito Kumamoto for the TEM measurements of carbon nanotubes.

I am grateful to Professor Mischa Bonn, Dr. Ellen H. G. Backus, and Dr. Akimitsu Narita in Max Planck Institute of Polymer Chemistry for the SFG spectroscopy and relevant discussion.

Financial supports from Advanced Leading Graduate Course for Photon Science (ALPS) is greatly appreciated. I also appreciate Professor Hideo Higuchi for giving me insightful comments and suggestions as a sub supervisor in the ALPS program.

Finally, but not least, I would like to show my deep gratitude to my family, Naoto, Keiko, and Mami to whom this thesis is dedicated. I thank them for always being there for me.

Hirohisa Nitta

Hirohisa Nitta
December 2014

Abbreviations

APCI	atmospheric pressure chemical ionization
AFM	atomic force microscopy
CCD	charge-coupled device
CFA	conical fullerene amphiphile
CMC	critical micelle concentration
CNH	carbon nanohorn
CNT	carbon nanotube
CTAB	cetyltrimethylammonium bromide
dec.	decomposition
DLS	dynamic light scattering
DMF	dimethylformamide
DMSO	dimethylsulfoxide
DNA	deoxyribonucleic acid
ESI	electrospray ionization
GPC	gel permeation chromatography
HLB	hydrophilic lipophilic balance
HPLC	high performance liquid chromatography
HRMS	high-resolution mass spectrometry
I.T.	interfacial tension
ITO	indium tin oxide
IR	infrared
LB	Langmuir-Blodgett
NIR	near infrared
MS	mass spectrometer/spectrometry
N/P	nitrogen/phosphate
NR	Nile red
NMR	nuclear magnetic resonance
MO	methyl orange
mp	melting point
MNP	magnetite nanoparticle
ODCB	*o*-dichlorobenzene
PBS	phosphate buffered saline
PMDETA	*N*,*N*,*N*’,*N*’’,*N*’’-pentamethyldiethylenetriamine
RNA	ribonucleic acid
rt	room temperature
siRNA	small interfering RNA
SDS	sodium dodecyl sulfate
SEM	scanning electron microscopy
SFG	sum frequency generation
STEM	scanning transmission electron microscopy
STM	scanning tunneling microscopy
TBS	tris buffered saline
TEM	transmission electron microscopy
THF	tetrahydrofuran
TIPS	triisopropylsilyl
TLC	thin layer chromatography
TMS	trimethylsilyl
TPFE	tetrapiperazinofullerene epoxide
UV	ultraviolet
Vis	visible

TABLE OF CONTENTS

CHAPTER 1. GENERAL INTRODUCTION 1
1.1. PROPERTIES OF ALKYL SURFACTANTS 3
1.2. FORMATION OF MICELLES AND VESICLES IN SOLUTION 4
1.3. INTERFACIAL ACTIVITY OF SURFACTANTS 6
1.4. ADSORPTION ON SOLID SURFACES 7
1.5. DESIGN OF SURFACTANTS BASED ON FULLERENE 8
1.6. SURFACTANT PROPERTIES OF FULLERENE AMPHIPHILES 9
1.7. SELF-ASSEMBLY TO FORM MICELLES AND VESICLES 9
1.8. ADSORPTION AT FLUID- AND SOLID-WATER INTERFACES 10
1.9. APPLICATION TO DISPERSION OF SOLID NANOMATERIALS 11
1.10. SYSTEMATIC STUDY OF FULLERENE SURFACTANTS FOR APPLICATION 12
1.11. REFERENCES 13
CHAPTER 2. MICELLIZATION OF CONICAL FULLERENE AMPHIPHILE AND APPLICATION AS A DNA BINDER 17
2.1. INTRODUCTION 19
2.2. SYNTHESIS OF THE CATIONIC CFA BY CLICK REACTION 19
2.3. MICELLIZATION OF THE CATIONIC CFA 20
2.4. BINDING OF THE CATIONIC CFA WITH DNA 23
2.5. CONCLUSION 26
2.6. EXPERIMENTAL SECTION 27
2.7. REFERENCES 33
CHAPTER 3. RETARDATION OF INTERFACIAL ACTIVITY OF NONIONIC CONICAL FULLERENE AMPHIPHILES AT AIR-WATER INTERFACE 35
3.1. INTRODUCTION 37
3.2. SYNTHESIS 38
3.3. MICELLIZATION OF THE NONIONIC CFAS 39
3.4. INTERFACIAL ACTIVITY 42
3.5. STRUCTURE OF GIBBS MONOLAYER 44
3.6. SUM FREQUENCY GENERATION SPECTROSCOPY 45
3.7. MOLECULAR MODELING OF CFA FRAMEWORKS 46
3.8. OIL-WATER INTERFACIAL ACTIVITY 48
3.9. CONCLUSION 50

3.10. EXPERIMENTAL SECTION 51
3.11. REFERENCES 60

CHAPTER 4. SOLID DISPERSION WITH IONIC CONICAL FULLERENE AMPHIPHILES WITHOUT INTERFACIAL ACTIVITY 63

4.1. INTRODUCTION 65
4.2. SYNTHESIS OF IONIC CFAS 66
4.3. CHARACTERIZATION OF MICELLE STRUCTURES 66
4.4. NILE RED ASSAY AND INTERFACIAL TENSION MEASUREMENT 68
4.5. NON-INTERFACIAL ACTIVITY 70
4.6. SFG SPECTROSCOPY OF AIR-WATER INTERFACE 73
4.7. INHIBITION OF ADSORPTION TO AIR-WATER INTERFACE BY MIRROR CHARGE 73
4.8. DISPERSION OF MAGNETITE NANOPARTICLES 75
4.9. DISPERSION OF CARBON NANOTUBES 78
4.10. AFM OBSERVATION OF CFA HEMIMICELLES ON CNTS 79
4.11. SEM OBSERVATION OF CARBON NANOHORNS DISPERSED BY IONIC CFAS 81
4.12. CONCLUSION 83
4.13. EXPERIMENTAL SECTION 83
4.14. REFERENCES 92

CHAPTER 5. SUMMARY AND OUTLOOK 95

Chapter 1. General introduction

1.1. Properties of alkyl surfactants

Surfactants have been studied in detail from old days due to its wide utility in daily use and in industry. When we focus on chemical structures, conventional surfactants such as sodium dodecyl sulfate (SDS) and cetyltrimethylammonium bromide (CTAB) have alkyl hydrophobic groups and polar hydrophilic groups. Because the functionalities can interact with each other by self-assembly as well as interact with other surfaces, the amphiphilic structure affords them of unique property, especially in water as shown in Figure 1-1.[1] Recently, not only the conventional alkyl surfactants but also a wide variety of amphiphiles with artificial backbone structures have been developed. Interestingly, such molecules share the characteristics with traditional surfactants, which enabled to enhance a specific feature by chemical design.

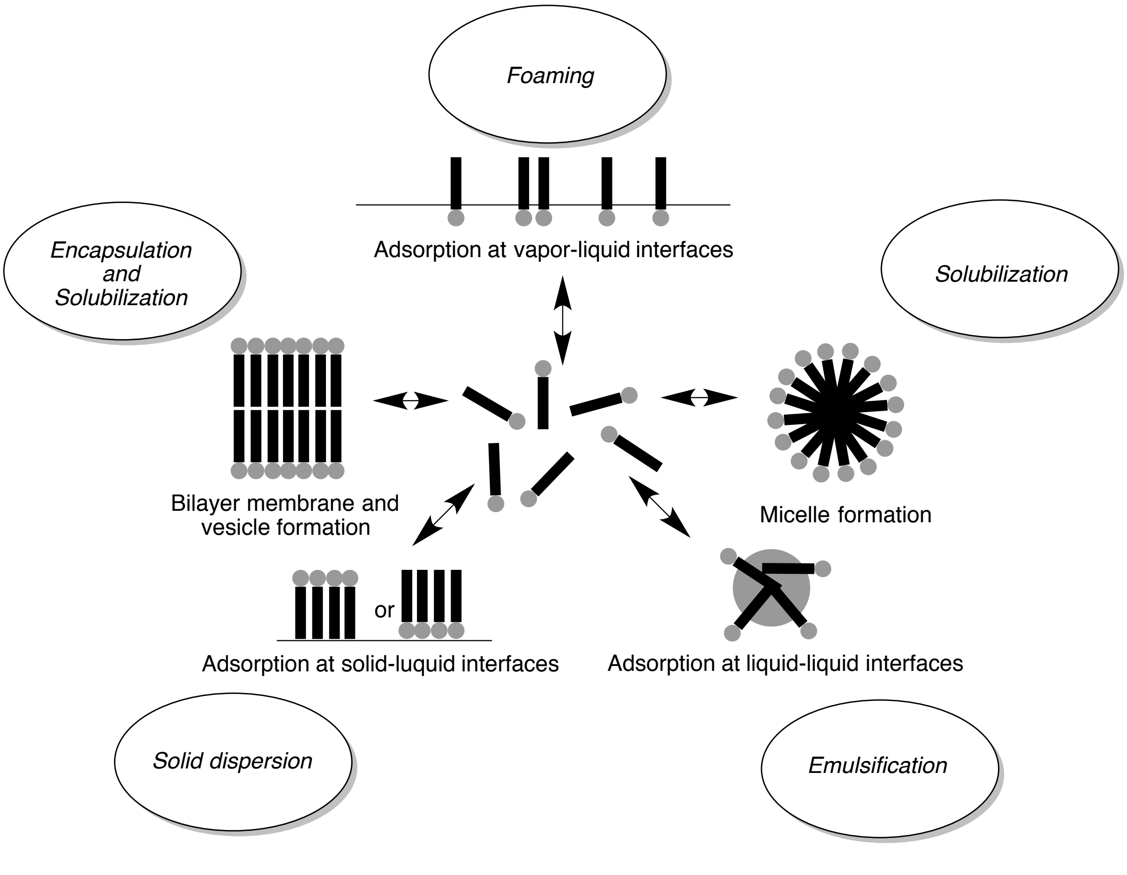
Foaming
Adsorption at vapor-liquid interfaces
Encapsulation and Solubilization
Solubilization
Bilayer membrane and vesicle formation
Micelle formation
or
Adsorption at solid-luquid interfaces
Adsorption at liquid-liquid interfaces
Solid dispersion
Emulsification

Figure 1-1. Surfactant properties in water or at vapor-liquid, liquid-liquid and solid-liquid interfaces and their application.

1.2. Formation of micelles and vesicles in solution

Self-assembly of surfactant molecules to form nano- to microstrucutres such as micelle or vesicle is driven by association of hydrophobic groups in polar solvent, in many cases, water.[2] The hydrophobic groups form apolar phase inside the nanostructures, while the hydrophilic groups face the aqueous phase. The geometry of the self-assembled structures varies with the molecular geometry of surfactant molecules, concentration etc. The shape of the packed molecules is called packing parameter, which is described by eq. 1.[3]

$$N_s = \frac{v_c}{a_0 \times l_c} \qquad \text{(eq. 1)}$$

Here, N_s is packing parameter, v_c and l_c are volume and length of hydrophobic groups, a_0 is area per molecule of surface of the hydrophobic aggregate. As shown in Figure 1-2, conical surfactants tend to form micelles, while rod-shaped surfactant tend to form bilayer structures.[4]

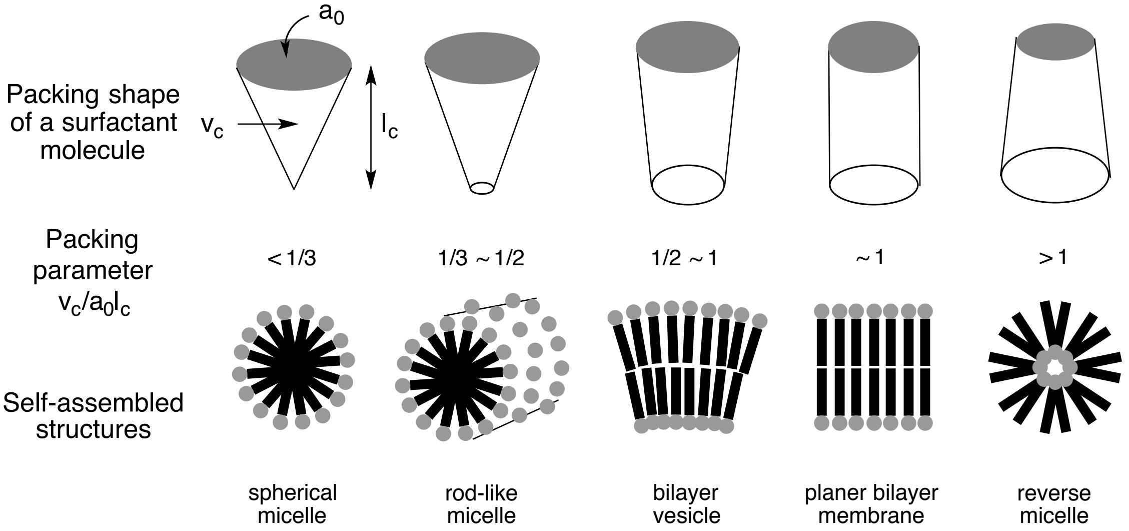
a_0
Packing shape of a surfactant molecule
v_c
l_c
Packing parameter v_c/a_0l_c
< 1/3
1/3 ~ 1/2
1/2 ~ 1
~ 1
> 1
Self-assembled structures
spherical micelle
rod-like micelle
bilayer vesicle
planer bilayer membrane
reverse micelle

Figure 1-2. Packing parameter of surfactants and self-assembled structures.

For artificial surfactants whose hydrophobic group is not an alkyl group, the concept of packing parameter may not be applicable but similar self-assembly behavior can be observed. Kim and Lee et al. reported micelle formation of aromatic rod amphiphiles with a hydrophilic oligoether dendron (Figure 1-3).[5] Packing of the molecules in the micelles formed by the amphiphiles is apparently different from that of alkyl surfactants, but its transformation into a linear nanostructure is similar to the conventional systems. Hydrogen bonding between a guest molecule and the pyridyl group led to further transformation to a tubular structure.

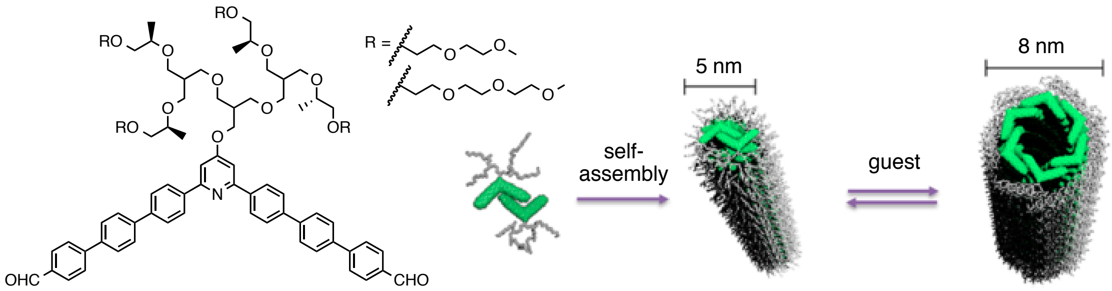

Figure 1-3. Micelle formation of surfactants with a rigid backbone. Reprinted with permission from ref 5. Copyright 2005 American Chemical Society.

The self-assembly of surfactants is dependent on concentration. Surfactants start to self-assemble at the concentration called critical micelle concentration (CMC). CMC is an important parameter to determine function of surfactants because effectiveness of each process including self-assembly, surface adsorption, and other accompanying phenomenon are enhanced above the concentration. For alkyl surfactants, CMC can be lowered by elongating an alkyl group or reducing polarity of a hydrophilic group, by shifting hydrophobic-lipophilic balance (HLB) of the surfactant in question. HLB is one of the widely used parameter, and was determined by Griffin by the following equation 2.[6]

$$HLB = 20 \times \frac{M_h}{M} \qquad \text{(eq. 2)}$$

Here, M_h is mass of hydrophilic groups and M is molecular weight. It should be noted that decrease of HLB reduces CMC, but at the same time solubility in water decreases. Such hydrophobic surfactants are not usable as detergents, but can be used instead as water-in-oil (w/o) emulsifiers or antifoaming agents.

The hydrophobic inner phase of the nanostructures can solubilize hydrophobic molecules. Solubilization of fluorescent molecules is used for determination of CMC by tracing change of the photoluminescence by solvatochromism.[7] For example, solubilization of drug molecules in vesicles has been used for tumor targeting in practice.[8]

The surface of the nanostructures exposing the polar functionalities of surfactants can interact with external systems via electrostatic interaction. Compaction of nucleic acids necessary for transfection has been achieved by complexation with cationic surfactants. Lipofectamine is so far the most widely used transfection agent that transports DNA to cell nuclei. More recently, cationic dendrons were shown to be applicable for complexation with nucleic acids and transfection (Figure 1-4a).[9] The multiple cationic functionalities of their micelles are expected to contribute to the effective complexation.

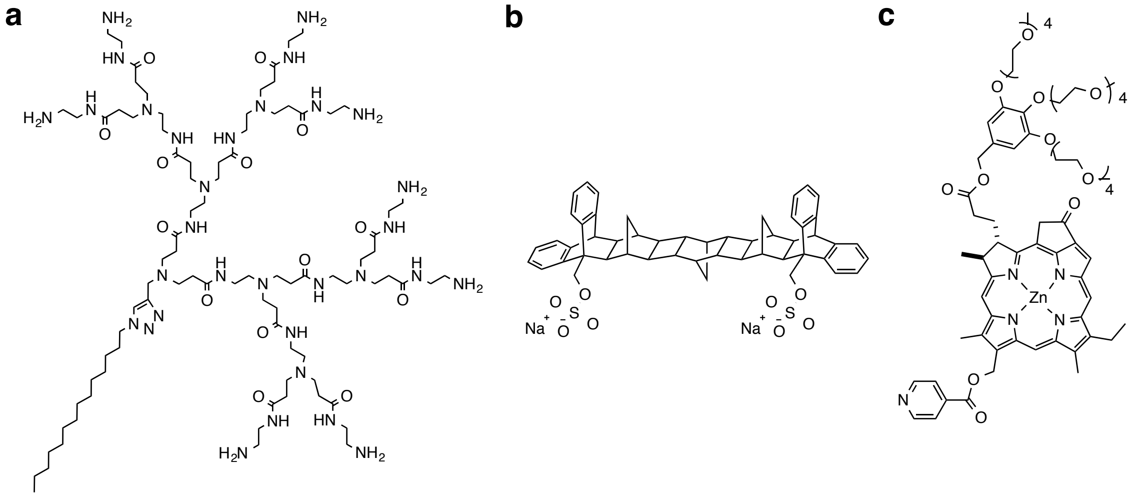

Figure 1-4. Structures of micelle-forming and emulsifying surfactants with artificial backbones.

1.3. Interfacial activity of surfactants

Adsorption on air-water and oil-water interfaces is another important property of surfactants. The driving force for the process is hydrophobic effect that repels hydrophobic groups from aqueous bulk solution.[10] Interfacial tension at air-water and oil-water interfaces decrease by the interfacial activity of surfactants, which leads to foaming at air-water interface and emulsification in the presence of organic liquids, as often utilized for detergents and cosmetics. With increasing bulk concentration, concentration of surfactant molecules at interface also increases until the interface is saturated (Figure 1-1). The surfactant membrane formed by water-soluble surfactants is called Gibbs monolayer, and further increase of bulk concentration results in micelle formation in bulk because no more molecules can adsorb.[11] The concentration where interfacial tension levels off (shown below as $C\gamma$), is thus generally accepted as CMC. (Figure 1-5). It has been known that molecular packing in Gibbs monolayer influences sensitivity of interfacial tension to bulk concentration (called 'efficiency') and the minimal interfacial tension (γ_{min}, called 'effectiveness').[12] For example, surfactants with large hydrophilic groups or those bearing a polar (e.g. ester) unit in hydrophilic groups loosely pack due to their conformation. This lowers both efficiency and effectiveness. Fluorination of hydrophobic groups improves efficiency and effectiveness due to lowered surface energy.

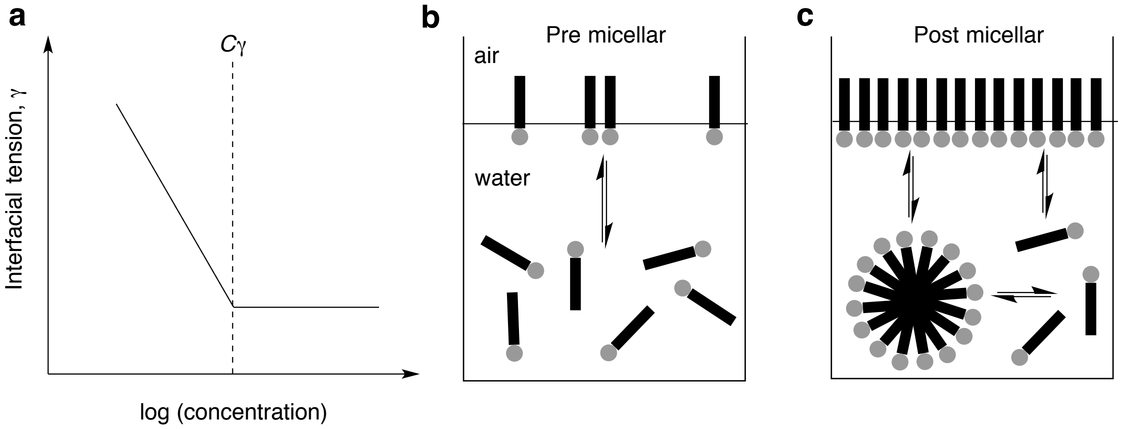

Figure 1-5. Adsorption of surfactants at air-water interface. (a) dependence of interfacial tension on log(concentration) of surfactants. (b, c) Equilibrium of surfactants at interface and in bulk below (pre micellar) and above (post micellar) Cγ.[11]

Adsorption to the interfaces could be achieved for completely new amphiphiles with rigid backbones. For example, emulsification of oil-water systems was reported for a rigid ladder-like molecule[13] and a zinc porphyrin bearing hydrophilic functionalities,[14] despite their obvious difference in the chemical structure from conventional surfactants (Figure 1-4b, c).

1.4. Adsorption on solid surfaces

Adsorption of surfactants on solid surfaces is another important function that causes change in wettability.[15] The process is influenced by chemical nature of surfactants (both hydrophilic and hydrophobic groups), solid surfaces, and solvents. Involvement of both hydrophilic interactions and hydrophobic interactions makes the system complex. Generally it has been known that longer alkyl groups of surfactants can saturate solid surface at lower concentration due to hydrophobic effect. For hydrophobic surfaces, the hydrophobic group of a surfactant adsorbs at the solid surface. For polar surface, first the charged hydrophilic group of a surfactant adsorbs on the surface, and then another layer of surfactant is formed by hydrophobic effect. Although there is some exception, the tendency is common with micelle formation, and thus CMC can be a measure to estimate dispersion ability of surfactants.

When solid particles are small enough to be dispersed in solvents by Brownian motion, we can obtain stable dispersion.[16] This is necessary for industrial process for production of paints, inks, as well as production of metallic nanoparticles. For example, surfactants are used for synthesis and dispersion of metallic nanoparticles that exhibit interesting optoelectronic and catalytic activities.[17]

Adsorption of surfactants on carbon nanotubes (CNTs) and dispersion in aqueous solvents have been extensively studied. CNT is an all-carbon materials like fullerene, having tubular structures with graphitic surface. The discovery goes back to Iijima's report in 1991.[18] Due to their (semi)conductivity, researchers focused on their application[19] as well as theoretical studies,[20] while their low solubility in solvents has been a drawback of the material. It is known that self-assembly of surfactant molecules on the surface promotes dispersion of CNTs in water, which is necessary for biological application.[21] While there have been sophisticated dispersants specifically designed for CNTs, the versatile utility of surfactants is important for practical application.[22,23]

1.5. Design of surfactants based on fullerene

As described above, researchers have achieved enhancement of particular surfactant functions, e.g. self-assembly, adsorption at oil-water interface, and solid dispersion, by substituting the alkyl backbone of surfactants with more complex molecular frameworks. However, a problem is that, the above designs are so varied that it is difficult to offer a general guideline to overwhelm the efficacy of conventional alkyl surfactants.

When overlooking the history of artificial surfactants, one realizes that fullerene has attracted much attention for the molecular design since its discovery in 1985 by Kroto et al.[24] Fullerene is hydrophobic, and has high cohesive power and symmetric structure, which is suitable as a general molecular unit that can be an alternative for alkyl groups.[25] Fullerene can be modified easily by various synthetic methods to produce backbone structures. For example, nucleophilic addition reactions using organometallic reagents is a powerful technique to functionalize the C_{60} core of the fullerene derivatives.[26] Cycloaddition reactions including Diels-Alder reaction,[27] Bingel reaction,[28] and Plato reaction[29] are widely used for introduction of various functionalities for the use in supramolecular science,[30] biological assay,[31] and optoelectronic devices.[32] Our group has also reported functionalization reaction using tetraaddition reaction with amines[33] and pentaaddition reaction using organocopper reagents.[34] On the other hand, the high reactivity of the π-conjugated system of fullerene has somewhat limited further functionalization of the fullerene derivatives. Click reactions, represented by copper(I)-catalyzed Huisgen cycloaddition reactions,[35] offer mild synthetic routes to introduce complex, fragile or multiple functional groups to the hydrophobic fullerene core effectively for designing surfactants.[36]

1.6. Surfactant properties of fullerene amphiphiles

In this way, a variety of amphiphilic fullerene derivatives have been developed. Formation of vesicles has been reported by Tour,[37] and Shinkai[38] for aqueous solutions of fullerene amphiphiles with or without the presence of organic solvents. Also Hirsch reported vesicle and micelle formation for dendritic fullerenes.[39] Fiber formation was reported for a similar fullerene with dendritic hydrophilic groups introduced by click reaction as well.[30] Needless to say, the successful results are achieved by the hydrophobicity of fullerene that helped self-association. While the phenomenon is somewhat common with alkyl surfactants, our group has found that the rigidity of the functionalized fullerene leads to stable bilayer vesicles.[40] The stability of the membrane inhibited permeation of water,[41] while retaining ability to solubilize hydrophobic molecules.[42]

1.7. Self-assembly to form micelles and vesicles

The effective aggregation of the fullerene core was applied for condensation of DNA and RNA.[43] Cationic fullerene derivatives adsorb on the anionic surface of the nucleic acid via electrostatic attraction. For effective folding, aggregation of the hydrophobic fullerene core is essential (Figure 1-6).[44]

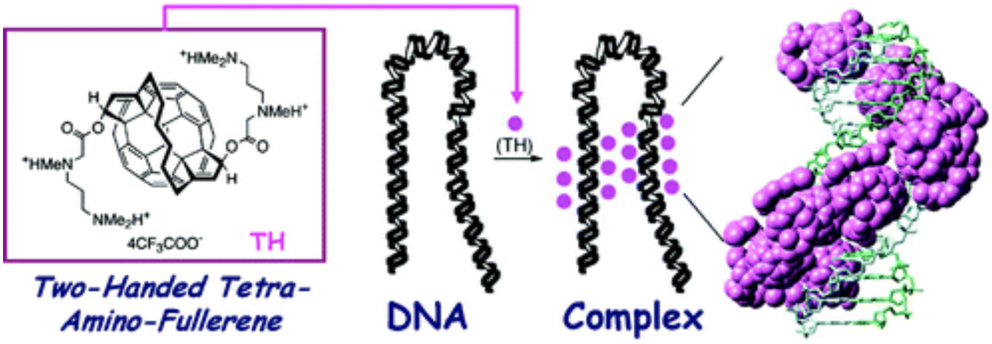

Figure 1-6. Complexation between a cationic fullerene amphiphile and DNA. Reprinted with permission from ref 44. Copyright 2005 American Chemical Society.

1.8. Adsorption at fluid- and solid-water interfaces

Adsorption of amphiphilic fullerenes on the air-water interface has been studied for Langmuir-Blodgett (LB) films.[45] Unlike Gibbs monolayer, a LB film is formed by water-insoluble molecules that mainly exist on air-water interface. We have reported LB film formation by a fullerene derivative bearing a carboxylic group. The area per molecule was 0.78 nm^2, which is close to the value of a single fullerene. The result implies that fullerene is suitable for tight packing at two-dimensional interfaces.

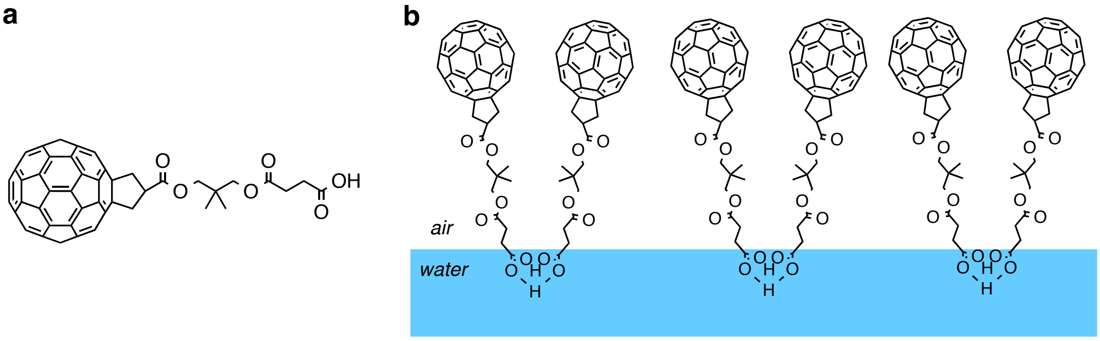

Figure 1-7. LB film of fullerene carboxylic acid (ref. 45).

Similar to the adsorption of fullerene surfactants to air-water interface, adsorption and assembly of fullerene deviatives at solid surfaces have been studied. $CpFeC_{60}Me_5$, a fullerene derivative bearing symmetrically introduced methyl groups, forms a tightly packed layer on Au(111) surface (Figure 1-8a).[46] The structure was characterized by scanning tunneling electron microscopy (STM). The significance of the molecular geometry of the fullerene-based framework was clearly shown in comparison with pentacarboxylated fullerene (Figure 1-8b). The latter compound has extended biphenyl arms that consist the C_5-symmetric structure. Unlike the former compound, the pentapod fullerene is unsuitable for tight packing on the surface. As shown in the figure, the molecules form disordered membrane. This suggests that the rigid molecular framework of the conical fullerene derivatives can be used to alter the characteristics of a self-assembled membrane by choosing an appropriate functionalization method.

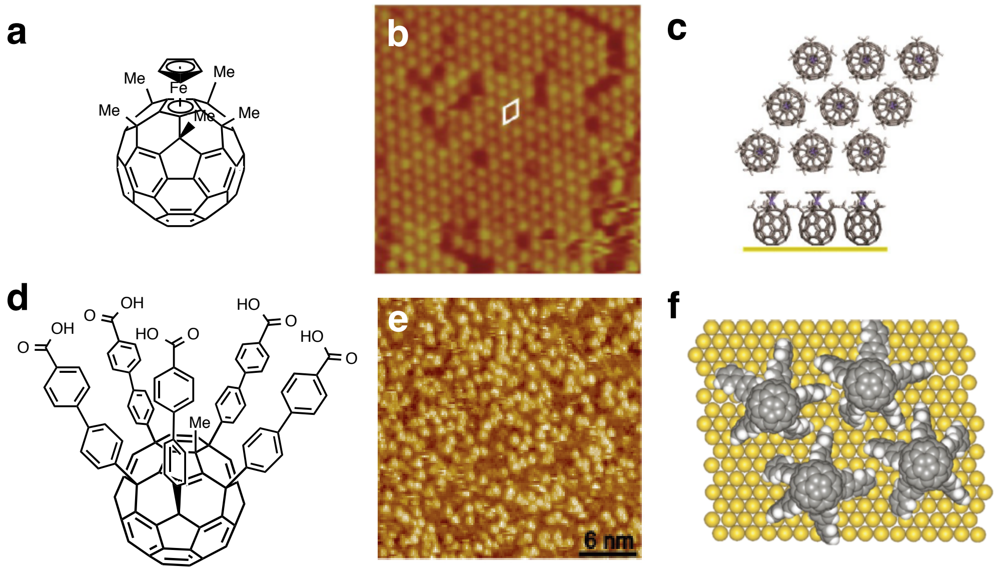

Figure 1-8. Adsorption of fullerene derivatives on Au(111) surface (ref46). (a, d) chemical structures, (b, e) STM images, and (c, f) Modeled structures of monolayer membranes of (a-c) a compact derivative and (d-f) a conical derivative, respectively. (b, c) Reprinted with permission from ref46a. Copyright 2014 American Chemical Society. (e, f) Reprinted with permission from ref46c. Copyright 2010 American Chemical Society.

1.9. Application to dispersion of solid nanomaterials

The above-mentioned properties of fullerene amphiphiles suggest their possible effectiveness as surfactants for solid dispersion. Although the number of report focusing on the purpose is limited, some researches utilized fullerene for dispersion of carbon nanotubes (CNTs). Fullerene has π-conjugated surface that can interact with CNT surface by dispersion force. Luzzi et al. showed that fullerene can be internalized in CNTs and also can adsorb on the surface.[47] As for functionalized fullerenes, Britz et al. showed adsorption of a fullerene dicarboxylic acid around CNTs (Figure 1-9a-c).[48] The amphiphilic fullerene formed a cage by hydrogen bonding between adjacent molecules. As such, it is expected that adsorption of fullerene molecules around CNTs involves multiple interactions between fullerene and CNTs and fullerene amphiphiles themselves. Dispersion of CNTs in water using a fullerene amphiphile with a dendritic hydrophilic group was demonstrated by Takaguchi et al (Figure 1-9d).[36] Although clear indication of fullerene adsorption on CNT is not shown, they successfully prepared CNT dispersion with the water-soluble fullerene. More recently, Hilmer et al. reported on electronic interaction between amphiphilic fullerenes adsorbed on CNT surfaces.[49] In this work, they could disperse CNTs successfully using fullerene derivatives conjugated with PEG groups and aliphatic groups (Figure 1-9e, f).

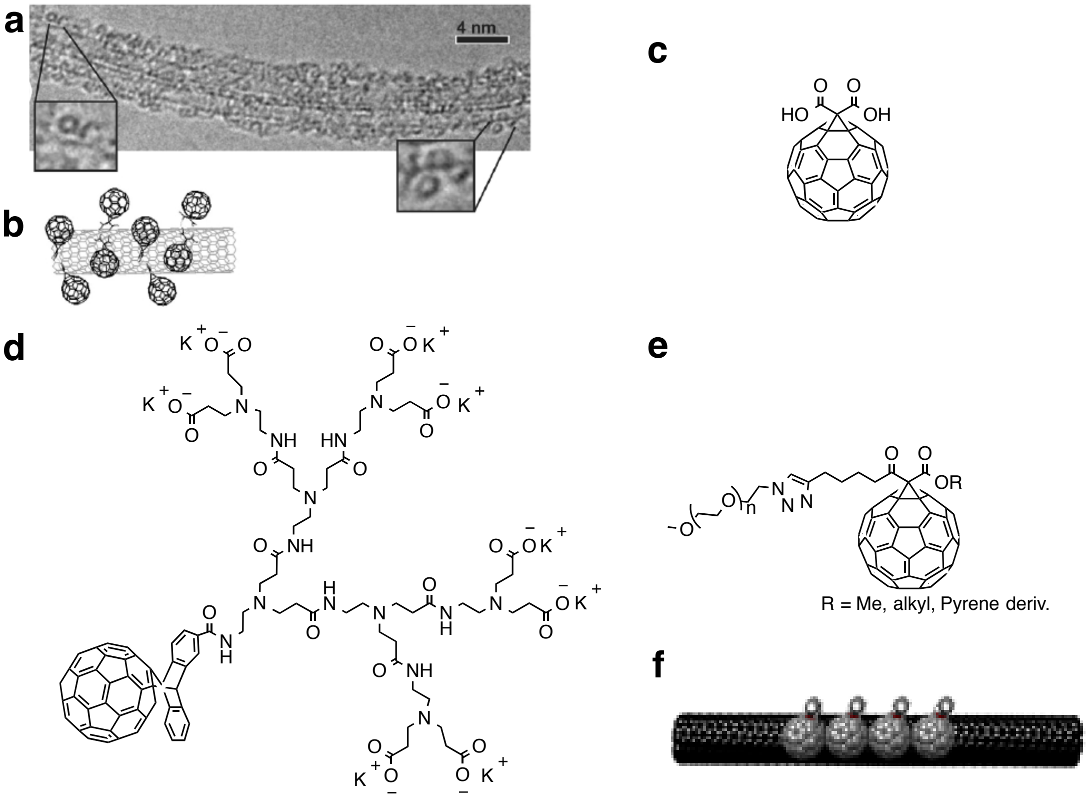

Figure 1-9. Interaction between amphiphilic fullerenes and CNTs. (a, b) TEM image and illustration of CNTs covered by fullerene dicarboxylic acid (ref 48). (c). (d) Dendritic fullerene amphiphile (ref 36) and (e) PEG-attached fullerene amphiphile used for dispersion of CNTs in water. (f) Illustration of CNT/PEG-fullerene. Reprinted with permission from ref 49. Copyright 2014 American Chemical Society.

1.10. Systematic study of fullerene surfactants for application

As shown above, fullerene amphiphiles can 1) self-assemble, 2) adsorb at air-water interfaces, and 3) solid-water interfaces. The previous studies suggest that not only the hydrophobicity of fullerene but also molecular geometry and interactions originating in hydrophilic groups are responsible for the functions of fullerene amphiphiles. Systematic study on structure-activity relationship of fullerene amphiphiles will open a way for on-demand control of dynamics of the surfactant molecules based on precise chemical modification.

1.11. References

[1] Myers, D. An Overview of Surfactant Science and Technology. *Surfactant Science and Technology,* 3rd ed.; John Wiley & Sons, Inc.: New Jersey, 2006; pp 1–28.

[2] a) Maibaum, L.; Dinner, A. R.; Chandler, D. *J. Phys. Chem. B* **2004**, *108*, 6778–6781. b) Lum, K.; Chandler, D.; Weeks, J. D. *J. Phys. Chem. B* **1999**, *103*, 4570–4577.

[3] Cullis, P. R.; Hope, M. J.; Tilcock, C. P. S. *Chem. Phys. Lipids* **1986**, *40*, 127–144.

[4] Israelachvili, J. N. *Intermolecular and surface forces*, Revised 3rd Edition, Academic Press, London, 2011.

[5] Wang, Y.; Huang, Z.; Kim, Y.; He, Y.; Lee, M. *J. Am. Chem. Soc.* **2014**, *136*, 16152–16155.

[6] Griffin, W. C. *J. Soc. Cosmet. Chem.* **1949**, *1*, 311–326.

[7] Misra, P. K.; Somasundaran, P. *Adv. Polym. Sci.* **2008,** *218*, 143–188.

[8] AmBisome® is a representative liposomal drug commercialized by Astellas Pharma Inc.

[9] Yu, T.; Liu, X.; Bolcato-Bellemin, A.-L.; Wang, Y.; Liu, C.; Erbacher, P.; Qi, F.; Rocchi, P.; Behr, J. P.; Peng, L. *Angew. Chem.* **2012**, *124*, 8606–8612.

[10] Scamehorn, J. F.; Schechter, R. S.; Wade, W. H. *J. Colloid. Interf. Sci.* **1982**, *85*, 463–478.

[11] Eastoe, J.; Dalton, J. S. *Adv. Colloid Interface Sci.* **2000**, *85*, 103–144.

[12] Myers, D. Fluid Surfaces and Interfaces. *Surfactant Science and Technology,* 3rd ed.; John Wiley & Sons, Inc.: New Jersey, 2006; pp 80–106.

[13] Menger, F. M.; Sorrells, J. L. *J. Am. Chem. Soc.* **2006**, *128*, 4960–4961.

[14] Numata, M.; Kinoshita, D.; Taniguchi, N.; Tamiaki, H.; Ohta, A. *Angew. Chem., Int. Ed.* **2012**, *51*, 1844–1848.

[15] Myers, D. Solid Surfaces and Dispersions. *Surfactant Science and Technology,* 3rd ed.; John Wiley & Sons, Inc.: New Jersey, 2006; pp 323–369.

[16] Eastman, J. A.; Phillpot, S. R.; Choi, S. U. S.; Keblinski, P. *Annu. Rev. Mater. Res.* **2004**, *34*, 219–246.

[17] Sapsford, K. E.; Algar, W. R.; Berti, L.; Gemmill, K. B.; Casey, B. J.; Oh, E.; Stewart, M. H.; Medintz, I. L. *Chem. Rev.* **2013**, *113*, 1904–2074.

[18] Iijima, S. *Nature* **1991**, *354*, 56–58.

[19] Baughman, R. H.; Zakhidov, A. A.; de Heer, W. A. *Science* **2002**, *297*, 787–792.

[20] Rao, A. M.; Richter, E.; Bandow, S.; Chase, B.; Eklund, P. C.; Williams, K. A.; Fang, S.; Subbaswamy, K. R. Menon, M. Thess, A.; Smalley, R. E.; Dresselhaus, G.; Dresselhaus, M. S. *Science* **1997**, *275*, 187–191.

[21] Moore, V. C.; Strano, M. S.; Haroz, E. H.; Hauge, R. H.; Smalley, R. E.; Schmidt, J.; Talmon, Y. *Nano Lett.* **2003**, *3*, 1379–1382.

[22] Nakashima, N.; Tomonari, Y.; Murakami, H. *Chem. Lett.* **2002**, 638–639.

[23] Shcn, C.; Ma, D.; Meany, B.; Isaacs, L.; Wang, Y. *J. Am. Chem. Soc.* **2012**, *134*, 7254–7254.

[24] Smalley, R. E.; Kroto, H. W.; Heath, J. R. *Nature* **1985**, *318*, 162–163.

[25] Labille, J.; Masion, A.; Ziarelli, F.; Rose, J.; Brant, J.; Villiéras, F.; Pelletier, M.; Borschneck, D.; Wiesner, M. R.; Bottero, Y. *Langmuir* **2009**, *25*, 11232–11235.

[26] a) Hirsch, A.; Soi, A.; Karfunkel, H. R. *Angew. Chem., Int. Ed.* **1992**, *31*, 766–768. b) Nagashima, H.; Terasaki, H.; Saito, Y.; Jinno, K.; Itoh, K. *J. Org. Chem.* **1995**, *60*, 4966–4967.

[27] a) Shlueter, J. A.; Seaman, J. M.; Taha, S.; Cohen, H.; Lykke, K. R.; Wang, H. H.; Williams, J. M. *J. Chem. Soc., Chem. Commun.* **1993**, 972–974. b) Ohno, M; Azuma, T.; Kojima, S.; Shirakawa, Y.; Eguchi, S. *Tetrahedron* **1996**, *52*, 4983–4994.

[28] Bingel, C. *Chem. Ber.* **1993**, *126*, 1957–1959.

[29] Maggini, M.; Scorrano, G.; Prato, M. *J. Am. Chem. Soc.* **1993**, *115*, 9798–9799.

[30] Muñoz, A.; Illescas, B. M.; Sánchez-Navarro, M.; Rojo, J.; Martín, N. *J. Am. Chem. Soc.* **2011**, *133*, 16758–16761.

[31] Bosi, S.; Feruglio, L.; Da Ros, T.; Spalluto, G.; Gregoretti, B.; Terdoslavich, M.; Decorti, G.; Passamonti, S.; Moro, S.; Prato, M. *J. Med. Chem.* **2004**, *47*, 6711–6715.

[32] Li, G.; Shrotriya, V.; Huang, J.; Yao, Y.; Moriarty, T.; Emery, K.; Yang, Y. *Nat. Mater.* **2005**, *4*, 864–868.

[33] Isobe, H.; Tanaka, T.; Nakanishi, W.; Lemiègre, L.; Nakamura, E. *J. Org. Chem.* **2005**, *70*, 4826–4832.

[34] Zhong, Y.-W.; Matsuo, Y.; Nakamura, E. *Org. Lett.* **2006**, *8*, 1463–1466.

[35] Meldal, M.; Tomøe, C. W. *Chem. Rev.* **2008**, *108*, 2952–3015.

[36] Takaguchi, Y.; Tamura, M.; Sako, Y.; Yanagimoto, Y.; Tsuboi, S.; Uchida, T.; Shimamura, K.; Kimura, S.; Wakahara, T.; Maeda, Y.; Akasaka, T. *Chem. Lett.* **2005**, *34*, 1608–1609.

[37] Cassell, A. M.; Asplund, C. L.; Tour, J. M. *Angew. Chem., Int. Ed.* **1999**, *38*, 2403–2405.

[38] Sano, M.; Oishi, K.; Ishi-I, T.; Shinkai, S. *Langmuir* **2000**, *16*, 3773–3776.

[39] Schade, B.; Ludwig, K.; Böttcher, C.; Hartnagel, U.; Hirsch, A. *Angew. Chem., Int. Ed.* **2007**, *46*, 4393–4396.

[40] Zhou, S.; Burger, C,; Chu, B.; Sawamura, M.; Nagahama, N.; Toganoh, M.; Hackler, U. E.; Isobe, H.; Nakamura, E. *Science* **2001**, *291*, 1944-1947.

[41] Isobe, H.; Homma, T.; Nakamura, E. *Proc. Natl. Acad. Sci. U.S.A.* **2007**, *104*, 14895-14898.

[42] Harano, K.; Gorgoll, R. M.; Nakamura, E. *Chem. Commun.* **2013**, *49*, 7629-7631.

[43] a) Maeda-Mamiya, R.; Noiri, E.; Isobe, H.; Nakanishi, W.; Okamoto, K.; Doi, K.; Sugaya, T.; Izumi, T.; Homma, T.; Nakamura, E. *Proc. Natl. Acad. Sci. U.S.A.* **2010**, *107*, 5339–5344. b) Minami, K.; Okamoto, K.; Doi, K.; Harano, K.; Noiri, E.; Nakamura, E. *Sci. Rep.* **2014,** *4*, doi:10.1038/srep04916.

[44] Ying, Q.; Zhang, J.; Liang, D.; Nakanishi, W.; Isobe, H.; Nakamura, E.; Chu, B. *Langmuir* **2005**, *21*, 9824–9831.

[45] Matsumoto, M.; Tachibana, H.; Azumi, R.; Tanaka, M.; Nakamura, T.; Yunome, G.; Abe, M.; Yamago, S.; Nakamura, E. *Langmuir* **1995**, *11*, 660–665.

[46] a) Chen, T.; Wang, D.; Gan, L.-H.; Matsuo, Y.; Gu, J.-Y.; Yan, H.-J.; Nakamura, E.; Wan, L.-J. *J. Am. Chem. Soc.* **2014**, *136*, 3184–3191. b) Chen, T.; Pan, G.-B.; Yan, H.-J.; Wan, L.-J.; Matsuo, Y.; Nakamura, E. *J. Phys. Chem. C* **2010**, *114*, 3170–3174. c) Lacher, S.; Matsuo, Y.; Nakamura, E. *J. Am. Chem. Soc.* **2011**, *133*, 16997–17004.

[47] Smith, B. W.; Monthioux, M.; Luzzi, D. E. *Nature* **1998**, *396*, 323–324.

[48] Britz, D. A.; Khlobystov, A. N.; Wang, J.; O'Neil, A. S.; Poliakoff, M.; Ardavan, A.; Briggs, G. A. D. *Chem. Commun.* **2004**, 176–177.

[49] Hilmer, A. J.; Tvrdy, K.; Zhang, J.; Strano, M. S. *J. Am. Chem. Soc.* **2013**, *135*, 11901–11910.

Chapter 2. Micellization of conical fullerene amphiphile and application as a DNA binder

2.1. Introduction

Aminofullerenes are protonated in neutral water and aggregate together with DNA[1] and siRNA[2], serving as a vector[3] both *in vitro* and *in vivo*.[4] Tetrapiperazino fullerene epoxide (TPFE) is one of these cationic fullerene vectors that form sub-μm to μm sized nucleic acid aggregates in a buffer and in serum.[5] However, an excess amount of the aminofullerene is required to achieve efficient DNA binding (terminal amine/phosphate (N/P) ratio of 5; the more reagent is expected a priori to cause the more side effects), since the basicity of the secondary amines in TPFE is attenuated by the strong electron-withdrawing effect of the fullerene moiety. In addition, being a little too compact in its structure, TPFE is not easily amenable to further structural modification and functionalization for tuning and targeting of the gene delivery.[6] To remedy these issues, I have designed a modular synthetic route to a new pentaaminofullerene (***p*-hex-DMA**) via click cycloaddition chemistry,[7] and examined its behavior in micelle formation[8] and DNA binding. The conical fullerene amphiphile (CFA) bearing five cationic groups shows high solubility in water to form micelles of ca. 12 nm in diameter. Upon mixing with a double stranded DNA, it forms reproducibly a spherical aggregate of 50-nm diameter at a N/P ratio as small as 0.5–1 in a hepes buffer. This diameter of the fullerene/DNA aggregate was previously shown to be useful for gene delivery across cell membrane.[9]

2.2. Synthesis of the cationic CFA by click reaction

The click approach to the new pentaminofullerenes is straightforward as shown in Scheme 1.[10] A Grignard reagent bearing a terminal acetylene protected by tris(isopropyl)silyl group (TIPS) was added five-times to [60]fullerene in the presence of a stoichiometric amount of copper(I) salt, which was followed by methylation[11] to obtain a pentaacetylenic fullerene **1**. The TIPS protection was removed by fluoride anion, and the terminal acetylene **2** was allowed to undergo Huisgen cycloaddition reaction (click reaction) with 3-(dimethylamino)propyl azide in the presence of copper(I) bromide dimethylsulfide complex and *N*,*N*,*N*',*N*'',*N*''-pentamethyldiethylenetriamine (PMDETA) (Scheme 2-1).[12] This ligand accelerates the reaction and also prevents premature precipitation of the catalyst from the reaction mixture. THF was solvent of choice, while DMSO gave poor results perhaps because of charge transfer between the dimethylamino groups and the fullerene moieties in this solvent.[13] The product was purified by removal of copper contaminants with aqueous ammonia solution followed by extraction in dichloromethane. The pentaaminofullerene **3** was finally converted into water-soluble hydrochloride salt ***p*-hex-DMA** and used for further studies.

Scheme 2-1. Synthesis of ***p*-hex-DMA** and the structure of TPFE.

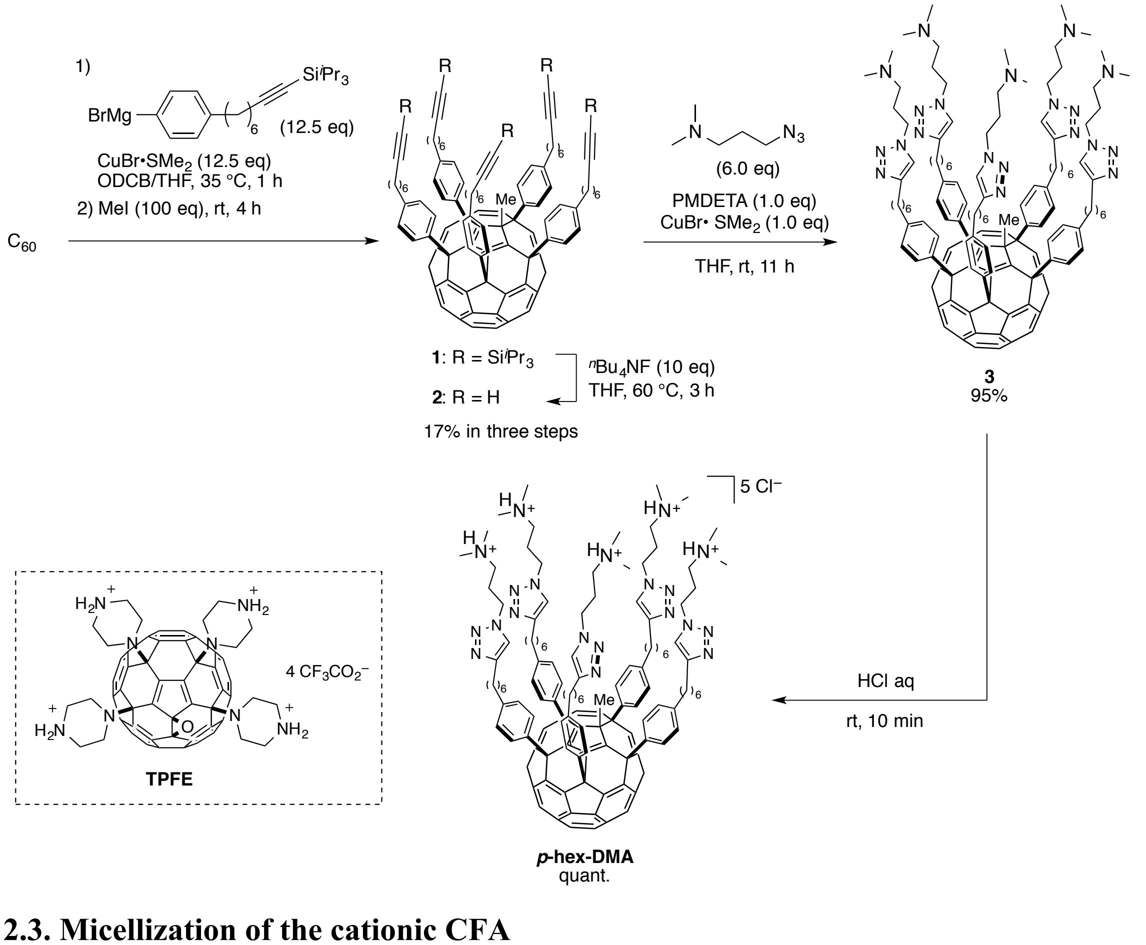

1)
BrMg
Si*i*Pr3
6 (12.5 eq)
CuBr•SMe2 (12.5 eq)
ODCB/THF, 35 °C, 1 h
2) MeI (100 eq), rt, 4 h
C60
R
Me
1: R = Si*i*Pr3
2: R = H
17% in three steps
*n*Bu4NF (10 eq)
THF, 60 °C, 3 h
N3
(6.0 eq)
PMDETA (1.0 eq)
CuBr• SMe2 (1.0 eq)
THF, rt, 11 h
3
95%
HCl aq
rt, 10 min
5 Cl⁻
p-hex-DMA
quant.
H2N
NH2
4 CF3CO2⁻
TPFE

2.3. Micellization of the cationic CFA

The cationic CFA ***p*-hex-DMA** dissolves well in water (≥ 25 g/L or ≥ 10 mM) and in a buffer by forming a micellar aggregate. Critical micelle concentration (CMC) in phosphate-buffered saline (PBS) as determined by the solvatochromic shift of a hydrophobic probe Nile red (NR)[14] was 3.6 ± 0.5 μM (Figure 2-1), which is much lower than those of ionic amphiphiles such as SDS (3.5 mM)[15] and CTAB (74 μM)[16], and comparable to high molecular-weight dendritic amphiphiles.[17] The fluorescence of 638 nm at concentration higher than 10 mM is the same as the value reported for a lipid micelle,[14] suggesting that NR is located in an environment similar to that in a lipid micelle. Comparison of the blue shift data in Figure 2-1b with the fluorescence intensity in Figure 2-1c provides support to this conjecture; that is, below CMC, the NR fluorescence was partially quenched,[18] suggesting proximity of NR and the fullerene part of ***p*-hex-DMA** as illustrated on the left of Figure 2-1c. A marked increase of the intensity above CMC suggest that NR is now located close to the aliphatic region of the micelle as illustrated on the right.[19,20]

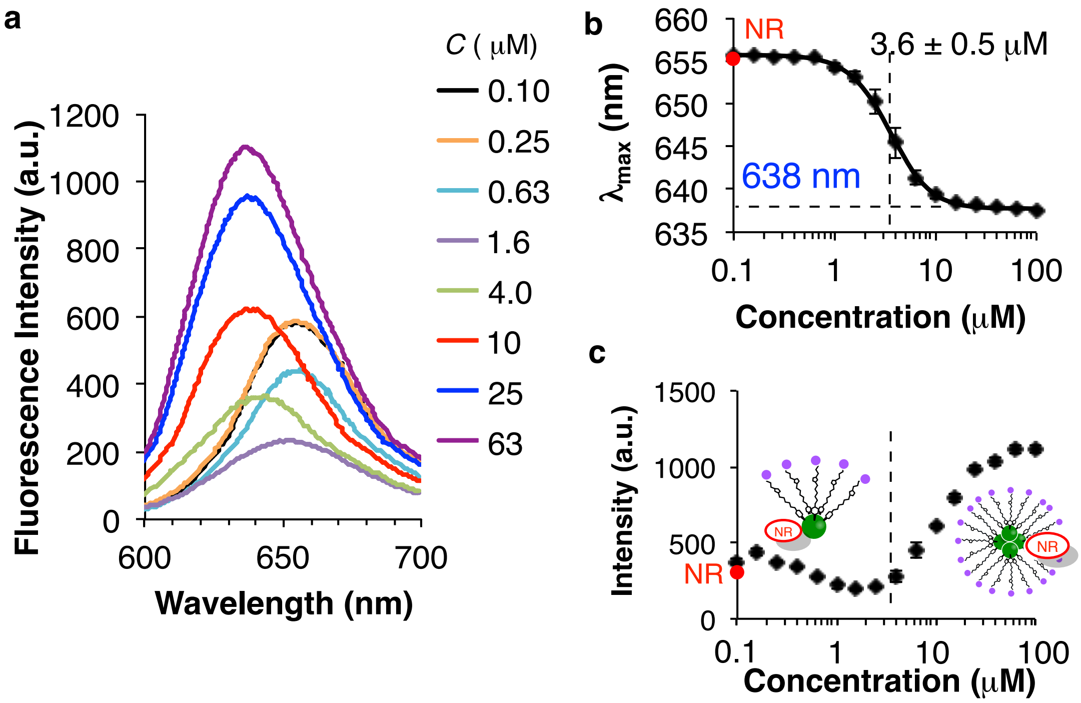

Figure 2-1. Solubilization of Nile red (NR) in a micelle of ***p*-hex-DMA**. (a) Emission spectra of NR at various concentrations of ***p*-hex-DMA**. (b) Emission wavelength (λ_{max}) vs. concentration. (c) Change of intensity recorded at 635 nm. The red dots in (b) and (c) show the intensity and the λ_{max} of NR fluorescence without ***p*-hex-DMA**.

Dynamic light scattering (DLS) analysis of ***p*-hex-DMA** in a hepes buffer showed two peaks at a hydrodynamic diameter of 14.1 ± 1.1 nm and 340 ± 90 nm (Figure 2-2a top; in red). Similarly, a 0.1 mM solution of ***p*-hex-DMA** in water showed peaks at 12.0 ± 0.2 nm and at 237 ± 21 nm. Only the smaller fraction was observed, by scanning transmission electron microscopy (STEM), as micellar particles of an average diameter of 6.1 ± 2.6 nm (Figure 2-2c).

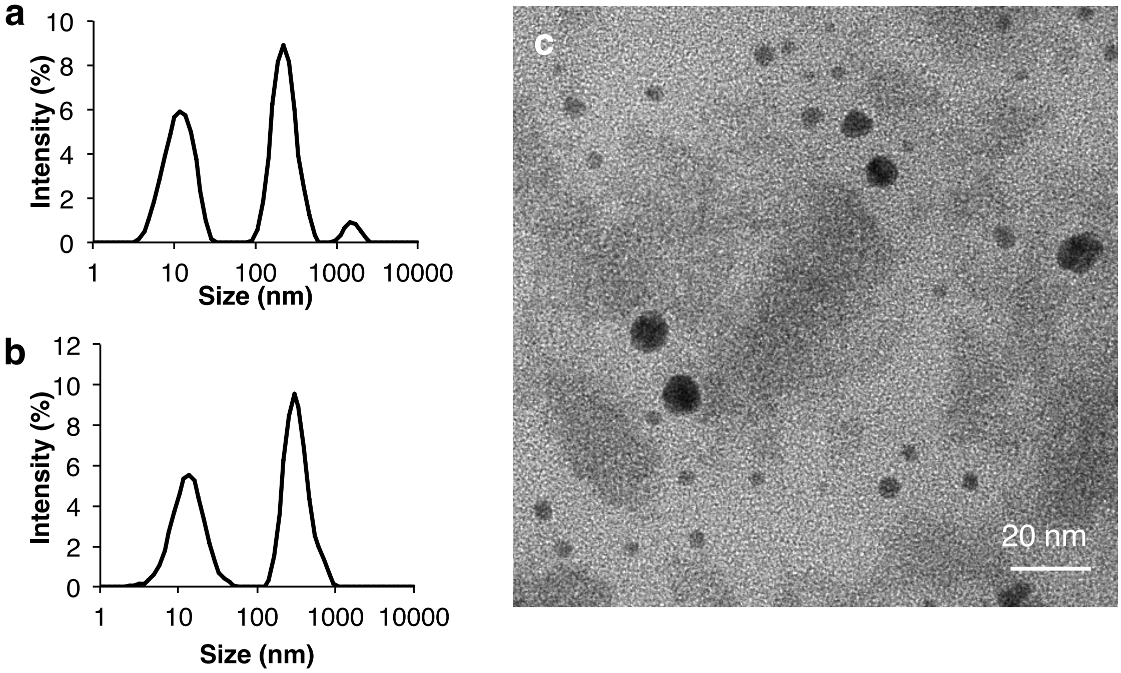

Figure 2-2. Analysis of self-assembled structure of ***p*-hex-DMA**. (a) Size distribution in a hepes buffer. (b) Size distribution in water. (c) STEM image of ***p*-hex-DMA** micelles on an amorphous carbon film.

The micellar structure was found to be stable between pH 3 and pH 8 (0.5 M KOH aq added to a pH 3 solution containing 25 mM KCl; little change of diameter and zeta potential, Figure 2-3),[6] while the size significantly increased above pH 9. At pH ≥ 6.2 ***p*-hex-DMA** precipitated by centrifugation due to partial neutralization of the dimethylamino group. The precipitate could be redispersed easily by shaking (Figure 2-3b). Interestingly, the smaller object could be separated from that larger by centrifugation, suggesting that the smaller and the large particles are not equilibrating with each other.[21] I used a solution of ***p*-hex-DMA** without removal of the larger fraction because all fractions appear to contribute equally well to DNA compaction upon addition double stranded DNA.

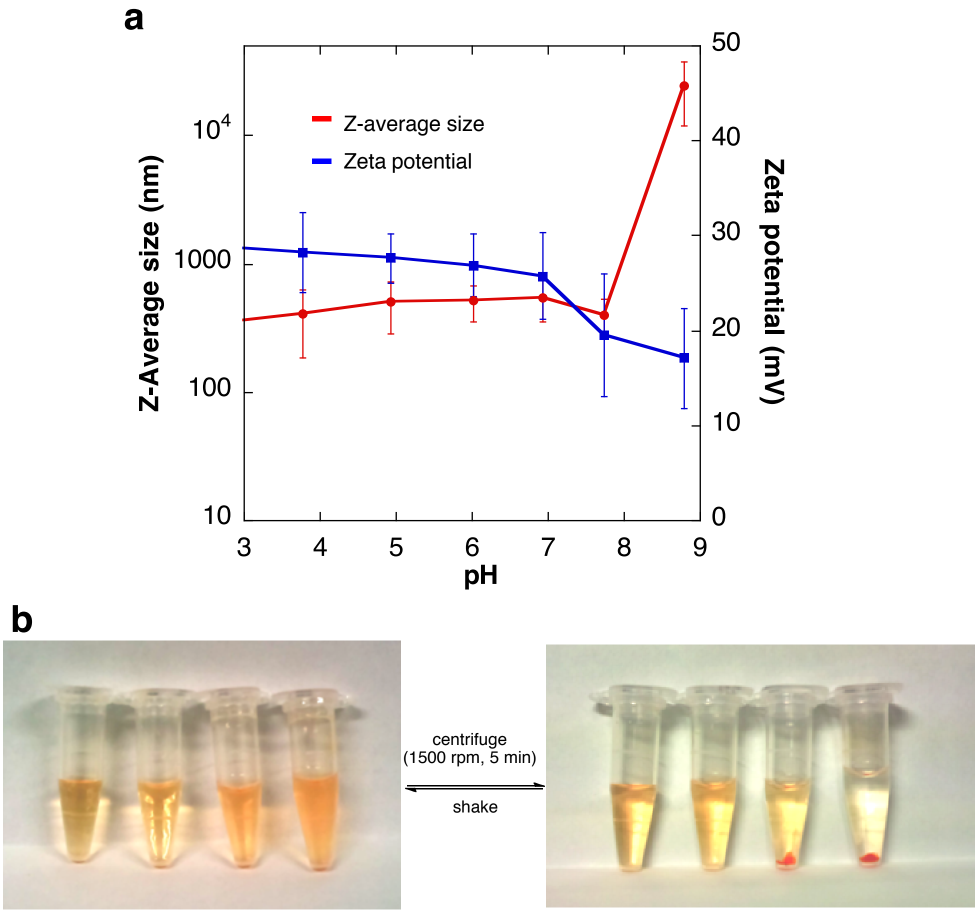

Figure 2-3. pH titration experiment. (a) pH dependence of Z-average size and zeta potential. (b) Precipitation and redispersion of ***p*-hex-DMA** in water at pH 6.0, 6.2, 6.3, and 7.8 from the left.

2.4. Binding of the cationic CFA with DNA

***p*-hex-DMA** was found to be an efficient agent for compacting double stranded DNA into cationic nanoparticles. Aliquots of ***p*-hex-DMA** were added to a 0.1 mg/mL solution of calf thymus DNA (≤ 2 kbp, 1%TAE agarose gel) in a hepes buffer (2 mM, pH 7.4) containing NaCl (10 mM), which showed a broad DLS size distribution between 10-1000 nm (Figure 2-4b, N/P = 0). The two DLS peaks in the solution of ***p*-hex-DMA** (Figure 2-4b top) disappeared upon mixing with the DNA and gave rise to a single peak at 46-50 nm by further addition of ***p*-hex-DMA** to N/P ratio of 1.0-2.0 and gave a single broad peak. Figure 2c shows the correlation of the N/P ratio and the aggregate size, illustrating a sharp initial increase of the size to 7 mm followed by precipitous decrease to 50 nm at N/P = 1.0. The size then remained constant suggesting that stable compaction of DNA was achieved. The zeta potential also suggests the formation of a cationic nanoparticle composed of **_p_-hex-DMA** and DNA (Figure 2-4c). The AFM images of the compacted calf thymus DNA on mica (Figure 2-5) were obtained by deposition of the **_p_-hex-DMA** /DNA complexes dispersed in a hepes-Mg buffer containing 10 mM $MgCl_2$, followed by washing with 1 mL of water.[22] At N/P = 0.5, particles to which DNA strands are attached can be observed (Figure 2-5f). This image is consistent with the 136 nm hydrodynamic diameter determined by DLS (Figure 2-4b). At N/P = 1.0, only fully compacted particles can be observed (Figure 2-5c), which is consistent with the data in Figure 2-4b at N/P = 1.0. Figure 2-5h illustrates one of such particles of about 20 nm in height. A mean height of 17.1 ± 4.9 nm and a diameter of 51.6 ± 36.2 nm were obtained for 135 particles at N/P = 1.0 by particle analysis (Figure 2-6). These data agree well with the hydrodynamic diameters in solution determined by DLS analysis (Figure 2-4b, c), and suggest that the particles are soft enough to deform upon deposition on mica. The amount of DNA in a particle is estimated to be ca. 1 kbp, which agrees with the size of the calf thymus DNA used for the experiment (≤ 2 kbp).

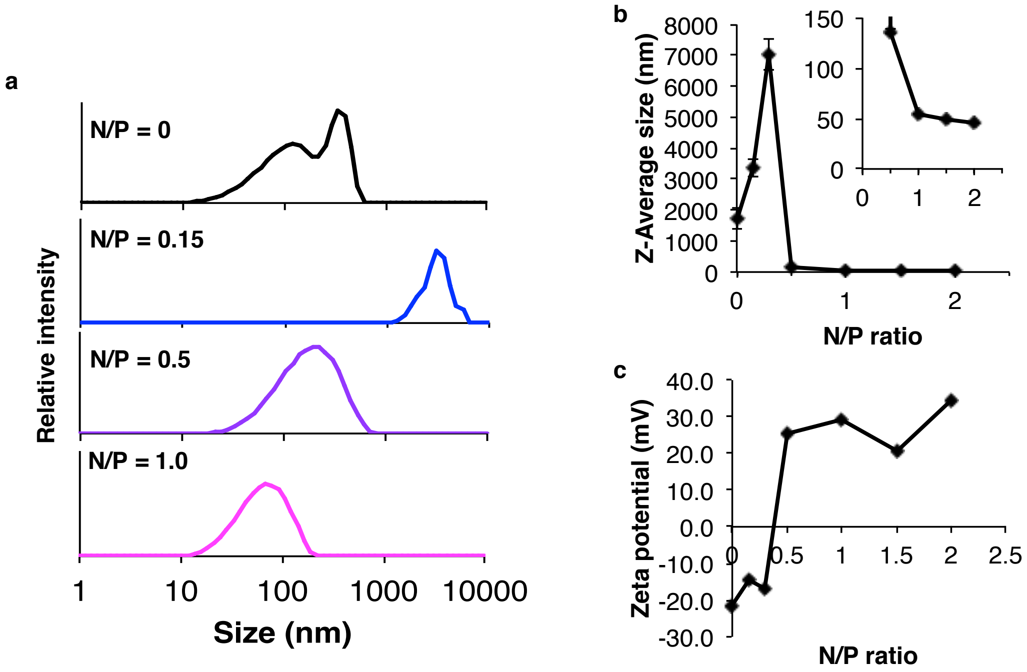

Figure 2-4. Compaction of calf thymus DNA (≤ 2 kbp) strands upon binding with **_p_-hex-DMA**. (a) Size distribution of **_p_-hex-DMA**/DNA complexes at varying N/P ratio obtained by CONTIN analysis of DLS. The concentration of DNA base pairs is determined by average molecular weight of a base (330 Da). Note that the size distribution at N/P = 0.3 was not obtained because

the average size (7 mm) was too large to be suitable for CONTIN analysis. (b) Z-average size change. (c) Zeta-potential change.

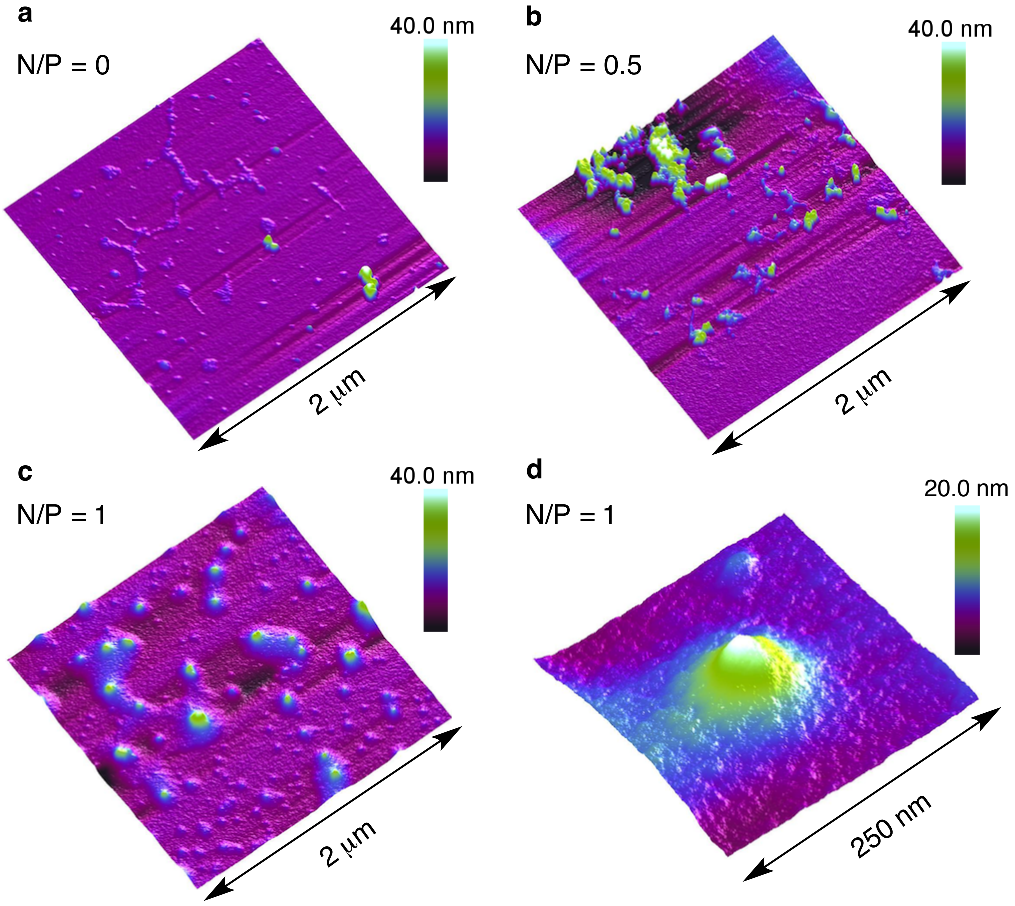
a
N/P = 0
40.0 nm
2 μm
b
N/P = 0.5
40.0 nm
2 μm
c
N/P = 1
40.0 nm
2 μm
d
N/P = 1
20.0 nm
250 nm

Figure 2-5. (a-c) AFM images of ***p*-hex-DMA** /DNA complexes at N/P = 0, 0.5, and 1, respectively. (d) Magnified image of a ***p*-hex-DMA** /DNA complex at N/P = 1.

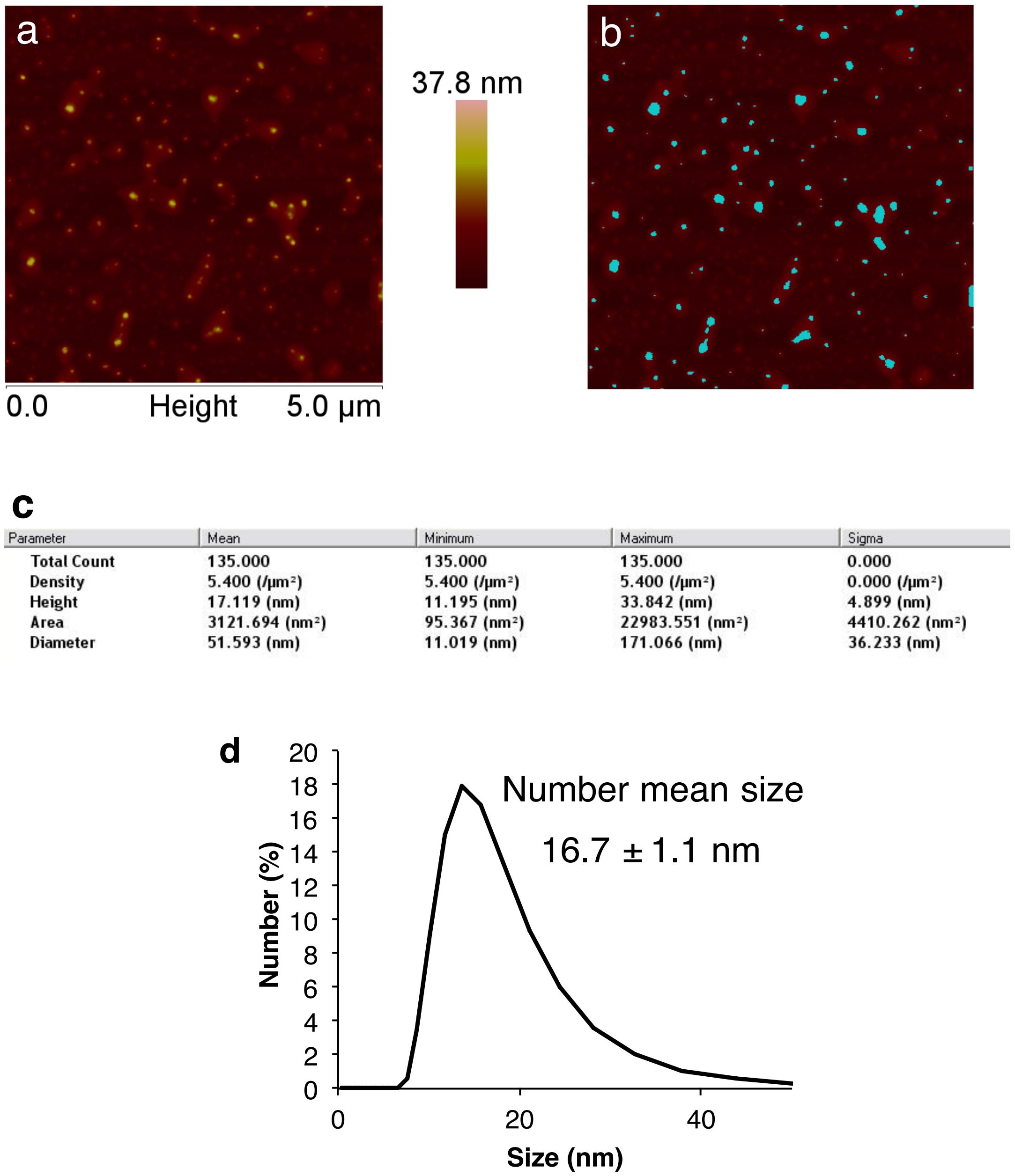

Parameter	Mean	Minimum	Maximum	Sigma
Total Count	135.000	135.000	135.000	0.000
Density	5.400 (/µm²)	5.400 (/µm²)	5.400 (/µm²)	0.000 (/µm²)
Height	17.119 (nm)	11.195 (nm)	33.842 (nm)	4.899 (nm)
Area	3121.694 (nm²)	95.367 (nm²)	22983.551 (nm²)	4410.262 (nm²)
Diameter	51.593 (nm)	11.019 (nm)	171.066 (nm)	36.233 (nm)

Figure 2-6. Particle analysis of ***p*-hex-DMA** /DNA complex at N/P =1. (a) Original image used for the analysis, (b) Selected particles colored blue. (c) Obtained parameters. (d) Number distributeion of ***p*-hex-DMA** /DNA at N/P = 1 obtained by DLS.

2.5. Conclusion

In conclusion, I have developed a synthesis of ***p*-hex-DMA** by modular assembly of a pentaorganofullerene and an amino group via click cycloaddition chemistry, and found that ***p*-hex-DMA** forms a stable micelle in water and in a buffer at low CMC. The micelle of ***p*-hex-DMA** tolerates a considerably wide range of pH and forms a structurally defined stable complex with DNA in a buffer solution. The N/P ratio =1 needed for efficient DNA compaction is expected to render this new aminofullerene a transfection agent with minimum side effects.[23] Finally the modular synthetic strategy[24] will provide an easy access of a variety of derivatives to be useful for targeting biomolecules such as RNA[25] and proteins. [26,10]

2.6. Experimental section

General

All the reactions dealing with air- or moisture-sensitive compounds were carried out in a dry reaction vessel under a positive pressure of nitrogen or argon. The water content of the solvent was confirmed with a Karl-Fischer Moisture Titrator (MKC-210, Kyoto Electronics Company) to be less than 100 ppm. Flash silica gel column chromatography was performed on silica gel 60N (Kanto, spherical and neutral, 140-325 mesh) as described by Still.[27] Analysis with high-pressure liquid chromatography (HPLC) was performed on a Shimadzu HPLC system equipped with Buckyprep column (Nakalai Tesque Inc., 4.6 mm ID x 250 mm). Melting points of solid materials were determined on a Mel-Temp capillary melting-point apparatus and were uncorrected. Infrared (IR) spectra were recorded on a JASCO FT/IR-6100 with an attenuated total reflection (ATR) instrument. NMR spectra were measured on JEOL ECX-400 and ECA-500 spectrometers and reported in parts per million from tetramethylsilane. ^{1}H NMR spectra in $CDCl_3$ were referenced internally to tetramethylsilane as a standard. ^{1}H NMR and ^{13}C NMR spectra in other solvents were referenced internally to the solvent resonance. High resolution mass spectra were acquired by atmospheric pressure chemical ionization (APCI) using a time-of-flight mass analyzer on a JEOL MS-T100LC spectrometer with a calibration standard of polyethylene glycol (M_W 2000) or by electrospray ionization (ESI) using a time-of-flight mass analyser on a Micromass LCT Premier XE mass spectrometer. Water was deionized with Millipore Milli-Q. Dynamic laser light scattering (DLS) study was carried out on a Malvern Zetasizer Nano ZS machine. Atomic force microscopy measurement was performed on a JEOL JSPM-4200 with a silicon cantilever (NSC-35, resonant frequency 120-190 kHz) or Bruker

Multimode 8 with a silicon nitride cantilever (SCANASIST-AIR, resonant frequency 70 kHz). Scanning transmission electron microscopy (STEM) observations were performed on a JEOL JEM-2100. Fluorescence spectra were recorded on a HITACHI F-4500 Fluorescence Spectrophotometer.

Materials

Unless otherwise noted, materials were purchased from Tokyo Kasei Co., Aldrich Inc. and other commercial suppliers, and used after appropriate purification before use. Anhydrous ethereal solvents (stabilizer-free) were purchased from WAKO Pure Chemical and purified by a solvent purification system (GlassContour)[28] equipped with columns of activated alumina and supported copper catalyst (Q-5) prior to use. All other solvents were purified by distillation and stored over 4 Å molecular sieves. [8-(4-Bromophenyl)oct-1-ynyl]tri(1-methylethyl)silane and 3-azidopropyl-*N*,*N*-dimethylamine was synthesized as described in a literature.[2930] [60]Fullerene was purchased from Frontier Carbon Co. Calf thymus DNA (≤ 2 kbp) was purchased from Life Technologies.

Determination of CMC by Nile red assay

Nile red assay was conducted following the procedure reported in ref 17. 1 mL of Nile red solution in ethanol (2.5 mM) was added to 1 mL of solutions of ***p*-hex-DMA** in PBS buffer (pH 6.9) at various concentrations. The solutions were prepared by dilution of aliquots of the stock solution in water. The fluorescence emission was measured using an excitation wavelength of 550 nm. Intensity of the emission was recorded at 635 nm. Maximum emission wavelengths were determined by curve fitting with quadratic functions. CMC values were determined from equilibrium points of the curves.

pH titration experiment

0.5 M KOH aq was added sequentially to a buffered solution (25 mM KCl) of ***p*-hex-DMA** (initial concentration of 0.1 mM), and size and zeta potential of particles in the solution was measured at each pH.

DLS experiment

Dynamic light scattering (DLS) measurements were performed using a Malvern Zetasizer Nano ZS instrument equipped with a He-Ne laser operating at 4 mW power and 633 nm wavelength, and a computer-controlled correlator, at 173° accumulation angle. Measurements were carried out in a polystyrene or glass cuvette. Samples were equilibrated for 2 min at the set temperature each time. The data were processed using Dispersion Technology software version 5.10 to give the particle size distribution and average particle sizes. Data were obtained as average of triplicated experiments.

STEM experiment

STEM measurement was conducted on a JEOL JEM-2100F at 294 K with a spherical aberration coefficient Cs = 1.0 mm at an acceleration voltage of 200 kV under reduced pressure of 1.0 x 10^{-5} Pa in the sample column. The current density was ca. 0.5 pA cm^{-2}. The imaging instrument used was an ultrascan charge-coupled device (CCD) camera (512 x 512 pixels). Aqueous solution of ***p*-hex-DMA** (0.1 mM, 2 mL) was deposited on a transmission electron microscopy (TEM) copper mesh coated with carbon film (Super Ultra High Resolution Carbon film, thickness < 6 nm, Oken Shoji Co., Ltd.), then dried under reduced pressure (1.5 Pa) at room temperature for 1 h.

Complexation between DNA and *p*-hex-DMA

A 10 mM stock solution of ***p*-hex-DMA** in water was added to 0.1 mg/mL solutions of DNA in hepes buffer (2 mM) containing NaCl (10 mM) in Eppendorf tubes, followed by vortex mixing. The mixed solutions were left standing for 3 h before DLS experiments.

Particle analysis

Size distribution of ***p*-hex-DMA** /DNA particles on mica at N/P = 1 was analyzed by particle analysis function using NanoScope Analysis software.

Synthesis

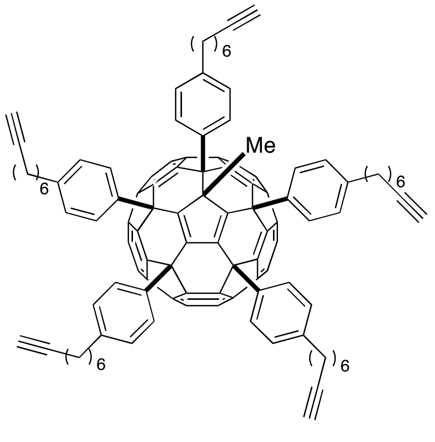

1-Methyl-6,9,12,15,18-penta[4-(oct-7-ynyl)phenyl]-1,6,9,12,15,18-hexahydro(C_{60}-*I*$_h$)[5,6]fullerene (2). To a solution of copper (I) bromide dimetyl sulfide complex (2.45 g, 11.9 mmol) in THF was added 0.298 M of 4-[8-(triisopropylsilyl)oct-7-ynyl]phenyl magnesium bromide in THF (40 mL, 12 mmol). After stirring for 10 min at 35 °C, a solution of [60]fullerene (720 mg, 1.00 mmol) in ODCB (70 mL) was added. The reaction was monitored by HPLC (Bucky Prep, eluent: 30% 2-propanol/toluene). After stirring for 1 h, methyl iodide (6.2 mL, 99 mmol) was added at room temperature, and stirred for 4 h. The reaction mixture was filtrated through a pad of silica gel eluted with toluene to remove copper salt, and then was concentrated under reduced pressure to afford compound **1** as a crude material. The crude material was then dissolved in THF (100 mL). 1.0 M of *n*-tetrabutylammonium fluoride in THF (10 mL, 10 mmol) was added to the solution at room temperature. The reaction was monitored by HPLC (Bucky Prep, eluent: 30% 2-propatnol/toluene). After stirring for 3 h at 60 °C, toluene (50 mL) was added to the reaction mixture and then washed with saturated aq. NH_4Cl (50 mL x 3) and water (50 mL x 1) successively. The combined organic layer was dried with $MgSO_4$, and concentrated in vacuo. The obtained crude material was purified by GPC (eluent: $CHCl_3$) to afford the title compound (282 mg, 17% in two steps) as a red solid. mp 350 °C dec.; IR (powder): 2931, 2855, 1508, 1461, 1186, 1020, 842, 634 cm^{-1}; ^1H NMR (500 MHz, $CDCl_3$): δ 1.20–1.70 (m, 43H), 1.90 (t, *J* = 2.5 Hz, 1H), 1.93–1.95 (m, 4H), 2.13 (dt, *J* = 2.5 Hz, 6.9 Hz, 2H) 2.16–2.22 (m, 8H), 2.46 (t, *J* = 8.0 Hz, 2H), 2.61–2.69 (m, 8H), 6.87 (d, *J* = 8.0 Hz, 2H), 7.10–7.18 (m, 10H), 7.62 (d, *J* = 8.0

Hz, 4H), 7.72 (d, $J = 8.0$ Hz, 4H); ^{13}C NMR (100 MHz, $CDCl_3$): δ 18.47, 18.55, 18.60, 28.44, 28.58, 28.62, 28.73, 28.77, 28.79, 28.83, 28.89, 31.18, 31.28, 31.43, 35.44, 35.57, 35.59, 58.12, 60.99, 62.31, 62.32, 68.30, 68.37, 68.41, 84.75, 128.06, 128.07, 128.35, 128.70, 128.93, 128.95, 130.12, 130.13, 135.55, 137.29, 140.40, 141.37, 142.08, 142.32, 142.82, 144.05, 144.11, 144.12, 144.33, 144.39, 144.47, 144.66, 145.11, 145.69, 145.95, 147.23, 147.42, 147.43, 147.45, 147.93, 148.13, 148.20, 148.33, 148.34, 148.44, 148.58, 148.69, 148.83, 148.86, 152.04, 153.43, 157.54, 160.27, 160.28; HRMS (APCI$^-$) calcd for $C_{131}H_{88}Cl^-$ [M+Cl]$^-$ 1695.6575, found 1695.6616.

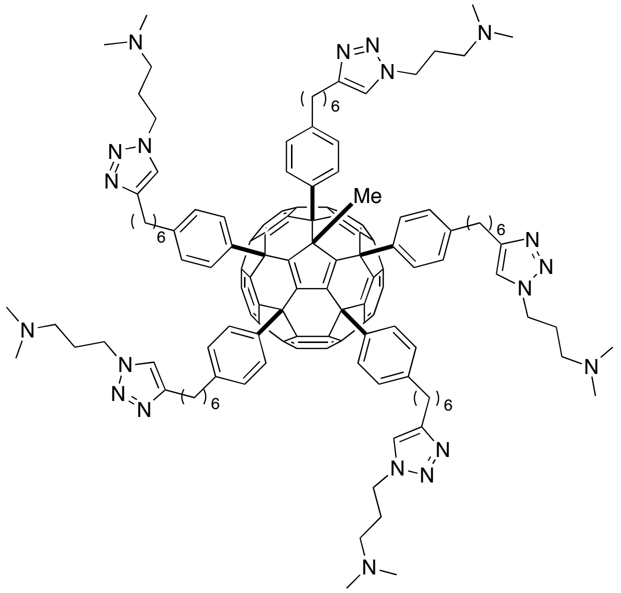

1-Methyl-6,9,12,15,18-penta{4-(6-[1-{3-(dimethylamino)propyl}-1,2,3-triazolyl]hexyl)phenyl}-1,6,9,12,15,18-hexahydro(C_{60}-*I*$_h$)[5,6]fullerene (3). 3-(Dimethylamino)propylazide (20.9 mg, 163 mmol) was added to a mixture of **2** (45.7 mg, 27.2 mmol), CuBr•SMe_2 (5.59 mg, 27.2 mmol), and PMDETA (5.7 mL, 27.2 mmol) in THF (2.0 mL) at room temperature, and the reaction mixture was stirred at room temperature for 11 h. The reaction mixture was diluted with dichloromethane (20 mL), washed with 10% aq. NH_4OH (3 mL x 3), and concentrated in vacuo to give the title compound (59.7 mg, 95%) as a red solid which was further converted into a hydrochloride salt (***p*-hex-DMA**) by addition of 1 M hydrochloric acid followed by condensation in vacuo. mp 350 °C dec.; IR (powder): 2929, 2855, 2818, 2766, 1508, 1461, 1044 cm^{-1}; ^{1}H NMR (500 MHz, $CDCl_3$): δ 1.26–1.46 (m, 23H), 1.63–1.69 (m, 20H), 2.00–2.05 (m, 10H), 2.19–2.20 (m, 30H), 2.22-2.26 (m, 10H), 2.44 (t, *J* = 7.3 Hz, 2H), 2.60–2.73 (m, 28H), 4.34–4.38 (m, 10H), 6.87 (d, *J* = 8.0 Hz, 2H), 7.09–7.12 (m, 10H), 7.25 (s, 1H), 7.28 (s, 2H), 7.29 (s, 2H), 7.61 (d, *J* = 8.0 Hz, 4H), 7.72 (d, *J* = 8.0 Hz, 4H); ^{1}H NMR (500 MHz, CDCl$_3$): δ 25.60, 25.67, 25.70, 28.25, 28.94, 29.05, 29.10, 29.16, 29.39, 29.49, 29.53, 31.11, 31.21, 31.36, 34.38, 35.34, 35.48, 45.35, 47.85, 55.91, 57.97, 60.85, 62.17, 62.29, 120.87, 120.92, 120.94, 127.94, 128.17, 128.56, 128.78, 129.96, 135.32, 137.05, 140.20, 141.25, 141.26, 142.03, 142.26, 142.64, 142.66, 143.93, 143.94, 143.99, 144.17, 144.23, 144.24, 144.31, 144.53, 144.54, 144.99, 145.55, 145.83, 147.07, 147.27, 147.30, 147.31, 147.77, 147.78, 148.03, 148.04, 148.09, 148.11, 148.17, 148.28, 148.43, 148.52, 148.67, 148.70, 148.71, 151.91, 151.92, 153.34, 157.45, 160.15, 160.16; HRMS (ESI$^+$) calcd for C$_{156}$H$_{148}$N$_{20}$H$^+$ [M+H]$^+$ 2303.2305, found 2303.2290.

2.7. References

[1] Klumpp, C.; Lacerda, L.; Chaloin, O.; Ros, T. D.; Kostarelos, K.; Prato, M.; Bianco, A. *Chem. Commun.* **2007**, *36*, 3762–3764.

[2] Minami, K.; Okamoto, K.; Doi, K.; Harano, K.; Noiri, D.; Nakamura, E. *Sci. Rep.* **2014**, *4*, 4916.

[3] Mintzer, M. A.; Simanek, E. E. *Chem. Rev.* **2009**, *109*, 259–302.

[4] Nakamura, E.; Isobe, H. *Chem. Rec.* **2010**, *10*, 260–270.

[5] Maeda-Mamiya, R.; Noiri, E.; Isobe, H.; Nakanishi, W.; Okamoto, K.; Izumi, T.; Homma, T.; Nakamura, E. *Proc. Natl. Acad. Sci. U.S.A.* **2010**, *107*, 5339–5344.

[6] Yu, H.; Nie, Y.; Dohmen, C.; Li, Y.; Wagner, E. *Biomacromolecules* **2011**, *12*, 2039–2037.

[7] Rostovtsev, V. V.; Green, L. G.; Fokin, V. V.; Sharpless, K. B. *Angew. Chem., Int. Ed.* **2002**, *41*, 2596–2599.

[8] Burghardt, S.; Hirsch, A.; Schade, B.; Ludwig, K.; Böttcher, C.; *Angew. Chem., Int. Ed.* **2005**, *44*, 2976–2979.

[9] Cabral, H.; Matsumoto, Y.; Mizuno, K.; Chen, Q.; Murakami, M.; Kimura, M.; Terada, Y.; Kano, M. R.; Miyazono, K.; Uesaka, M.; Nishiyama, N.; Kataoka, K. *Nat. Nanotechnol.* **2011***,* *6*, 815–823.

[10] Isobe, H.; Cho, K.; Solin, N.; Werz, D. B.; Seeberger, P. H.; Nakamura, E. *Org. Lett.* **2007**, *9*, 4611–4614.

[11] Hamasaki, R.; Matsuo, Y.; Nakamura, E. *Chem. Lett.* **2004**, *33*, 328–329.

[12] Meldal, M.; Tomøe, C. W. *Chem. Rev.* **2008**, *108*, 2952–3015.

[13] Isobe, H.; Tanaka, T.; Nakanishi, W.; Lemiègre, L.; Nakamura, E. *J. Org. Chem.* **2005**, *70*, 4826–4832.

[14] Stuart, M. C. A.; van de Pas, J. C.; Engberts, J. B. F. N. *J. Phys. Org. Chem.* **2005**, *18*, 929–934.

[15] Moore, B. M.; Flurkey, W. H. *J. Biol. Chem.* **1990**, *265*, 4982–4988.

[16] Techen, A.; Hille, C.; Dosche, C.; Kumke, M. U. *J. Colloid Interface Sci.* **2012**, *377*, 251–261.

[17] Barnard, A.; Posocco, P.; Pricl, S.; Calderon, M.; Haag, R.; Hwang, M. E.; Shum, V. W. T.; Pack, D. W.; Smith, D. K. *J. Am. Chem. Soc.* **2011**, *133*, 20288–20300.

[18] Harano, K.; Gorgoll, R. M.; Nakamura, E. *Chem. Commun.* **2013**, *49*, 7629–7631.

[19] van Rijn, P.; Janeliunas, D.; Brizard, A. M.; Stuart, M. C.; Koper, G. J.; Eelkema, R.; van Esch, J. H. *New J. Chem.* **2011**, *35*, 558–567.

[20] Synatschke, C. V.; Nomoto, T.; Cabral, H.; Förtsch, M.; Toh, K.; Matsumoto, Y.; Miyazaki, K.; Hanisch, A.; Schacher, F. H.; Kishimura, A.; Nishiyama, N.; Müller, A. H. E.; Kataoka, K. *ACS Nano* **2014**, *8*, 1161–1172.

[21] Israelachvili, J. N. *Intermolecular and surface forces*, Revised 3rd Edition, Academic Press, London, 2011.

[22] Isobe, H.; Nakanishi, W.; Tomita, N.; Jinno, S.; Okayama, H.; Nakamura E. *Chem. Asian. J.* **2006**, *1–2*, 167–175.

[23] Wang, M.; Liu, H.; Li, L.; Cheng, Y. *Nat. Commun.* **2014**, *5*, 3053.

[24] Muñoz, A.; Illescas, B. M.; Sánchez-Navarro, M.; Rojo, J.; Martín, N. *J. Am. Chem. Soc.* **2011**, *133*, 16758–16761.

[25] Yu, T.; Liu, X.; Bolcato-Bellemin, A-L.; Wang, Y.; Liu, C.; Erbacher, P.; Qu, F.; Rocchi, P.; Behr, J-P.; Peng, L. *Angew. Chem*. **2012**, *124*, 8606–8612.

[26] Torres, D. A.; Garzoni, M.; Subrahmanyam, A. V.; Pavan, G. M.; Thayumanavan, S. *J. Am. Chem. Soc.* **2014**, *136*, 5385–5399.

[27] Still, W. C.; Kahn, M.; Mitra, A. *J. Org. Chem.* **1978**, *43*, 2923–2925.

[28] Pangborn, A. B.; Giardello, M. A.; Grubbs, R. H.; Rosen, R. K.; Timmers, F. J. *Organometallics* **1996**, *15*, 1518–1520.

[29] Harano, K.; Minami, K.; Noiri, E.; Okamoto, K.; Nakamura, E. *Chem. Commun.* **2013**, *49*, 3525-3527.

[30] Engler, A. C.; Bonner, D. K.; Buss, H. G.; Cheung, E. Y.; Hammond, P. T. *Soft Matter* **2011**, *7*, 5627–5637.

Chapter 3. Retardation of interfacial activity of nonionic conical fullerene amphiphiles at air-water interface

3.1. Introduction

It has been generally considered for a long time that surfactants in water preferencially adsorb at air-water interfaces by hydrophobic effect, and it is only after saturation of the interface that micellization starts in bulk. [1] Indeed for water-soluble surfactants, critical micelle concentrations (CMC) determined from various methods, e.g. surface tension measurement, solubilization, conductivity, etc. are known to be close in their values. The traditionally accepted behavior was disprobed by Menger et al., who reported preferential interfacial adsorption of a surfactant cation with polyaromatic anions, which was expected to be caused by more favarable geometry of the ion pairs at the interface than in micelles.[2] On the other hand, lowering CMC than saturation of interface by controlling molecular geometry will also be beneficial to prevent foaming upon solubilization process, [3] or to improve stability of nanocomposites solubilizing molecules.[4,5,6] To address the issue, I envisioned that the conical fullerene amphiphile (CFA) is a suitable motif due to its micellization ability[7] and its disfavorable packing at two-dimensional surfaces.[8] Herein this work, I demonstrate that the molecular geometry of CFA is crutial for preferencial micellization at significantly lower bulk concentration than saturation of air-water interface. For this study, two regioisomers of nonionic CFAs, ***p*-HEO** and ***m*-HEO**, bearing different frameworks were syntheized to systematically evaluate the effect of molecular geometry (Figure 3-1). [9] ***p*-HEO** micellizes at more than 50 times smaller concentration than saturation of air-water interface, in contrast to the merely 1.5 times smaller value for ***m*-HEO**. Sum frequency generation (SFG) spectroscopy of the air-liquid interfaces indicated that both ***p*-HEO** and ***m*-HEO** adsorb on air-water interface. The results suggest that packing of the molecules in the Gibbs monolayer is crutial for alternation of dyanamics of surfactants and promoting micellization in bulk. This work demonstrates that tendency of surfactants for interfacial adsorption and micellization can be separately controlled by precise design of molecular geometry.

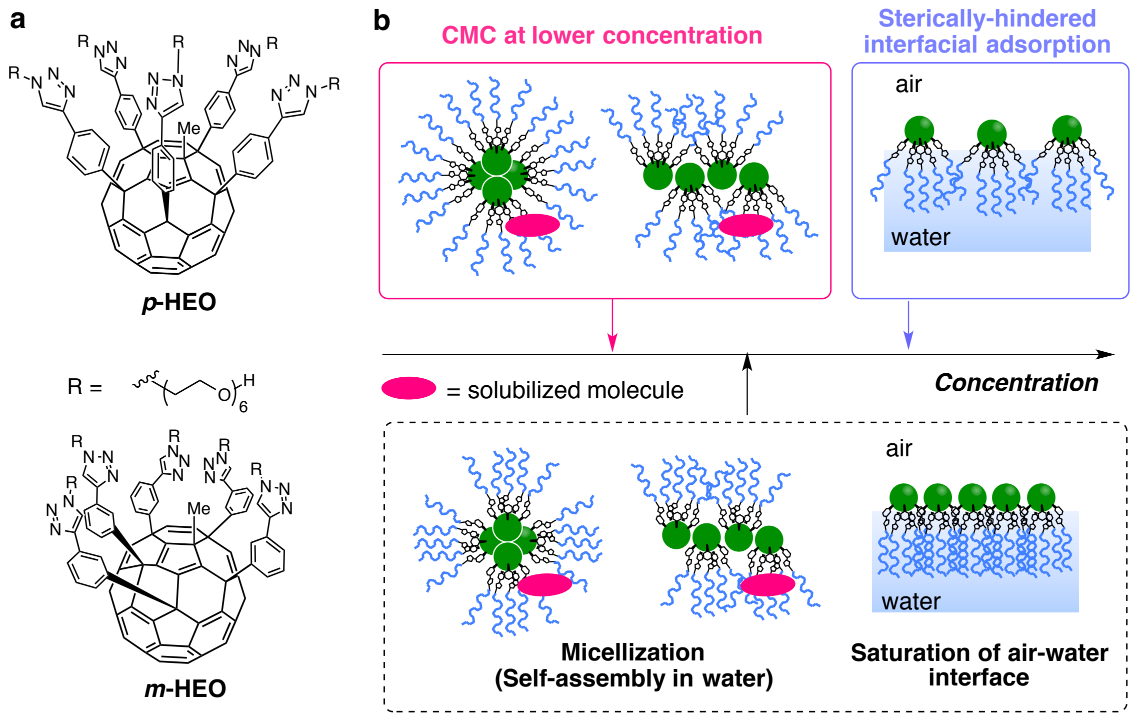
a
p-HEO
R =
6
m-HEO
Me
b
CMC at lower concentration
Sterically-hindered interfacial adsorption
air
water
= solubilized molecule
Concentration
air
water
Micellization (Self-assembly in water)
Saturation of air-water interface

Figure 3-1. Separated micellization and saturation of air-water interface for nonionic CFAs. (a) Structures of nonionic CFAs, ***p*-HEO** and ***m*-HEO**. (b) Comparison of ***p*-HEO** and ***m*-HEO** showing lowered CMC and suppressed interfacial adsorption of ***p*-HEO** compared with ***m*-HEO**.

3.2. Synthesis

***m*-HEO** and ***p*-HEO**, hexa(ethyleneoxide)-decorated CFAs with 3-(triazolo)phenyl groups (*m*-CFA) and 4-(triazolo)phenyl groups (*p*-CFA), were synthesized by the procedure established previously (Scheme 3-1).[7] The hydrophobic frameworks were synthesized by introduction of *p*/*m*-ethynyphenyl groups by pentaaddition reaction followed by methylation of a cyclopentadienyl anion.[10] The introduction of the rigid and compact substituents facilitated isolation merely by reprecipitation with addition of methanol to the reaction mixtures. Trimethysilyl groups were successfully cleaved by addition of the fluoride ion[11] in the presence of acetic acid to neutralize the system. The modified procedure resulted in better yield than the previous synthesis of **2** in chapter 2. Hexa(ethylene oxide) groups were introduced by the click cycloaddition reaction following the previous procedure.[12] High water solubility of ***p*/*m*-HEO** (≥ 30 g/L or ≥ 10 mM) enabled further study in aqueous solutions.

Scheme 3-1. Synthesis of ***p*-HEO** and ***m*-HEO**

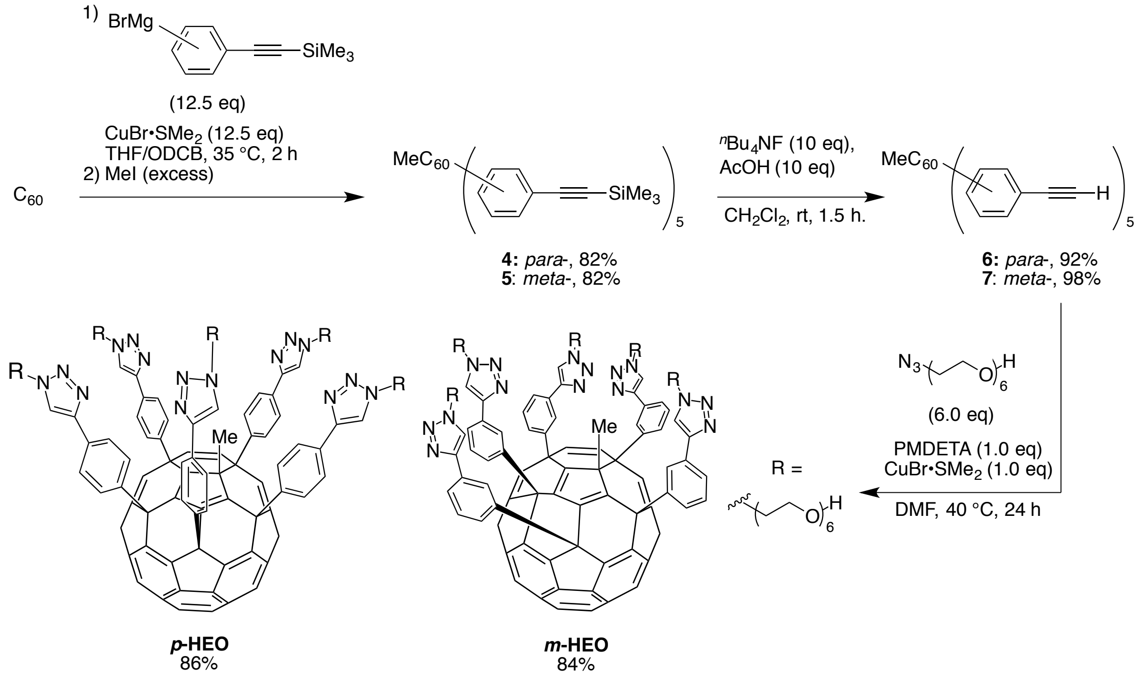
1) BrMg
SiMe3
(12.5 eq)
CuBr•SMe2 (12.5 eq)
THF/ODCB, 35 °C, 2 h
2) MeI (excess)
C60
MeC60
SiMe3
5
4: para-, 82%
5: meta-, 82%
nBu4NF (10 eq),
AcOH (10 eq)
CH2Cl2, rt, 1.5 h.
MeC60
H
5
6: para-, 92%
7: meta-, 98%
N3
O
H
6
(6.0 eq)
PMDETA (1.0 eq)
CuBr•SMe2 (1.0 eq)
DMF, 40 °C, 24 h
R =
O
H
6
R
N
Me
p-HEO
86%
m-HEO
84%

3.3. Micellization of the nonionic CFAs

The size distribution obtained at 100 μM by CONTIN analysis of DLS measurement data shows two peaks for both of the compounds, at 12.6 ± 0.2 nm and 97 ± 0.6 nm for ***p*-HEO** and 7.0 ± 0.2 nm and 253 ± 26 nm for ***m*-HEO** (Figure 3-2a, b). The tendency of the CFAs to form bimodal size distribution is common with ***p*-hex-DMA**. The smaller particles are expected to be micelles rather than monomers considering the size of ***p*/*m*-HEO** of ca. 3.5 nm. The STEM image of ***p*-HEO** shows spherical particles with an average diameter of 84 ± 36 nm, which reasonably matches with the DLS data for the larger fraction (Figure 3-3a). The magnified image of a round-shaped object shows smaller particles, which suggests that the larger particles are collapsed into structurally stable micelles upon deposition on the substrate. Note that the size of ca. 3.5 nm for the dark spots in Figure 3-3c are apparently smaller than the DLS data, because only the core of micelles can be observed for high atomic density of a fullerene cluster (The diameter of fullerene is ca. 1 nm.) on a 6 nm-thick carbon film. On the other hand, ***m*-HEO** is spread on the substrate without formation of particles with defined size or shape (Figure 3-3b).

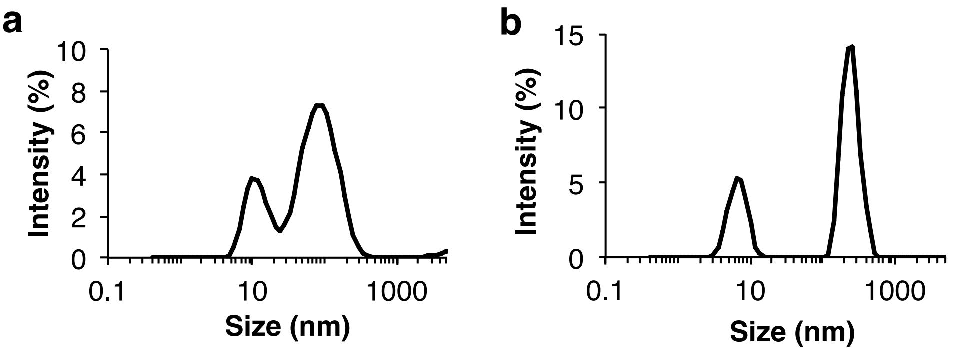

Figure 3-2. Size distributions of self-assembled structures of ***p*-HEO** (a) and ***m*-HEO** (b), respectively (100 μM concentration). The data are obtained by DLS measurement using CONTIN analysis.

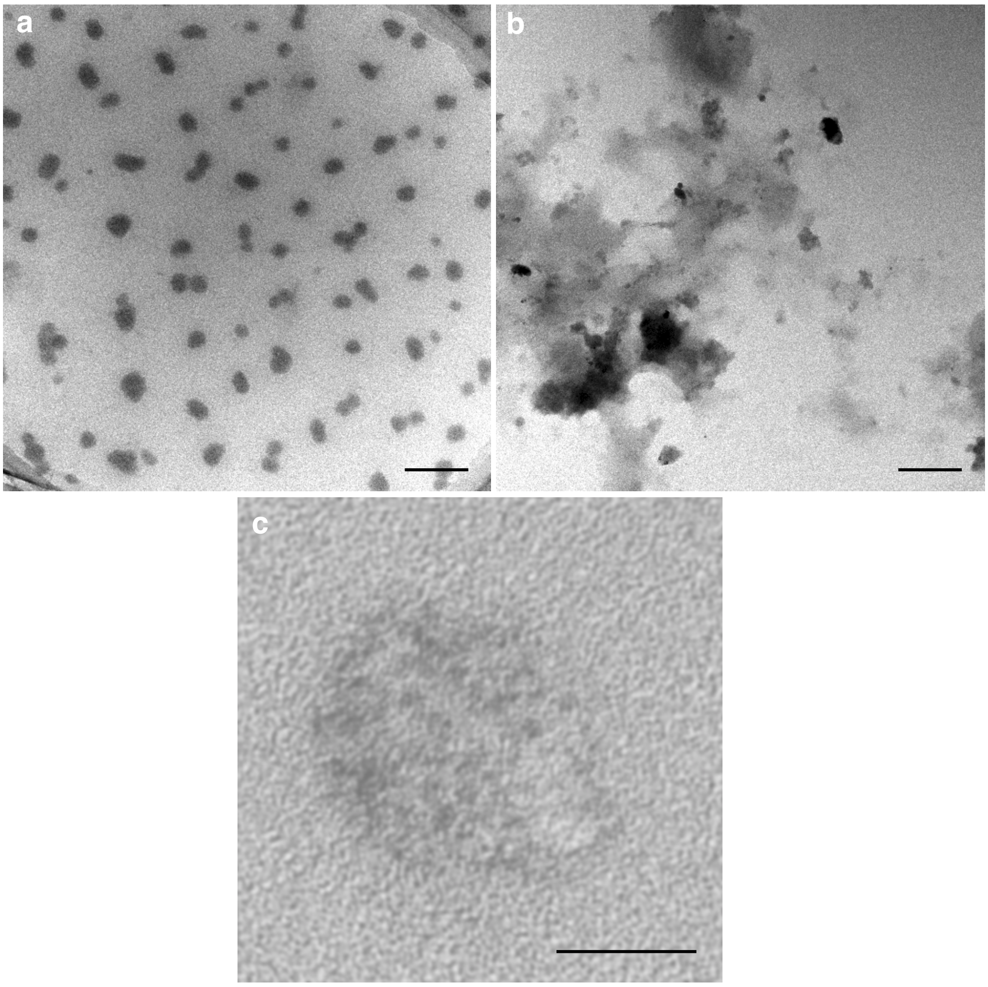

Figure 3-3. STEM imaging of ***p*-HEO** (a) and ***m*-HEO** (b) on a TEM grid with a carbon film. Scale bars are 200 nm. (c) Magnified image of a ***p*-HEO** particle consisting of smaller aggregates of CFAs. Scale bar is 20 nm.

AFM imaging of ***p*-HEO** and ***m*-HEO** on mica substrates also showed the difference between the morphologies of the self-assembled structures. 100 μM aqueous solutions were deposited on mica for the experiments. As shown in Figure 3-4a, micellar particles with average diameter of 16.4 ± 4.9 nm were observed for ***p*-HEO**, which is assumed to be corresponding to the smaller fraction observed by DLS. On the other hand for ***m*-HEO**, the micellar particles are interconnected with each other due to the difference of the molecular geometry of the hydrophobic frameworks (Figure 3-4b).

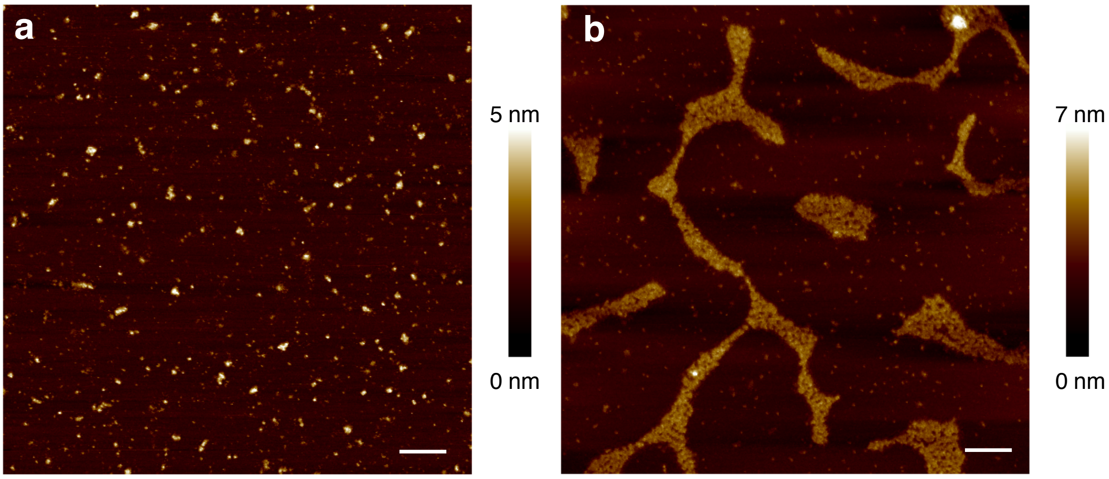

Figure 3-4. AFM images of ***p*-HEO** (a) and ***m*-HEO** (b) on mica. Scale bars are 100 nm.

Micellization of ***p*/*m*-HEO** in water was traced by Nile red (NR) fluorescence assay (Figure 3-5).[13] The shift of NR fluorescence maximum wavelengths shows solubilization of the dye in micelles. By triplication of the experiment, CMCs were determined to be 9.5 ± 1.1 μM for ***p*-HEO** and 31.4 ± 1.4 μM for ***m*-HEO**, respectively. The smaller value for ***p*-HEO** compared with ***m*-HEO** indicates more effective micellization and solubilization for ***p*-HEO**.

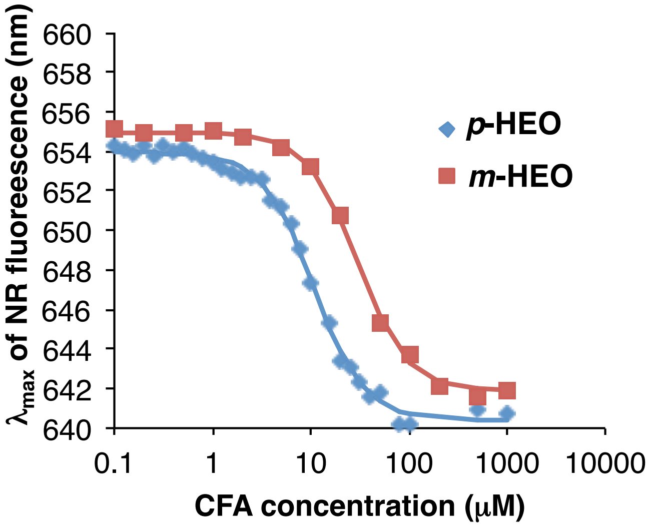

Figure 3-5. NR assay of ***p*/*m*-HEO.**

3.4. Interfacial activity

Interfacial activity of ***p*/*m*-HEO** was shown by drop of interfacial tension of their aqueous solutions (Figure 3-6a). Here, the concentration where interfacial tension levels off after precipitous decrease is determined as C_γ. Traditionally this concentration has been determined as CMC, because it indicates saturation of the water surface or Gibbs monolayer formation, and spontaneous formation of micelles in bulk.[14] For alkyl surfactants, CMC_{NR} (CMC determined by NR assay), and C_γ result in similar values. The C_γ value of 48 ± 11 μM for ***m*-HEO** is reasonably close with the CMC_{NR}, indicating that ***m*-HEO** behaves similarly to conventional surface-active alkyl surfactants (Figure 3-6b). On the other hand for ***p*-HEO**, the C_γ value of 515 ± 50 μM is an order of magnitude larger than the CMC_{NR}. The large disparity between the two regioisomers indicates alternation of dynamics between self-assembly and accumulation at air-water interface by introduction of the conical molecular framework of ***p*-HEO**.

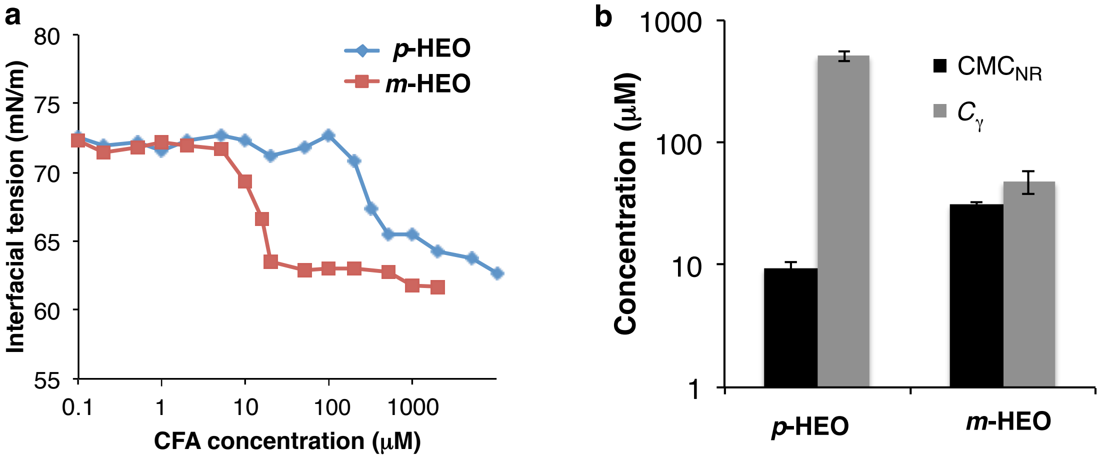

Figure 3-6. Interfacial activity and CMC of ***p*/*m*-HEO**. (a) Plot of interfacial tension in aqueous solutions of the CFAs at varying concentrations. (b) Comparison of CMC_{NR} and C_γ for the CFAs.

Similar to alkyl surfactants that start to form micelles after drop of interfacial tension with increasing concentration, the drop of interfacial tension for ***p*-HEO** also accompanies size change in self-assembled structures below and above its C_γ (Figure 3-7). Size distribution at 10^3 μM is almost similar to that at 100 μM. Note that size distributions at ≤10 μM show large experimental errors suggesting either instability of the aggregates or detection limit at the low concentration. Similarly, quantitative discussion for the size change of ***m*-HEO** is difficult due to its polydispersity. Upon increasing concentration from 10^3 μM to 10^4 μM, the peaks shift to larger sizes from 11.3 ± 0.4 nm to 34.4 ± 7.3 nm, and from 93.5 ± 2.1 nm to 216 ± 5 nm, adding to generation of larger particles that exceeds the measurable size range (Figure 3-7a). This is reflected by Z-average size, which suggests that further aggregation of micelles start to take place after drop of interfacial tension (Figure 3-7b).

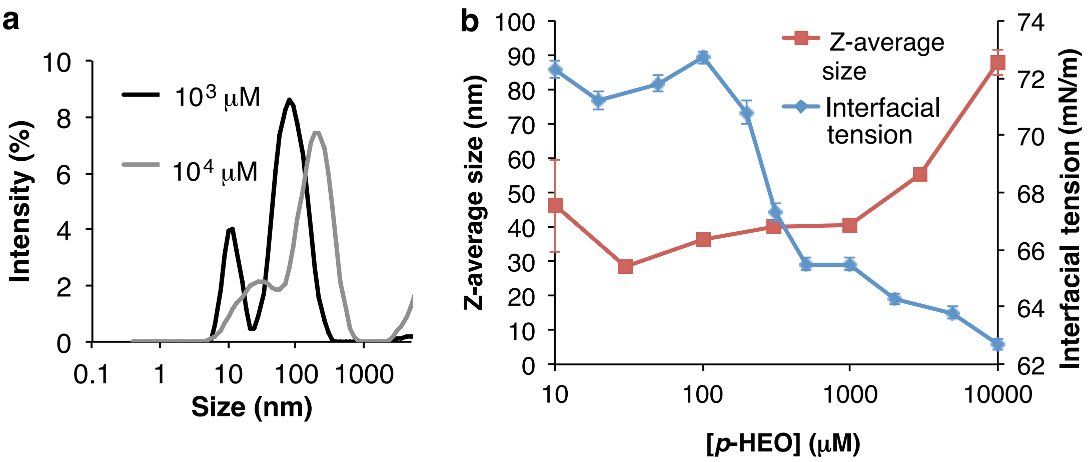

Figure 3-7. Size change of self-assembled structures of ***p*-HEO** accompanied by drop of interfacial tension. (a) Change of size distribution measured by DLS (CONTIN analysis). (b) Decrease of interfacial tension and increase of Z-average size with increased concentration.

3.5. Structure of Gibbs monolayer

To corroborate relationship between the molecular structures and accumulation at air-water interface, density of molecules in Gibbs monolayer was calculated from the plot of interfacial tension. Surface excess concentration (Γ) is calculated by the Gibbs equation of adsorption (eq. 1). Here, R is the gas constant, T is temperature, γ is interfacial tension, and C is a concentration of a surfactant. Areas per molecules in in the saturated Gibbs monolayers (a) are thus calculated as shown in eq.2. N_A is the Avogadro constant.

$$\Gamma = -\frac{1}{2.303RT}\left(\frac{\partial \gamma}{\partial \log C}\right)_T \quad (mol/cm^2) \qquad \text{(eq. 1)}$$

$$a = \frac{10^{16}}{N_A \Gamma} \qquad (\mathring{A}^2) \qquad \text{(eq. 2)}$$

The values are obtained by analyzing the slope of the γ-C curve below the C_γ (Figure 3-6a). The areas per molecule for ***p*-** and ***m*-HEO** are 94.1 ± 7.7 Å^2 and 70.4 ± 10.1 Å^2, respectively. Previously, the area per molecule of a Langmuir-Blodgett (LB) film of an amphiphilic fullerene was estimated to be 78 Å.[15] Given that the van der Waals radius of C_{60} is 0.5 nm, the area per molecule of the C_{60} core is 79 Å. The values fit with that for ***m*-HEO** assuming formation of Gibbs monolayer at air-water interface, which suggests that the CFA is packed to the size of fullerene at saturated air-water interface. On the other hand, ***p*-HEO** has a ca. 20% larger value than C_{60} suggesting steric effect of the *p*-CFA structure.

Table 1. Parameters determined by Nile red assay and interfacial tension measurements of ***m*-HEO** and ***p*-HEO**.

CFA	CMC_{NR} (μM)	C_γ (μM)	Γ (x 10^{-10} mol/cm^2)	a (Å^2/molecule)
***p*-HEO**	9.51 ± 1.14	515 ± 50	1.81 ± 0.17	94.1 ± 7.7
***m*-HEO**	31.4 ± 1.4	48.3 ± 10.8	2.36 ± 0.34	70.4 ± 10.1

3.6. Sum frequency generation spectroscopy

Sum frequency generation (SFG) spectroscopy showed adsorption of ***p*/*m*-HEO** molecules at air-water interface and gave insight into difference in the structures of the Gibbs monolayer (Figure 3-8a, b). SFG spectroscopy is a surface-specific measurement detecting molecular vibration perpendicular to surfaces.[16] SFG occurs by irradiation of visible and IR light to a surface where symmetry is broken.[17] To observe change of surface by adsorption of surfactants, we used D_2O as solvent.[18] The spectrum of pure D_2O surface shows a broad band of hydrogen-bonding OD groups at 2400-2600 cm^{-1} and a peak of OD stretch directing toward air at 2870 cm^{-1}. The spectrum of both ***p*-HEO** and ***m*-HEO** solutions at ≤10 μM are similar with each other; even at 1 μM, a broad peak with its maxima shown at 2870 cm^{-1} that corresponds to CH_2 vibration of ethylene oxide groups appears, which indicates adsorption of the CFA molecules at D_2O surface (Figure 3-8c, d). Saturation of SFG intensity at 10 μM suggests coverage of the surface. The spectrum of ***m*-HEO** does not change even with the increase of concentration to 100 μM, which suggests preservation of molecular orientation and concentration. On the other hand, decrease of intensity for ***p*-HEO** at 100 μM implies randomized orientation of the molecule by increased concentration.

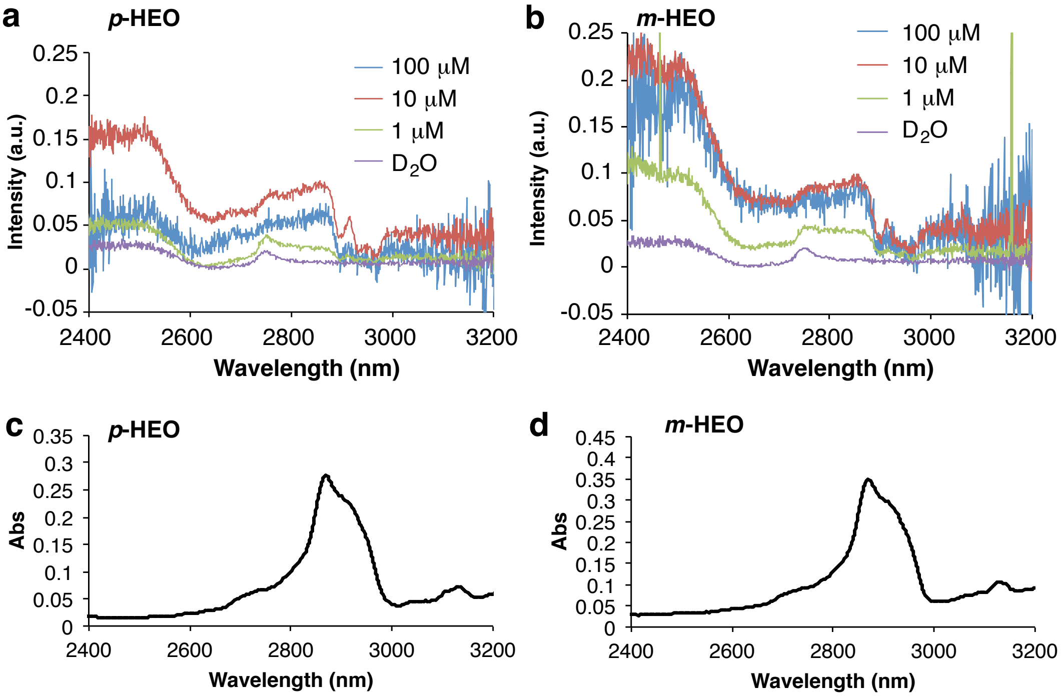

Figure 3-8. Sum frequency generation spectroscopy of aqueous solutions of (a) ***p*-HEO** and (b) ***m*-HEO** with varying concentration. IR spectra of (c) ***p*-HEO** (d) and ***m*-HEO**.

3.7. Molecular modeling of CFA frameworks

Molecular modeling suggested effect of molecular geometry on packing at air-water interface (Figure 3-9). Hydrophobic frameworks, ***p*/*m*-Me**, bearing *N*-methyl triazole groups were constructed as model structures to search the most stable conformation by calculation. Both the height and width of ***m*-Me** after energy minimization were estimated to be ca. 17 Å. For ***p*-Me**, the height and width were 17 Å and 21 Å, respectively due to the shrunk conformation of ***m*-Me** compared with ***p*-Me** having the expanded *p*-(triazoyl)phenyl arms. Areas per molecule for ***p*/*m*-Me** estimated from cross section were 2.4 x 10^2 Å and 2.9 x 10^2 Å, respectively. It should be noted that the areas per molecule of ***m*-Me** can shrink more by close packing at interface while it is difficult for ***p*-Me** due to its pseudo-C_5 symmetricity unsuitable for space filling. Our previous work on self-assembled membrane of conical fullerenes on Au(111) substrate showed disordered alignment of the molecules, while its less-bulky congener could tightly pack with each other in an ordered membrane.[19]

Combining the areas per molecule obtained by the interfacial tension measurements, the SFG data, and the modeled molecular structures of *p*- and *m*-CFA frameworks, the packing structures of the CFAs at air-water interface can be illustrated as Figure 3-9g. At $c \leq 10$ μM, ***p*/*m*-HEO** equally adsorb at air-water interface. While ***m*-HEO** can fully saturate the interface by Gibbs monolayer formation, ***p*-HEO** has looser packing of the molecule at higher concentration, which resulted in retained interfacial tension. The suppressed adsorption to the air-water interface led to lower CMC in bulk. At $c \geq 100$ μM, the increased concentration overcomes the steric repulsion between the ***p*-HEO** molecules at the interface. This leads to increased concentration at the air-water interface, accompanied by reduction of interfacial tension and disruption of molecular orientation.

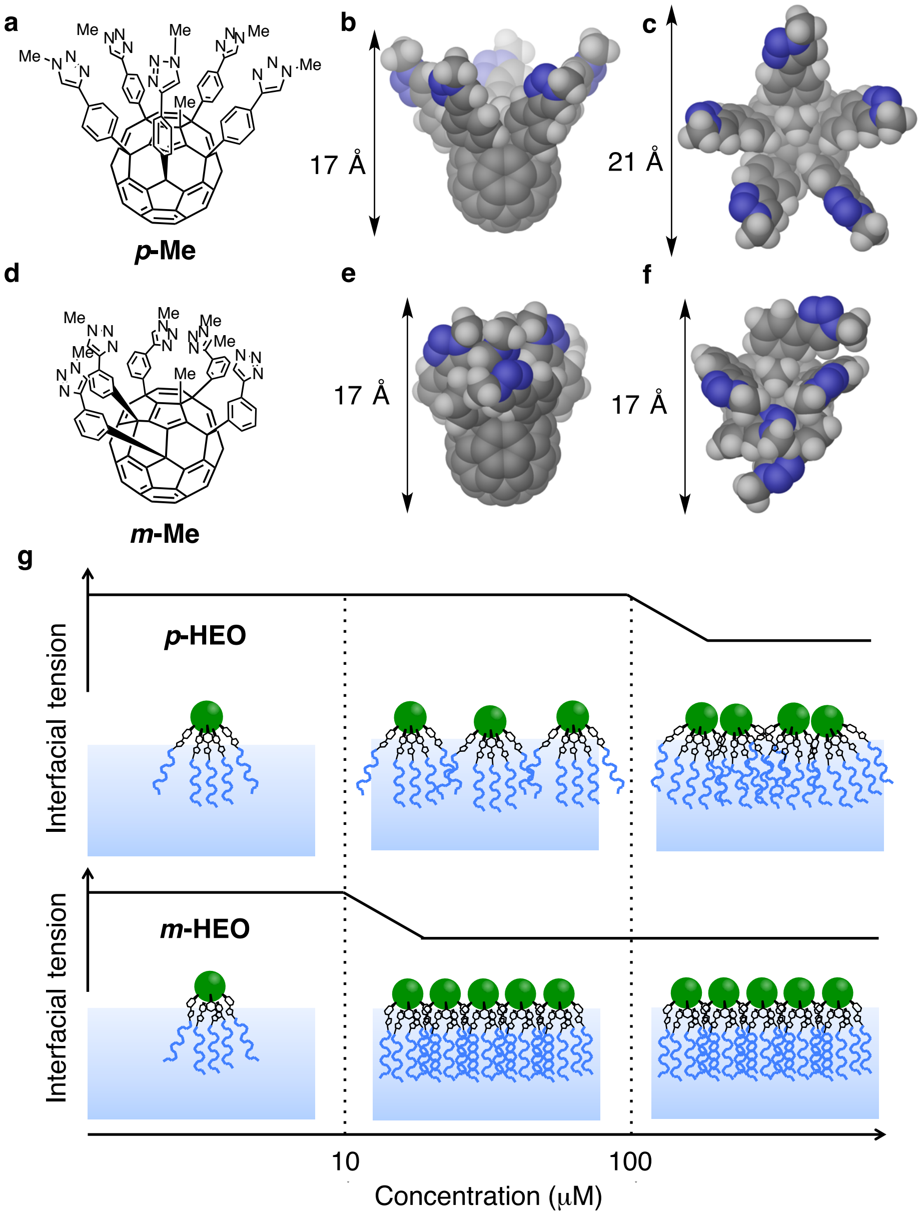
a
p-Me
b
17 Å
c
21 Å
d
m-Me
e
17 Å
f
17 Å
g
Interfacial tension
p-HEO
Interfacial tension
m-HEO
10
100
Concentration (μM)

Figure 3-9. Molecular modeling of ***p*-Me** (a, c) and ***m*-Me** (b, d) performed by macromodel under OPLS_2005 force field in vacuum. Side view (a, b) and top view (c, d). (e) Illustration describing Gibbs monolayer formation and reduction of interfacial tension for ***p*-HEO** and ***m*-HEO** with concentration increase.

3.8. Oil-water interfacial activity

***p*/*m*-HEO** showed interfacial activity at oil-water interfaces as well. Biphasic mixtures of hexane and the solutions of nonionic CFAs resulted in emulsification, while a reference solution colored with methyl orange remained biphasic (Figure 3-10). Microscopic images of the emulsions show oil droplets dispersed in aqueous phase orange colored with the CFA (Figure 3-10b-e). Emulsions were also obtained for toluene. The larger size of the droplet is due to the difference of interfacial tensions.

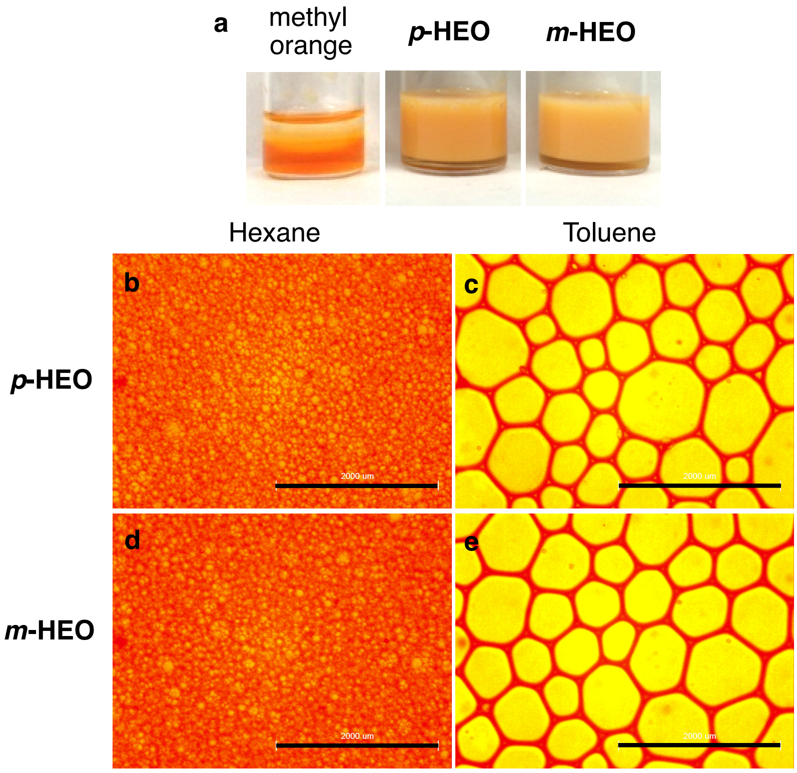

Figure 3-10. Emulsification of oil-water mixtures containing nonionic CFAs. (a) Pictures of the samples 30 min after homogenization of the hexane-water mixtures containing methyl orange (0.1 mg/mL), **_p_-HEO**, and **_m_-HEO** (1 mM). Optical microscopic images of emulsions of **_p_-HEO** (a, b) and **_m_-HEO** (c, d) with hexane (a, c) and toluene (b, d) as an oil phase. Scale bars are 2 mm.

Reduction of interfacial tension at oil-water interfaces was confirmed by pendant drop method in the organic solvents (Figure 3-11). The difference between the two regioisomers is still present in hexane, while the C_γ is shifted to lower concentrations. In toluene, the interfacial tension-concentration curves are even closer, which indicates that the steric effect is less critical than at the air-water interface due to affinity between toluene and fullerene.[20, 21]

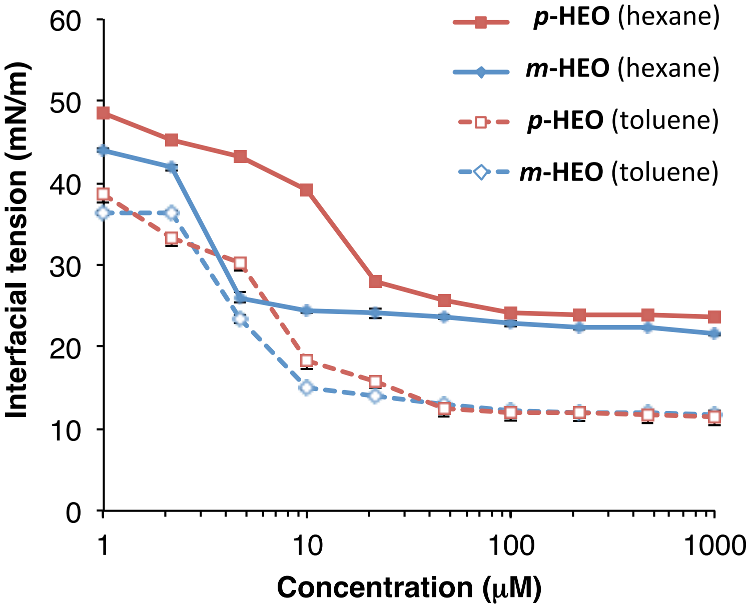

Figure 3-11. Interfacial tension at oil-water interfaces in the presence of ***p*/*m*-HEO**.

3.9. Conclusion

The framework structure of ***p*-HEO** enables suppression of interfacial activity at air-water interface and formation of micelles at $\mathrm{CMC_{NR}}$ more than one order of magnitude smaller than C_{γ}. Comparison of interfacial tension at air-water interface with ***m*-HEO** showed that the regioisomerism of the molecular framework suppressed the interfacial activity. Concentration-dependent structure change of the surface of the CFA solutions was observed by SFG spectroscopy, which suggests that the framework structure of the CFAs affects the molecular packing in the Gibbs monolayers. The above data corroborated with molecular modeling proved that expanded configuration with pseudo-C_5 symmetry for ***p*-HEO** prohibits of packing of the CFA framework at air-water interface, which made it possible to micellize without reducing interfacial tension. The interfacial activity was also present at oil-water interfaces to cause emulsification. The above finding is not limited to CFAs, and can be expanded to other amphiphiles with a rigid, conical framework. The molecules will be applicable as efficient detergents or drug carriers that can predominantly work in solution rather without sparing themselves to adsorption at air-water interfaces.

3.10. Experimental section

General

All the reactions dealing with air- or moisture-sensitive compounds were carried out in a dry reaction vessel under a positive pressure of nitrogen or argon. The water content of the solvent was confirmed with a Karl-Fischer Moisture Titrator (MKC-210, Kyoto Electronics Company) to be less than 100 ppm. Flash silica gel column chromatography was performed on silica gel 60N (Kanto, spherical and neutral, 140-325 mesh) as described by Still.[22] Analysis with high-pressure liquid chromatography (HPLC) was performed on a Shimadzu HPLC system equipped with Buckyprep column (Nakalai Tesque Inc., 4.6 mm ID x 250 mm). Melting points of solid materials were determined on a Mel-Temp capillary melting-point apparatus and were uncorrected. Infrared (IR) spectra were recorded on a JASCO FT/IR-6100 with an attenuated total reflection (ATR) instrument. NMR spectra were measured on JEOL ECX-400 and ECA-500 spectrometers and reported in parts per million from tetramethylsilane. ^{1}H NMR spectra in $CDCl_3$ were referenced internally to tetramethylsilane as a standard. ^{1}H NMR and ^{13}C NMR spectra in other solvents were referenced internally to the solvent resonance. High-resolution mass spectra were acquired by atmospheric pressure chemical ionization (APCI) or electrospray ionization (ESI) using a time-of-flight mass analyzer on a JEOL MS-T100LC spectrometer with a calibration standard of polyethylene glycol (M_W 2000). Water was deionized with Millipore Milli-Q. Dynamic laser light scattering (DLS) study was carried out on a Malvern Zetasizer Nano ZS machine. Scanning transmission electron microscopy (STEM) observations were performed on a JEOL JEM-2100. Fluorescence spectra were recorded on a HITACHI F-4500 Fluorescence Spectrophotometer.

Materials

Unless otherwise noted, materials were purchased from Tokyo Kasei Co., Aldrich Inc. and other commercial suppliers, and used after appropriate purification before use. Anhydrous ethereal solvents (stabilizer-free) were purchased from WAKO Pure Chemical and purified by a solvent purification system (Glass Contour) equipped with columns of activated alumina and supported copper catalyst (Q-5) prior to use. All other solvents were purified by distillation and stored over 4 Å molecular sieves. The following compounds were synthesized as described in literature: 3-(trimethylsilylethynyl)phenylmagnesium bromide [23] ,[10], 1-methyl-6,9,12,15,18-pentakis(4-trimethylsilylethynylphenyl)-1,6,9,12,15,18-hexahydro(C_{60}-I_h)[5,6]fullerene[10], 17-azido-3,6,9,12,15-pentaoxaheptadecan-1-ol[24]. [60]Fullerene was purchased from Frontier Carbon Co.

Synthesis

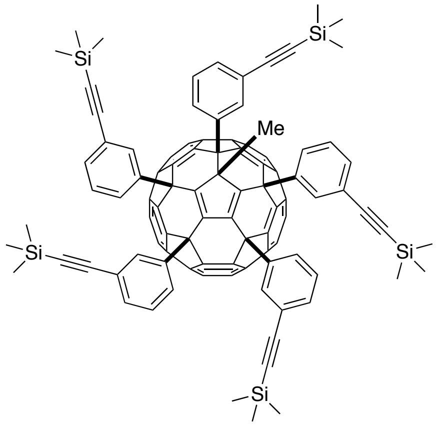

1-Methyl-6,9,12,15,18-Pentakis[3-(trimethylsilylethynyl)phenyl]-1,6,9,12,15,18-hexahydro(C_{60}-I_h)[5,6]fullerene (5)

3-(trimethylsilylethynyl)phenylmagnesium bromide was added to copper(I) bromide dimethylsulfide complex (2.46 g, 12.0 mmol) suspended in THF (6.0 mL) at room temperature. After stirring for 10 min at 35 °C, a solution of [60]fullerene (720 mg, 1.00 mmol) in 1,2-dichlorobenzene (35 mL) was added over 10 min. The reaction mixture was stirred for 2 h, and then was allowed to cool to room temperature followed by addition of methyl iodide (6.2 mL, 100 mmol). After stirring for 17 h, THF and methyl iodide were removed *in vacuo*, and filtered through a pad of silica gel. After evaporation of the solvents, methanol (500 mL) was added for reprecipitation. The resulting solid was collected by filtration followed by washing with acetonitrile (10 mL) to afford the title compound as a reddish solid (1.33g, 82%). mp 217–218 °C; IR (powder): 3064, 2958, 2158, 1598, 1477, 1249, 862, 841, 862, 759, 694 cm^{-1}; ^1H NMR (500 MHz, $CDCl_3$): δ 0.24 (s, 27H), 0.26 (s, 9H), 0.27 (s, 9H), 1.47 (s, 3H). 7.07 (t, J = 7.6 Hz, 1H), 7.27–7.32 (m, 4H), 7.37 (t, J =7.8 Hz, 1H), 7.42–7.46 (m, 4H), 7.54 (s, 2H), 7.68 (d, J = 7.8 Hz, 1H), 7.76 (s, 1H), 7.82 (s, 2H), 7.90 (s, 2H) 7.92 (s, 2H); ^{13}C

NMR (125 MHz, $CDCl_3$): δ 0.12, 0.16, 34.63, 57.83, 57.96, 60.74, 60.88, 62.26, 62.39, 94.81, 95.13, 95.15, 95.20, 95.23, 104.24, 104.53, 104.57, 104.63, 123.22, 124.05, 124.09, 124.27, 124.51, 128.08, 128.30, 128.32, 128.57, 128.61, 128.80, 128.82, 128.98, 129.01, 129.77, 130.86, 131.37, 131.63, 131.73, 131.78, 131.99, 132.09, 132.22, 133.74, 137.84, 138.18, 139.47, 139.54, 142.37, 142.58, 142.98, 143.02, 143.24, 143.69, 143.74, 143.82, 143.85, 144.03, 144.17, 144.25, 144.27, 144.45, 144.48, 144.50, 144.59, 144.71, 144.85, 145.40, 145.44, 145.62, 145.77, 147.24, 147.41, 147.44, 147.49, 147.93, 147.99, 148.29, 148.39, 148.46, 148.55, 148.64, 148.79, 148.83, 148.92, 148.95, 148.97, 151.18, 151.35, 152.56, 152.64, 156.90, 157.19, 159.56, 160.31; HRMS (APCI$^-$) calcd for $C_{116}H_{68}Si_5$ $[M]^-$ 1600.4167, found 1600.4192.

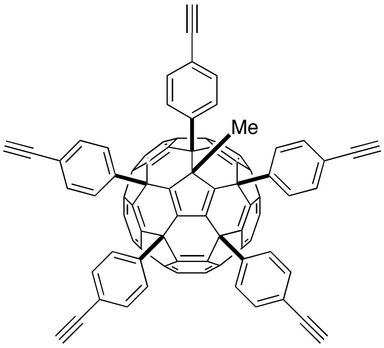

1-Methyl-6,9,12,15,18-penta(4-ethynylphenyl)-1,6,9,12,15,18-hexahydro(C_{60}-*I*$_h$)[5,6]fullerene (6). Acetic acid (92.0 μL, 1.60 mmol) and 1.0 M of *n*-tetrabutylammonium fluoride in THF (1.60 mL, 1.60 mmol) was added to a solution of 1-methyl-6,9,12,15,18-penta[4-(trimethylsilylethynyl)phenyl]-1,6,9,12,15,18-hexahydro(C_{60}-*I*$_h$)[5,6]fullerene (**4**) (250 mg, 0.156 mmol) in dichloromethane (35 mL) at 0 °C, and stirred at room temperature for 1.5 h. The reaction was monitored by TLC (eluent: 30% ethyl acetate/hexane). Methanol (100 mL) was added to the reaction mixture, and the resulting precipitate was filtered through a membrane filter to afford the title compound as an orange solid (178 mg, 92%). mp 350 °C dec.; IR (powder): 3032, 2928, 2863, 2109, 1706, 1502, 1234, 1178, 1018, 839 cm^{-1}; ^{1}H NMR (500 MHz, $CDCl_3$): δ 1.44 (s, 3H), 3.02 (s, 1H), 3.15 (s, 2H), 3.18 (s, 2H), 7.13 (d, *J* = 8.1 Hz, 2H), 7.24 (d, *J* = 8.5 Hz, 2H), 7.47–7.50 (m, 8H), 7.64 (d, *J* = 8.1 Hz, 4H), 7.77 (d, *J* = 8.6 Hz, 4H); ^{13}C NMR (125 MHz, $CDCl_3$): δ 34.59, 58.10, 60.96, 62.40, 62.44, 78.34, 78.50, 78.54, 82.82, 82.91, 83.04, 121.29, 122.03, 122.21, 128.18, 128.83, 129.82, 132.17, 132.65, 132.97, 138.47, 140.08, 142.55, 142.99, 143.05, 143.60, 143.70, 143.90, 144.32, 144.52, 144.55, 144.64, 144.67, 145.31, 145.62, 147.26, 147.31, 147.44, 147.47, 148.01, 148.37, 148.44, 148.55, 148.66, 148.90, 148.94, 149.02, 151.25, 152.54, 156.84, 160.14; HRMS (APCI$^-$) calcd for $C_{101}H_{28}$ [M]$^-$ 1240.2191, found 1240.2208.

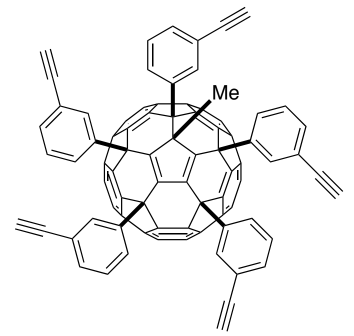

1-Methyl-6,9,12,15,18-Pentakis(3-ethynylphenyl)-1,6,9,12,15,18-hexahydro(C$_{60}$-I_h)[5,6]fullerene (7)

Acetic acid (71.5 μL, 1.25 mmol) and an 1 M solution of tetrabutylammonium fluoride in THF (1.25 mL, 1.25 mmol) were added to a solution of compound **5** (200 mg, 0.125 mmol) in dichloromethane (30 mL) at room temperature under argon atmosphere. After stirring for 2 h, the reaction mixture was concentrated and methanol (50 mL) was added. The resulting precipitate was filtered and purified by silica gel chromatography (eluent: toluene) to afford the title compound as a red solid (153 mg, 98%). mp 264–265 °C; IR (powder): 3065, 2924, 2109, 1597, 1575, 1477, 801 cm^{-1}; ^{1}H NMR (500 MHz, $CDCl_3$): δ 1.46 (s, 3H) 2.99 (s, 1H), 3.05 (s, 3H), 3.08 (s, 1H), 7.09 (t, J = 7.8 Hz, 1H), 7.207.27 (m, 2H), 7.32–7.38 (m, 5H), 7.46–7.50 (m, 4H), 7.66–7.71 (m, 2H), 7.79 (d, J = 8.7 Hz, 1H), 7.81 (d, J = 8.2 Hz, 1H), 7.87 (s, 1H), 7.90 (s, 1H), 7.96 (s, 1H), 7.97 (s, 1H); ^{13}C NMR (100 MHz, $CDCl_3$): δ 34.67, 57.80, 57.84, 60.71, 60.73, 62.18, 62.34, 78.01, 78.10, 78.27, 82.91, 83.20, 83.28, 122.31, 123.10, 123.14, 123.24, 123.41, 128.35, 128.45, 128.54, 128.59, 128.89, 129.06, 129.11, 129.16, 129.25, 129.98, 130.72, 131.67, 131.81, 131.84, 131.91, 132.03, 132.48, 134.30, 138.26, 138.33, 139.64, 139.83, 142.31, 142.62, 142.69, 142.98, 143.05, 143.56, 143.61, 143.71, 143.77, 144.08, 144.21, 144.25, 144.27, 144.44, 144.46, 144.49, 144.56, 144.61, 144.65, 144.76, 145.32, 145.40, 145.54, 147.20, 147.39, 147.42, 147.90, 147.96, 148.29, 148.37, 148.46, 148.51, 148.60, 148.78, 148.82, 148.88, 148.94, 148.96, 151.30, 151.34, 152.40, 152.70, 156.74, 160.12, 160.59; HRMS (APCI$^-$) calcd for $C_{101}H_{28}$ [M]$^-$ 1240.2191, found 1240.2155.

General procedure for the synthesis of CFAs.

17-azido-3,6,9,12,15-pentaoxaheptadecan-1-ol (149 mg, 484 μmol) was added to a mixture of **6** or **7** (100 mg, 80.5 μmol), CuBr•SMe_2 (16.5 mg, 80.5 μmol), and PMDETA (17.0 μL, 80.5 μmol) in DMF (16 mL) at 40 °C and stirred for 24 h. Diethyl ether (50 mL) was added to the crude mixture. The resulting precipitate collected by centrifugation was redissolved in chloroform (10 mL), followed by addition of diethyl ether (50 mL) and acetonitrile (1 mL). The precipitate was collected by centrifugation again to give the desired compounds as red solid.

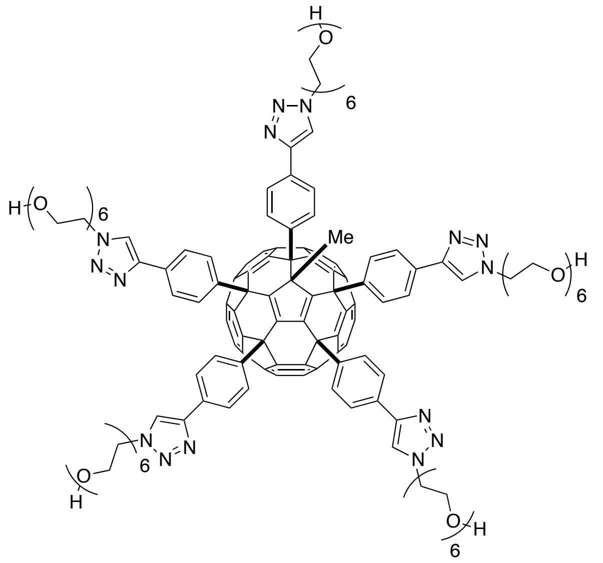

1-Methyl-6,9,12,15,18-Pentakis[4-{1-(17’-hydroxy-3’,6’,9’,12’,15’-hexaoxoheptadecyl)-1,2,3-triazoyl}phenyl]-1,6,9,12,15,18-hexahydro(C_{60}-I_h)[5,6]fullerene (*p*-HEO). 86% yield (193 mg). mp 350 °C dec.; IR (powder): 3422, 3134, 2867, 1667, 1460, 1350, 1231, 1112, 842 cm^{-1}; ^{1}H NMR (500 MHz, $CDCl_3$): δ 1.60 (s, 3H), 2.93-3.00 (br s, 5H), 3.51-3.67 (m, 100H), 3.84 (t, J = 4.9 Hz, 2H), 3.92–3.96 (m, 8H), 4.51 (t, J = 4.9 Hz, 2H), 4.60–4.64 (m, 8H), 7.33 (d, J = 8.0 Hz, 2H), 7.57 (d, J = 8.0 Hz, 2H), 7.85-7.95 (m, 17H), 8.08 (s, 2H), 8.09 (s, 2H); ^{13}C NMR (100 MHz, $CDCl_3$): δ 34.70, 50.44, 58.17, 61.06, 61.70, 62.49, 62.57, 69.49, 69.59, 70.31, 70.58, 72.64, 121.32, 121.58, 121.67, 125.61, 126.15, 126.44, 128.71, 129.23, 129.68, 130.40, 130.55, 130.74, 137.63, 139.31, 142.35, 142.77, 142.95, 143.65, 143.84, 143.98, 144.20, 144.41, 144.47, 144.55, 144.93, 145.56, 145.80, 146.76, 146.97, 147.00, 147.23, 147.42, 147.85, 147.96, 148.28, 148.37, 148.49, 148.60, 148.77, 148.89, 151.85, 152.98, 157.12, 160.47; HRMS (APCI$^+$) calcd for $C_{161}H_{153}N_{15}O_{30}Na^+$ $[M+Na]^+$ 2799.0805, found 2799.0822.

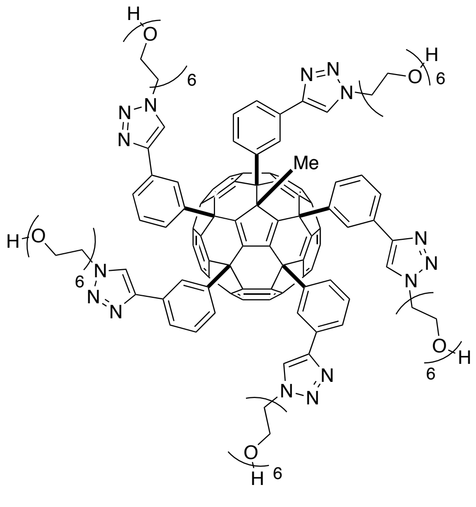

1-Methyl-6,9,12,15,18-Pentakis[3-{1-(17’-hydroxy-3’,6’,9’,12’,15’-hexaoxoheptadecyl)-1,2,3-triazoyl}phenyl]-1,6,9,12,15,18-hexahydro(C_{60}-*I_h*)[5,6]fullerene (*m*-HEO). 84% yield (189 mg). mp 350 °C dec.; IR (powder): 3435, 3132, 2870, 1610, 1456, 1350, 1230, 1113, 944, 797 cm^{-1}; ^{1}H NMR (400 MHz, $CDCl_3$): δ 1.68 (s, 3H), 3.02 (br, 5H), 3.51-3.67 (m, 100H), 3.77-3.80 (m, 2H), 3.88-3.89 (m, 8H), 4.32-4.34 (m, 2H), 4.53-4.54 (m, 8H), 7.12 (s, 1H), 7.18 (t, $J = 8.0$ Hz, 1H), 7.27-7.41 (m, 5H), 7.47 (s, 1H), 7.49 (t, $J = 8.0$ Hz, 1H), 7.55 (s, 2H), 7.70-7.78 (m, 4H), 7.82-7.90 (m, 4H), 7.95-7.98 (m, 2H), 8.09 (s, 1H), 8.16 (s, 1H), 8.33 (s, 2H); ^{13}C NMR (100 MHz, $CDCl_3$): δ 34.87, 50.06, 50.27, 58.19, 58.29, 61.20, 61.17, 61.70, 62.64, 62.66, 69.47, 69.56, 70.34, 70.53, 70.55, 70.59, 72.60, 120.84, 121.32, 121.39, 121.45, 121.79, 124.48, 124.99, 125.26, 125.31, 125.37, 125.84, 127.91, 128.14, 128.24, 129.12, 129.67, 129.73, 129.77, 130.22, 130.83, 131.67, 131.72, 131.95, 132.19, 138.63, 139.07, 140.20, 140.34, 142.29, 142.85, 143.00, 143.07, 143.44, 143.79, 143.92, 143.97, 144.06, 144.15, 144.25, 144.43, 144.51, 144.57, 144.61, 144.89, 145.06, 145.51, 145.75, 145.85, 146.52, 146.55, 146.59, 146.64, 146.81, 147.19, 147.41, 147.46, 147.48, 147.63, 147.87, 147.97, 148.31, 148.36, 148.48, 148.60, 148.63, 148.79, 148.89, 148.93, 151.53, 151.77, 153.01, 153.25, 157.21, 157.50, 159.71, 160.96; HRMS (APCI$^+$) calcd for $C_{161}H_{153}N_{15}O_{30}Na^+$ $[M+Na]^+$ 2799.0805, found 2799.0698.

Determination of CMC by Nile red assay

Nile red assay was conducted following the procedure reported in ref 25. One microliter of Nile red solution in ethanol (2.5 mM) was added to 1 mL of solutions of CFAs in water at various concentrations. The solutions were prepared by dilution of aliquots of 10 mL stock solutions in water. The fluorescence emission was measured using an excitation wavelength of 550 nm. The intensity of the emission was recorded at 635 nm. Maximum emission wavelengths were determined by curve fitting with quadratic functions. CMC values were determined from equilibrium points of the curves.

Interfacial tension measurement

Interfacial tension of CFA solutions was measured by pendant drop method using a Kyowa Interface Science Co., DM-301 instrument. A drop of CFA aqueous solutions with various concentrations (0.1 μM – 10 mM) was prepared on the point of a syringe needle. Interfacial tension was measured by fitting of the outline of the drop with the Young-Laplace theoretical curve. The interfacial tension values were obtained as average of ten measurements.

DLS experiments

Dynamic light scattering (DLS) measurements were performed using a Malvern Zetasizer Nano ZS instrucment equipped with a He-Ne laser operateing at 4 mW power and 633 nm wavelength, and a computer-controlled correlator, at 173° accumulation angle. Measuremnts were carried out in a polystyrene or glass cuvette. Samples were equilibrated for 2 min at 25 °C. The data were processed using Dispersion Technology software version 5.10 to give the particle sizee distribution and average particle sizes. Data were obtained as average of triplicated experiments.

STEM experiments

The STEM measurements were conducted using a JEOL JEM-2100F at 294 K with a spherical aberration coefficient Cs = 1.0 mm at an acceleration voltage of 200 kV under a reduced pressure of 1.0×10^{-5} Pa in the sample column. The current density was ca 0.5 pA cm^{-2}. The imaging instrument used was an ultrascan charge-coupled device (CCD) camera (512 × 512 pixels). Aqueous solution of ***p*****-** or ***m*****-HEO** (0.1 mM, 2 μL) was deposited on a transmission electron microscopy (TEM) copper mesh coated with carbon film (Super Ultra High Resolution Carbon film, thickness < 6 nm; Oken Shoji Co., Ltd.), then dried under reduced pressure at room temperature for 1 h.

SFG spectroscopy

In the SFG experiments an infrared and visible laser beam are overlapped on the sample. The laser pulses originate from an amplified Ti:sapphire laser system (Spitfire Ace, Spectra-Physics) giving 5 W at 800 nm with a repetition rate of 1 kHz and a pulse duration of ~ 40 fs. Part of the laser output is converted into IR light in an optical parametric generation/amplification stage (TOPAS, Light Conversion), resulting in pulses centered at 2800 cm^{-1} with a full width half maximum (FWHM) of 450 cm^{-1}. Another part of the amplifier output was passed through an etalon to obtain visible pulses with a bandwidth of 15 cm^{-1}. The visible and IR beam have a power of 23 and 6 μJ and an angle of incidence with respect to the surface normal around 35 and 40°, respectively. All experiments were performed in a rotating trough to avoid laser induced displacement of the molecules out of the laser focus especially at low concentrations due to heating (*J. Phys. Chem. B* **2012**, *116*, 2703−2712). The fluorescence has been subtracted by collecting data with the IR light blocked. The SFG spectra were measured under SSP (S: SFG, S: vis, P:IR) polarization and normalized to an SFG spectrum taken from z-cut quartz to account for the frequency-dependent IR power. All samples were dissolved in D_2O instead of H_2O, as more IR power can be obtained in the D_2O frequency range allowing a better signal to noise.

The SFG experiments were performed with an amplified Ti:sapphire laser system (Spitfire Ace, Spectra-Physics) delivering pulses of ~40 fs at 800 nm with a repetition rate of 1 kHz and a pulse energy of 5 mJ. Roughly 1.7 W from the laser output was frequency converted in an optical parametric generation/amplification (TOPAS, Light Conversion), resulting in tunable infrared (IR) pulses with a full width at half-maximum bandwidth of around 450 cm^{-1} and a power of ~2 and 6 μJ at a wavelength of 6 and 3.3 μm, respectively. To provide the spectral resolution of the experiment, a narrow-band visible (VIS) upconversion pulse was created by passing 1 mJ of the 800 nm laser output through an etalon, resulting in pulses with a bandwidth of 15 cm^{-1} and an energy of 20 μJ. The reflected SFG light was frequency dispersed in a spectrograph (Acton Instruments) and detected with an electron-multiplied charge coupled device (EMCCD, Andor Technologies). To account for the frequency-dependent IR power, all SFG spectra were normalized to a reference spectrum taken from z-cut quartz. The incident angles with respect to the surface normal of the IR and vis beams were 38° and 32°, respectively. Peak amplitudes and frequencies were obtained.

Molecular modeling

***m*-** and ***p*-Me** were modeled using Maestro, version 9.3, Schödinger, LLC, New York, NY, 2012. and MacroModel, version 9.9, Schödinger, LLC, New York, 2012. Conformational search was conducted using Macromodel program under OPLS_2005 force field in vacuum with a constant dielectric constant of 1.0. Energy minimization was conducted using the PROG method (maximum iteration of 500, convergence on Gradient, convergence threshold of 0.05). For conformational search, Mixed tortional/Low-mode sampling method (Multi-ligand) was selected. The searching condition was set as follows; torsion sampling options: intermediate with retained mirror-image conformations, maximum number of steps: 1000 using 100 steps per rotable bond, energy window for saving structures: 21.0 kJ/mol, elimination of redundant conformers using maximum atom deviation cutoff of 0.5 Å, probability of a torsion rotation/molecule translation: 0.5, minimum distance for low-mode move: 3.0, maximum distance for low-mode move: 6.0.

3.11. References

[1] Myers, D.; Wiley, J. *Surfactant science and technology*; 3rd ed.; Wiley Online Library, 2005, pp118.

[2] Menger, F. M.; Shi, L. *J. Am. Chem. Soc.* **2009**, *131*, 6672–6673.

[3] Höfer, R., Jost, F., Schwuger, M. J., Scharf, R., Geke, J., Kresse, J., Lingmann, H., Veitenhansl, R., Erwied, W. *Foams and Foam Contrrol*, Ulmann's encyclopedia of Industrial Chemistry, Electronic Release, vol 15, Wiley-VCH, Weinheim, 2012.

[4] Carless, J. E.; Chalis, R. A.; Mulley, B. A. *J. Colloid Sci.* **1964**, *19*, 201–212.

[5] Djekic, L.; Primorac, M.; Filipic, S.; Agbaba, D. *Int. J. Pharm.* **2012**, *433*, 25–33.

[6] Edwards, D. A.; Luthy, R. G.; Liu, Z.. *Environ. Sci. Technol.* **1991**, *25*, 127–133.

[7] Nitta, H.; Minami, K.; Harano, K.; Nakamura, E. *Chem. Lett.* in Press.

[8] Chen, T.; Pan, G.-B.; Yan, H.-J.; Wan, L.-J.; Matsuo, Y.; Nakamura, E. *J. Phys. Chem. C* **2010**, *114*, 3170–3174.

[9] Li, P. X.; Li. Z. X.; Shen. H.-H.; Thomas, R. K.; Penfold, J.; Lu, J. R. *Langmuir* **2013**, *29*, 9324–9334.

[10] Zhong, Y.-W.; Matsuo, Y.; Nakamura, E. *J. Am. Chem. Soc.* **2007**, *129*, 3052–3053.

[11] Zhong, Y.-W.; Matsuo, Y.; Nakamura, E. *Org. Lett.* **2006**, *8*, 1463–1466.

[12] Isobe, H.; Cho, K.; Solin, N.; Werz, D. B.; Seeberger, P. H.; Nakamura, E. *Org. Lett.* **2007**, *9*, 4611–4614.

[13] Stuart, M. C. A.; van de Pas, J. C.; Engberts, J. B. F. N. *J. Phys. Org. Chem.* **2005**, *18*, 929–934.

[14] Li, P. X.; Li, Z. X.; Shen, H.-H.; Thomas, R. K.; Penfold, J.; Lu, J. R. *Langmuir* **2013**, *29*, 9324–9334.

[15] Matsumoto, M.; Tachibana, H.; Azumi, R.; Tanaka, M.; Nakamura, T.; Yunome, G.; Abe, M.; Nakamura, E. *Langmuir* **1995**, *11*, 660–665.

[16] Nihonyanagi, S.; Yamaguchi, S.; Tahara, T. *J. Am. Chem. Soc.* **2014**, *136*, 6155–6158.

[17] Shultz, M. J.; Schnitzer, C.; Simonelli, D.; Baldelli, S. *Int. Rev. Phys. Chem.* **2000**, *19*, 123–153.

[18] Sovago, M.; Campen, R.; Wurpel, G.; Müller, M.; Bakker, H.; Bonn, M. *Phys. Rev. Lett.* **2008**, *100*, 173901.

[19] Chen, T.; Pan, G.-B.; Yan, H.-J.; Wan, L.-J.; Matsuo, Y.; Nakamura, E. *J. Phys. Chem. C* **2010**, *114*, 3170–3174.

[20] Labille, J.; Masion, A.; Ziarelli, F.; Rose, J.; Brant, J.; Villiéras, F.; Pelletier, Borschneck, D.; Wiesner, M.R.; Bottero, J. –Y. *Langmuir* **2009**, *25*, 11232–11235.

[21] Ma, X.; Wigington, B.; Bouchard, D. *Langmuir* **2010**, *26*, 11886–11893.

[22] Still, W. C.; Kahn, M.; Mitra, A. *J. Org. Chem.* **1978**, *43*, 2923–2925.

[23] Henze, O.; Lentz, D.; Dieter, S. A. *Chem. –Eur. J.* **2000**, *6*, 2362–2367.

[24] Ngai, M. H.; Yang, P. –Y.; Liu, K.; Shen, Y.; Wenk, M. R.; Yao, S. Q.; Lear, M. J. *Chem. Commun.* **2010**, 46, 8335–8337.

[25] Barnard, A.; Posocco, P.; Pricl, S.; Calderon, M.; Haag, R.; Hwang, M. E.; Shum, V. W. T.; Pack, D. W.; Smith, D. K. *J. Am. Chem. Soc*. **2011**, *133*, 20288–20300.

Chapter 4. Solid dispersion with ionic conical fullerene amphiphiles without interfacial activity

4.1. Introduction

Ionic surfactants such as SDS and CTAB disperse magnetite nanoparticles (MNPs)[1] and carbon nanotubes (CNTs) in water by forming micelles not only in solution but also on the solid surfaces (also called 'hemimicelles') using both hydrophobic and Coulombic interactions.[2,3,4] The micelle formation is competitive with adsorption at air-water interface, and their balance is determined by the alkyl groups and the charged groups of the surfactants. The hydrophobic alkyl groups induce micellization, but at the same time their small surface energy leads to adsorption at air-water interface and reduction of interfacial tension.[5] On the other hand, electrostatic repulsion of ionic groups prohibits micelle formation, but is also known to suppress adsorption at air-water interface.[6,7,8] If we aim at promoting the micelle formation and resulting dispersibility of nanomaterials using the surfactants, we should select a hydrophobic backbone with large surface energy and enough amount of charged groups to suppress adsorption at air-water interface. Based on my finding that introduction of five hydrophilic groups to a conical fullerene framework leads to effective surfactant with low CMC,[9] I envisioned that ionic groups of CFAs should shift the balance to micelle formation by the large surface energy of fullerene[10] and repulsive force of the five charged groups. Interestingly, fullerene has affinity with water, but at the same time has strong tendency to self-assemble.[10,11] Here I show that non-surface activity of ionic CFAs promotes micelle formation and thus leads to effective dispersion of nanomaterials at low concentration of the surfactants. Ionic CFAs have low critical micelle concentration (CMC) of less than 10 μM without adsorption at air-water interface. MNPs were dispersed in water at less than 5 μM, while CTAB required ≥ 500 μM to achieve equivalent dispersibility. CNTs were also dispersed at similarly low concentration, while SDS required ≥ 100 μM for dispersion. Formation of micelle was confirmed on CNTs, which was promoted by low CMC and absence of interfacial activity at air- and oil-water interfaces. The 'mirror charge' effect together with the large surface energy of the fullerene moiety are expected to be the cause of suppressed interfacial activity and effective micelle formation. The property of the ionic CFAs will be applicable for formulation of nanomaterials with a small amount of additives, and without impediment of foaming process, which is impossible to achieve using conventional surfactants.

4.2. Synthesis of ionic CFAs

Ionic CFAs were synthesized by the copper-catalyzed Huisgen cycloaddition with the pentasubstituted fullerene framework **6** bearing the conical structure.[12] The obtained neutral compounds (compounds **8** and **9**, see experimental section) were used for dispersion of solid materials after converting to corresponding salts by addition of 1 M aq. HCl or 10% aq. NH_4OH, followed by condensation *in vacuo*. Cationic CFAs with quaternary ammonium groups (***p*-TMA**), dimethyl ammonium groups (***p*-DMA**), and carboxylate groups (***p*-CA**), and a nonionic congener ***p*-HEO** were used for the study (Figure 4-1). Every compound was well soluble in water (≥ 10 mM or ≥ 28 g/L) to produce a reddish orange-colored clear solution.

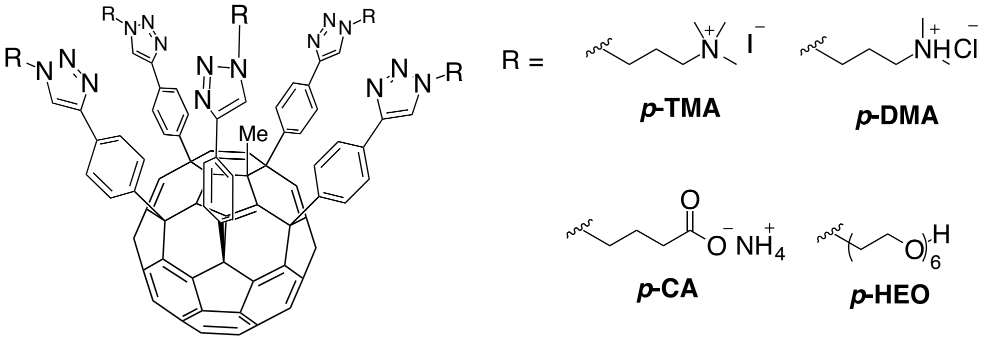

Figure 4-1. Structures of CFAs used for dispersion of solid materials in water.

4.3. Characterization of micelle structures

DLS study of ionic CFAs showed multimodal peaks in pure water (Figure 4-2). This tendency is common between the CFAs regardless of the existence of charge or the size of the hydrophilic groups, which suggests the major contribution of the pentasubstituted fullerene framework on the self-assembly behavior. The multimodal size distribution for the 100 μM solutions indicates that varying nanostructures were formed. STEM images of CFA solutions (100 μM) deposited on a substrate suggests that the smaller particles are micelles (Figure 4-3). The large particles with ≥100 nm are not identified in the STEM images due to instability of the structures compared with the micelles.

Previous reports on cluster formation by a hydrophilic fullerene derivative in water[13] and a liquid-crystalline conical fullerene[14] suggested assembly of more than four molecules in clusters, which also suggests the possibility of a similar structure for the CFAs.

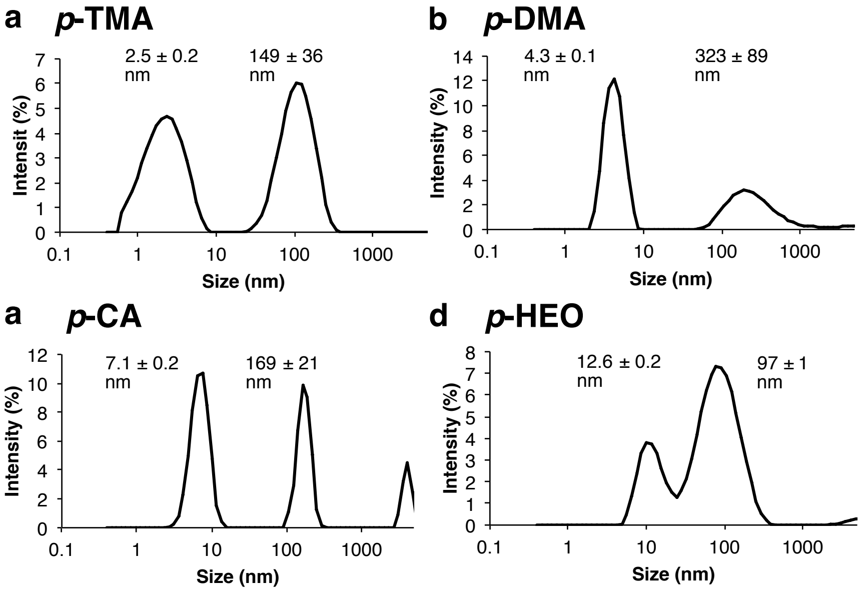

Figure 4-2. DLS of (a-c) ionic CFAs and (d) a nonionic CFA in water, analyzed with CONTIN analysis. The values shown are average sizes corresponding to the peak top.

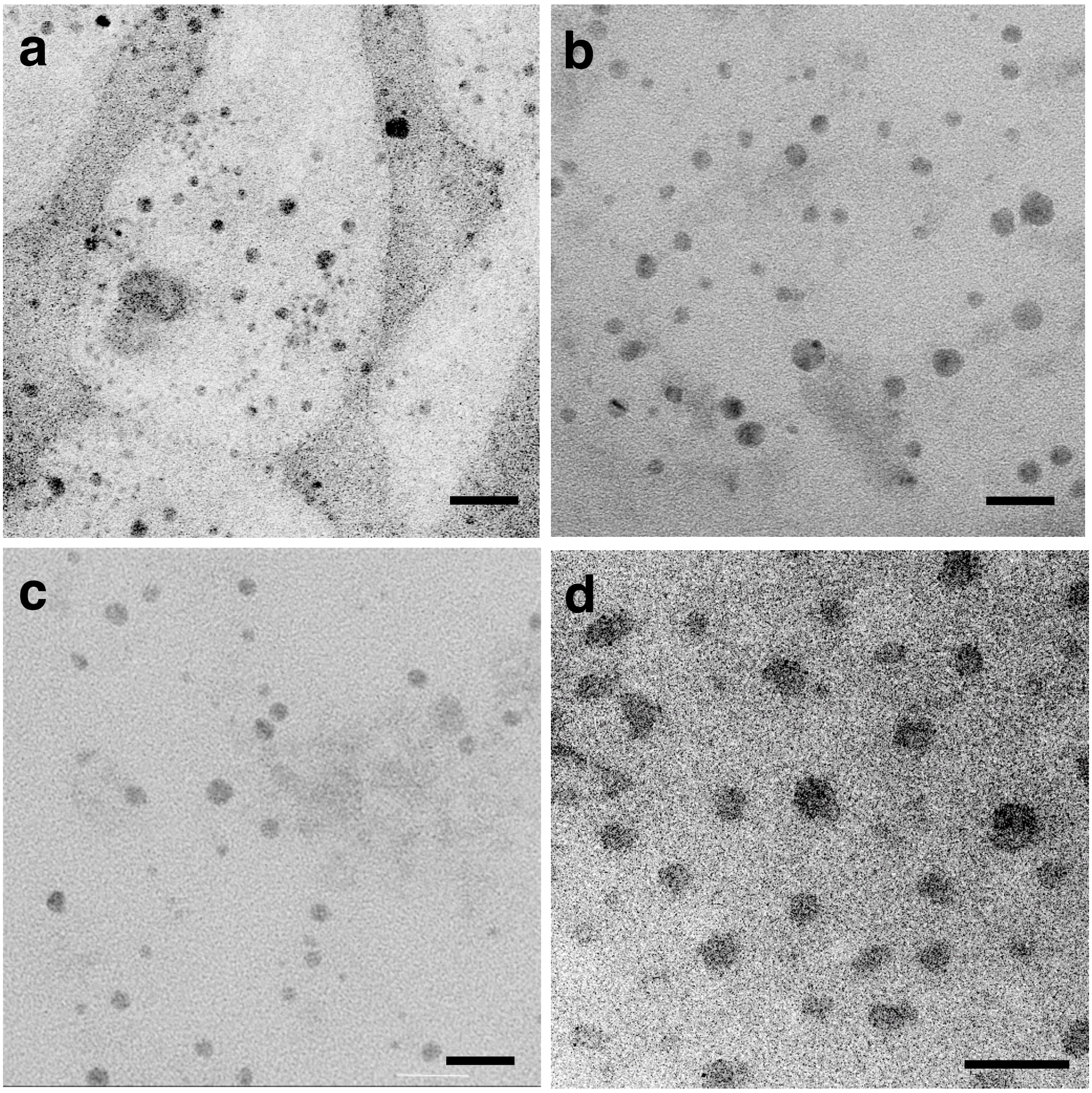

Figure 4-3. STEM images of CFAs on an amorphous carbon film. (a) ***p*-TMA**, (b) ***p*-DMA**, (c) ***p*-CA**, and (d) ***p*-HEO**. Scale bars: 20 nm (a-c) and 200 nm (d).

4.4. Nile red assay and interfacial tension measurement

CMC values of the ionic CFAs were determined by Nile red (NR) assay (Figure 4-4).[15] The blue shift of the maximum emission wavelengths indicates incorporation of NR molecules in the self-assembled structures in water, as discussed for the other CFAs in the previous chapters. The degree of the shift, however, is smaller for the ionic CFAs than ***p*-HEO.** While the hexa(ethyleneoxide) groups of ***p*-HEO** can serve not only as hydrophilic groups but also as hydrophobic shells due to their amphiphilicity, the short propyl linker between the fullerene core and the charged hydrophilic groups may not offer high hydrophobicity. The CMC values of 7.4 ± 2.3 μM (***p*-TMA**), 3.4 ± 0.2 μM (***p*-DMA**), and 2.2 ± 0.4 μM (***p*-CA**) were obtained from equilibrium points of the curves. The values are similar to that of ***p*-hex-DMA** at 3.6 ± 0.5 μM, despite the lack of the hexyl groups between the phenyl and the triazol groups for the newly synthesized ionic CFAs. Note that the CMC values only slightly change in PBS buffer (Figure 4-4e). Notably, the CMCs of the ionic CFAs are lower than ***p*-HEO** despite prevention of self-assembly by electrostatic repulsion. For example, a dodecyl-based surfactant with hexa(ethylene oxide) group, $C_{12}H_{25}(OC_2H_4)_6OH$ has its CMC at 8.7 x 10^{-5} M (20 °C), but its ionic congeners $C_{12}H_{25}N^{+}(CH)_3Br^{-}$ (CMC:1.6 x 10^{-2} M at 25 °C) and $C_{12}H_{25}COO^{-}K^{+}$ (1.2 x 10^{-2} M at 30 °C, pH10.5) have more than 10^3 times larger CMC values due to electrostatic repulsion.[6]

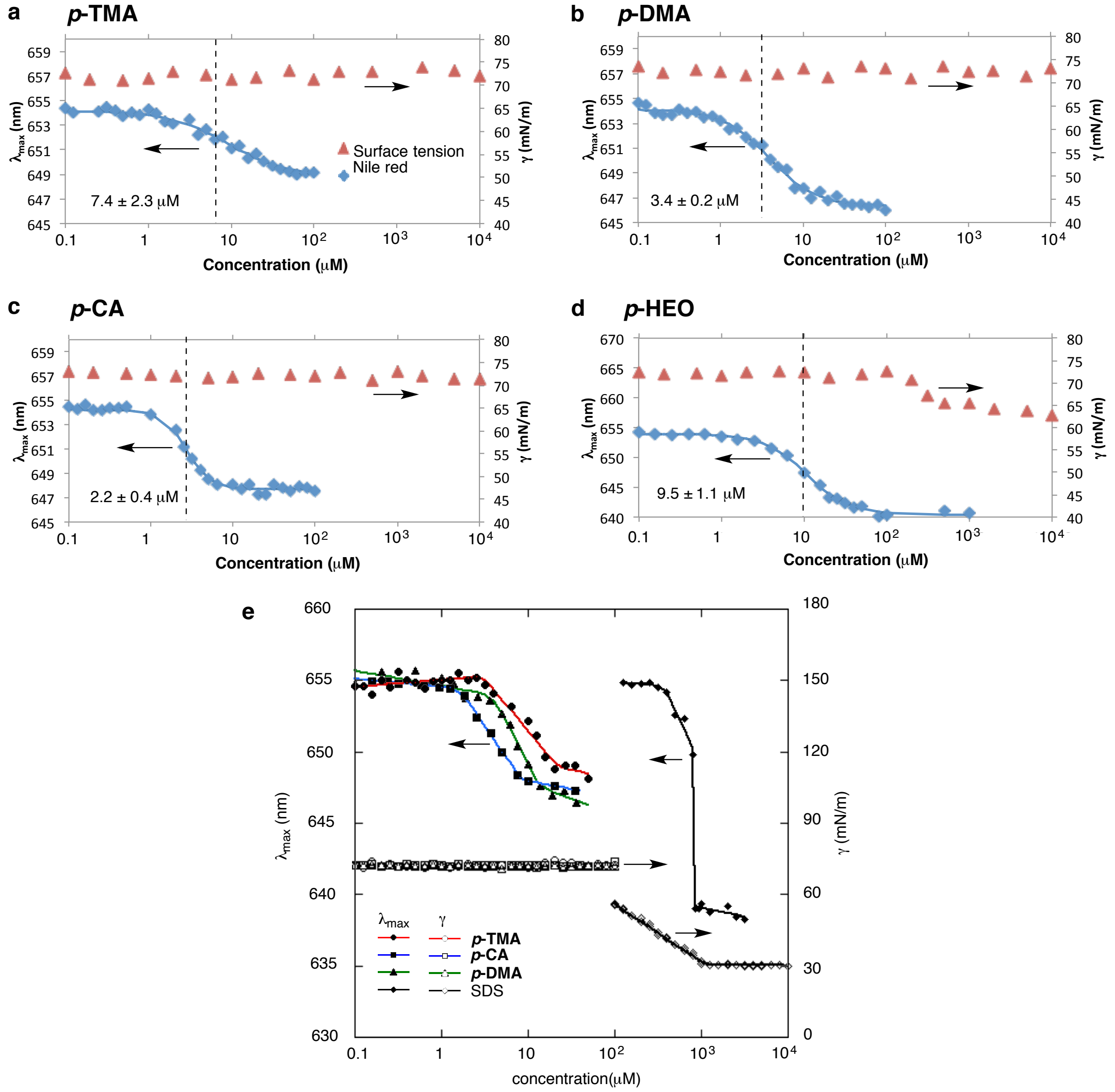

Figure 4-4. Interfacial tension measurement and NR assay of CFAs in water for (a) ***p*-TMA**, (b) ***p*-DMA**, (c) ***p*-CA**, and (d) ***p*-HEO**. (e) Interfacial activity and micelle formation of the ionic CFAs and sodium dodecyl sulfate (SDS) in PBS buffer (pH 7.4).

4.5. Non-interfacial activity

Most notably, ionic CFAs cause neither foaming of an aqueous solution nor lowering of the air-water interfacial tension (pure water; 72.0 ± 0.4 mN/m at 22 °C) up to the limit of solubility of ca. 30 g/L (from 0.1 μM to 10 mM) as shown in Figure 4-5. The interfacial tensions were measured by pendant drop method. On the other hand, ***p*-HEO** lowered the air-water interfacial tension at the concentration of 515 μM. The lack of the air-water interfacial activity is also demonstrated by suppressed foaming for ***p*-TMA** solution after shaking (Figure 4-5a). Similarly to the lack of air-water interfacial activity, the ionic CFAs showed no interfacial activity at oil-water interface either. This is also proven by emulsification experiment of hexane-water mixtures showing that aqueous solutions without any surfactant (colored with methyl orange, MO) and with ***p*-TMA** remained biphasic after homogenization (Figure 4-5c). The interfacial tension of hexane-pure water is 47.6 ± 0.5 mN/m, and a 1.0 mM aqueous solution of ***p*-TMA** showed an essentially the same value of 49.1 ± 0.2 mN/m (Figure 4-5d). ***p*-DMA** and ***p*-CA** slightly decreased the interfacial tension, suggesting that the lower degree of ionization of the tertiary ammonium (pK_a ~10) and the carboxylate (pK_a ~5) than ***p*-TMA**, a quaternary ammonium, results in adsorption of the CFAs to hexane-water interface to some degree. On the contrary, neutral CFA, ***p*-HEO** at 1.0 mM, reduces the hexane-water interfacial tension to half into 25.3 ± 0.2 mN/m. As summarized in Figure 4-5d, the air-water (square), hexane-water (triangle) interfacial tension data, and the CMC data (diamond) are complementary to each other.

Figure 4-5d show complementary relationship between micelle formation and reduction of surface tension. SDS, an alkyl surfactant, has the largest CMC among shown surfactants and a large degree of reduction of interfacial tension ($\Delta\gamma$ ~30 mN/m at air-water interface). In the case of ***p*-HEO**, the CMC decreased to ~1/1000 with a smaller degree of $\Delta\gamma$ (~10 mN/m). $\Delta\gamma$ can be interpreted as decrease in the surface energy when hydrophobic groups face to the air. The reported surface energies of dodecane (the hydrophobic group of SDS) and fullerene are 25.0 mN/m and 41.7 mN/m, which indicates the effectiveness of the large surface energy of fullerene for both suppression of interfacial activity and promotion of micellization.[16,17] The ionic CFAs, having multiple charges, are thus expected to be even more unfavorable for adsorption to the interface, as shown by the negligible $\Delta\gamma$ and among the smallest CMC values.

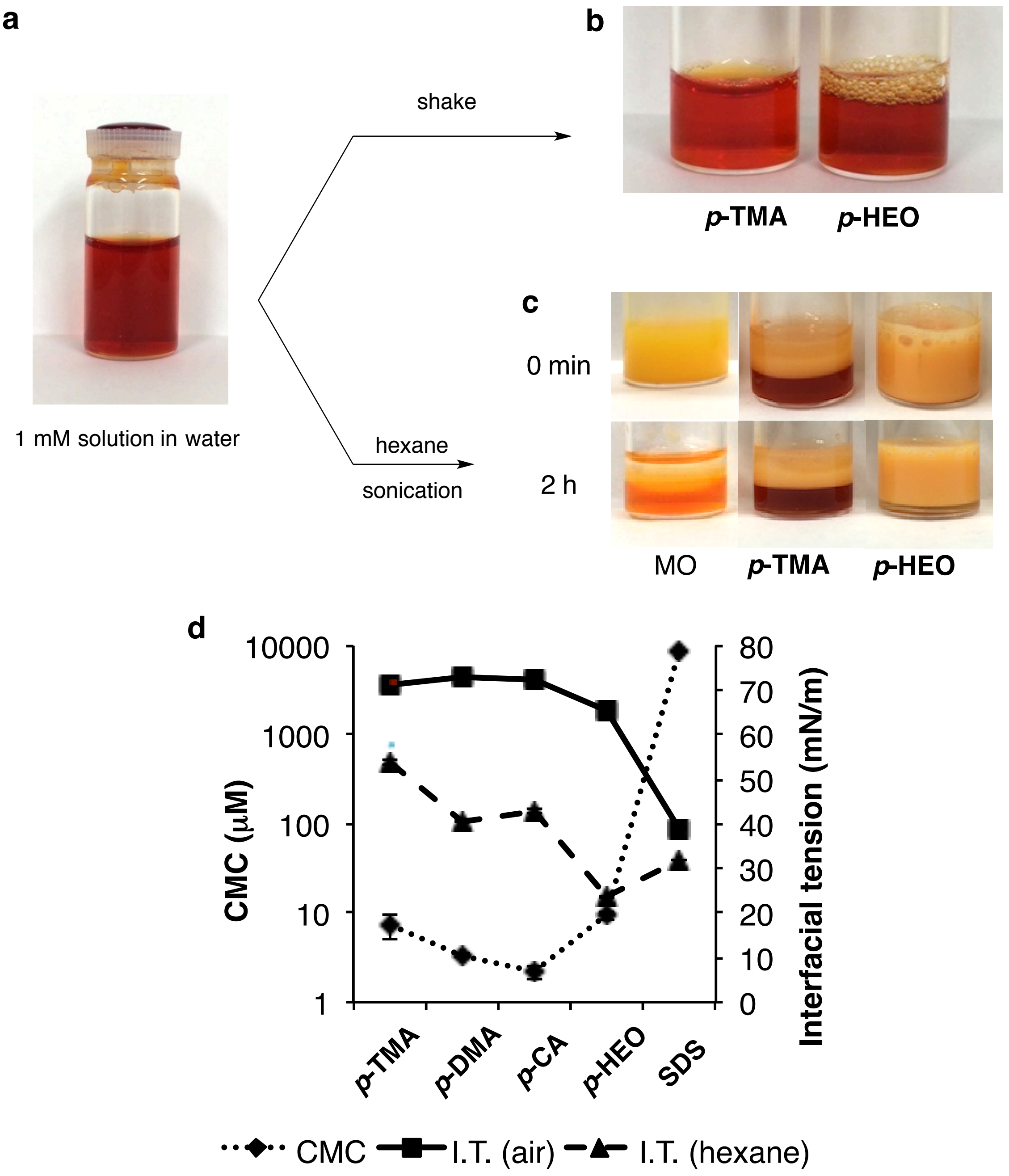

Figure 4-5. Schematic images showing non-surface activity of ionic CFA at air-water and hexane-water interfaces. (a) 1 mM aqueous solution of CFAs (***p*-TMA**). (b) The 1 mM solutions of CFAs after vigorous shaking for 30 s. (c) Mixtures of hexane and aqueous solutions of methyl orange (MO, 0.1 mg/mL), ***p*-TMA** (1 mM), and ***p*-HEO** (1 mM), 0 min and 2 h after shaking for 30 s.

4.6. SFG spectroscopy of air-water interface

The sum frequency generation spectroscopy (SFG) analysis is a method sensitive enough to analyze the topmost layer of a surface and hence provided a proof of the presence and the absence of the Gibbs monolayer of CFAs at air-water interface (Figure 4-6). The SFG spectra of pure D_2O and D_2O solutions of ***p*****-HEO** at 1, 10, and 100 μM solution indicates the formation of a Gibbs monolayer of ***p*****-HEO** and the loss of D_2O layer at the higher concentration. Thus, the 2750 cm^{-1} signal originating from the O-D bond of D_2O perpendicular to water surface disappeared at 100 μM concentration. Instead, a broad CH_2 stretching signal centered at 2870 cm^{-1} appeared, already at 10 μM. In contrast, the spectra of ionic CFAs showed only the O-D signal (2750 cm^{-1}) and even at 100 μM concentration (Figure 4-6b).

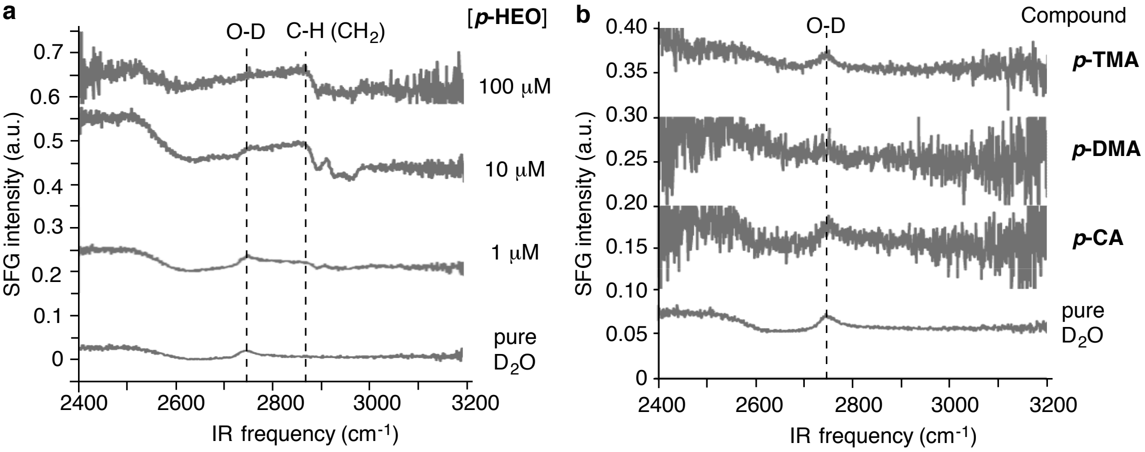

Figure 4-6. SFG spectra of D_2O and different CFA solutions. (a) The spectra of nonionic CFA ***p*****-HEO** at different concentrations. (b) The spectra of ionic CFAs at 100 μM. The low signal-to-noise ratio is attributed to fluorescence from the pentasubstituted [60]fullerene moiety.[18]

4.7. Inhibition of adsorption to air-water interface by mirror charge

The non-interfacial activity of the ionic CFAs can be attributed to 'mirror charges' induced at the interface between hydrophobic fluids and water. The concept originates from classical electromagnetism dealing with electric field originating from a point charge that crosses between an infinite boundary between two phases with different dielectric constants.[6] When a point charge q is placed near the boundary, its electric field induces charges spread at the interface. Although direct calculation of the induced charges is complicated, we can substitute them with a single charge q' at the other side of the boundary. The position of the mirror charge q' is determined so that its electric field is equivalent to the induced charges. Especially at the interface between air and water with dielectric constants of ε_a and ε_w, the relationship between q in water and q' in air is as follows;

$$q' = -\left(\frac{\varepsilon_a - \varepsilon_w}{\varepsilon_a + \varepsilon_w}\right) q \quad \text{(eq. 1)}$$

When $\varepsilon_a = 1$ and $\varepsilon_w = 80$, q' has the same sign as q with its quantity of 98% of q. Therefore, the ions at the interface feel repulsive force from the interface (Figure 4-7a). In fact, the increased surface tension for electrolytic solutions is explained by the mirror charge effect.[19] In the case of ionic surfactants such as SDS and CTAB, the molecules can adsorb at the air-water interface despite the repulsive force, due to the hydrophobic effect that overcomes the increased surface energy by the charge (Figure 4-7c, e).[20] One may expect the effect of counterion to reduce the repulsive force, but they are further from the interface than the amphiphilic ion, and the net force the ions feel should be repulsive.[21] The mirror charge effect on non-surface activity has been discussed only for block copolymers bearing multiple ionic groups, and the ionic CFAs are the first non-surface-active small molecules to our knowledge.[8]

It must be noted that the effect of mirror charges is not always critical for alkyl surfactants (Figure 4-7b,d). The hydrophobic group itself has tendency to adsorb at air-water interface and self-assemble to decrease interface in contact with water. The phenomena known as hydrophobic effect originate from interfacial energy (γ_{12}) between the hydrophobic group (1) and water (2). Therefore, the balance between Coulombic potential of mirror charge and γ_{12} determines the interfacial adsorption. As γ_{12} values for dodecane and fullerene are 52.5 mN/m and 24.0 mN/m, respectively, fullerene has greater affinity with water.[19,20] As a result, the adsorption of fullerene amphiphiles at air-water interface can be more easily prohibited by mirror charges.[17] Moreover, the multiplicity of the charged groups of CFAs amplifies the effect to cause larger repulsive force than monovalent surfactant ions (Figure 4-7c,e).

The influence of mirror charge on micelle formation is also important. Because dielectric constant of hydrocarbons ($\varepsilon \sim 2$)[22] and fullerene ($\varepsilon \sim 4$)[23] are both small, mirror charge should also be large enough to cause repulsion upon micelle formation,[24] which eventually increases CMC of ionic surfactants. The reason why the ionic CFAs have lower CMC than the nonionic CFA despite the charge repulsion can be attributed to the suppressed interfacial activity and resulting shift of equilibrium to micelle formation, as already discussed in chapter 3. In addition, cohesive energy between fullerene, deriving from reorganization of water around the fullerene cluster and dispersion forces of the π-conjugated surfaces, may also contribute to the low CMC of CFAs.[17, 25]

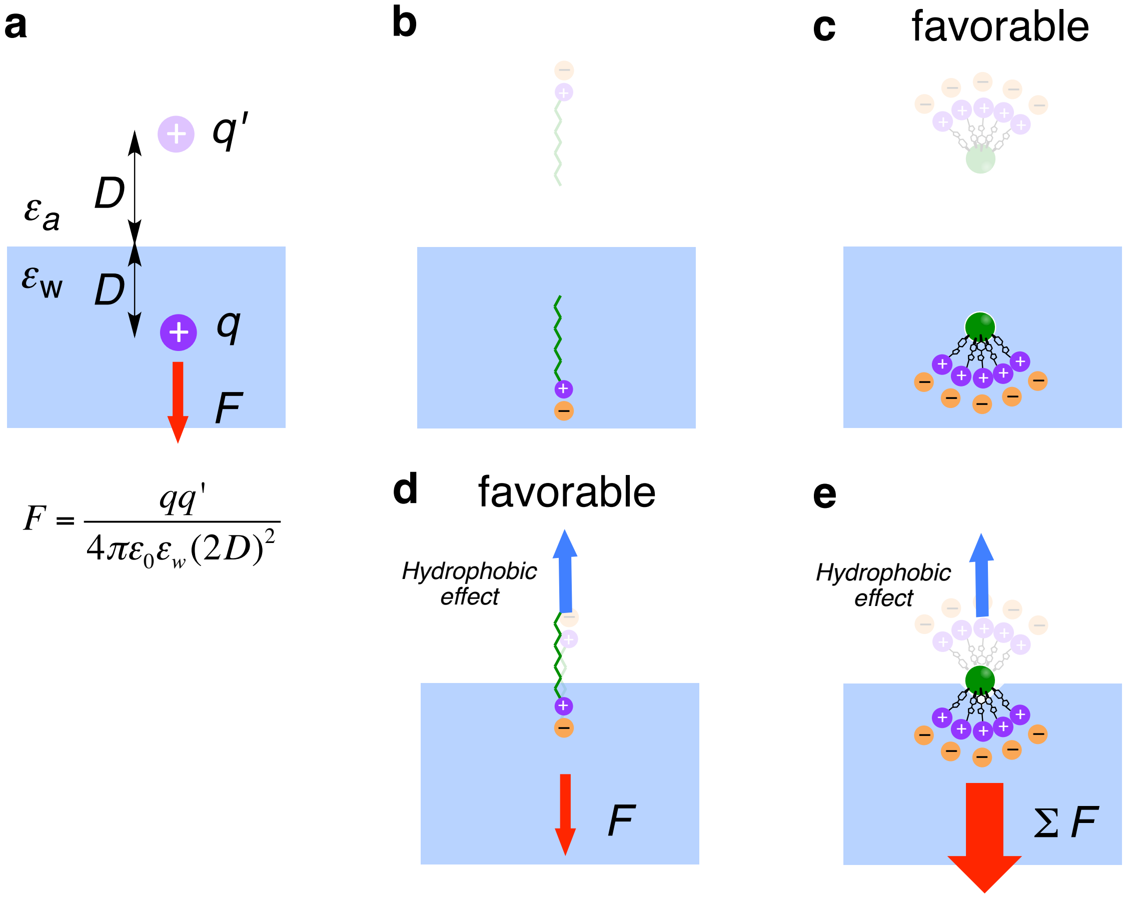

$$F = \frac{qq'}{4\pi\varepsilon_0\varepsilon_w(2D)^2}$$

Figure 4-7. Mirror charge effect of surfactants at air-water interface. (a) Illustration of repulsive force between real charge q and mirror charge q' at air-water interface. (b-e) Illustration of mirror charge when ionic CFAs (b, d) and an alkyl surfactant (c, e) are below (b, c) and at (d, e) the interface.

4.8. Dispersion of magnetite nanoparticles

Magnetite nanoparticles (MNPs) have attracted attention due to their utility in various applications including magnetic fluids, catalyst, bioapplications, etc.[1] Especially for biomedical applications, stable dispersion in water by surface modification is required. Surfactants are often used for modification of MNPs, in addition to fabrication of MNPs from their precursor solutions.[26] I expected that the micelle formation of CFAs on the surface of MNPs should effectively disperse MNPs in water.

A commercially available Fe_3O_4 MNPs (50-100 nm) were dispersed in aqueous solutions of surfactants by probe sonication. At first, dispersibility of MNPs in various surfactants at relatively high concentrations (1 and 10 mM) was screened. As shown in Figure 4-8, dispersion using SDBS, SDS, and Triton X-100 resulted in worse effectiveness. From the result, significance of CMC as well as surface charge is suggested.

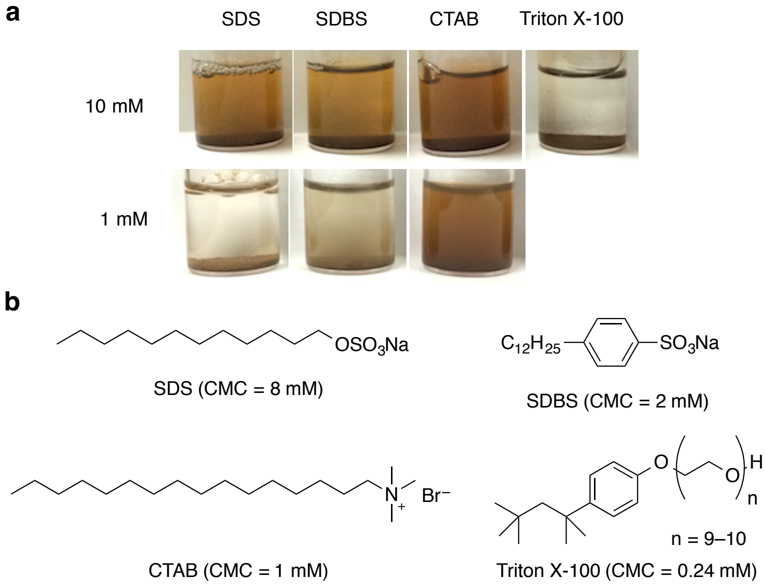

Figure 4-8. Dispersion of MNPs in surfactant solutions. (a) Comparison of dispersibility of MNPs at surfactant concentrations of 10 mM (Pictures are taken 5 h after sonication.) and 1 mM (Pictures are taken 2 h after sonication.) (b) Chemical structures of surfactants.

The stability of the MNP dispersion prepared in ionic CFAs was even better than CTAB. The sonicated dispersions were left stand for 24 h, to confirm dispersion stability. As illustrated in Figure 4-9a, 5-μM aqueous solution of the cationic CFA, ***p*-TMA** disperses MNPs very well, while CTAB is ineffective even at 5 x 10^2 μM due to its higher CMC (ca. 1 mM).[27] Evaluation of dispersions was done for supernatants collected by decantation of the precipitated dispersions. The Z-average sizes of MNPs dispersed with ***p*-TMA** (5 μM) showed a similar value of 110 ± 1 nm compared with

101 ± 0 nm for CTAB (7.5 x 10^2 μM, a concentration where MNPs could be dispersed), with identical unimodal size distribution obtained by CONTIN analysis. Disappearance of peaks observed for pure CFA solutions (Figure 4-2) is indicative for complete adsorption of the CFA molecules to the surface of MNPs. Relative concentration of dispersed MNPs was characterized by optical density of the dispersions (Figure 4-9c).

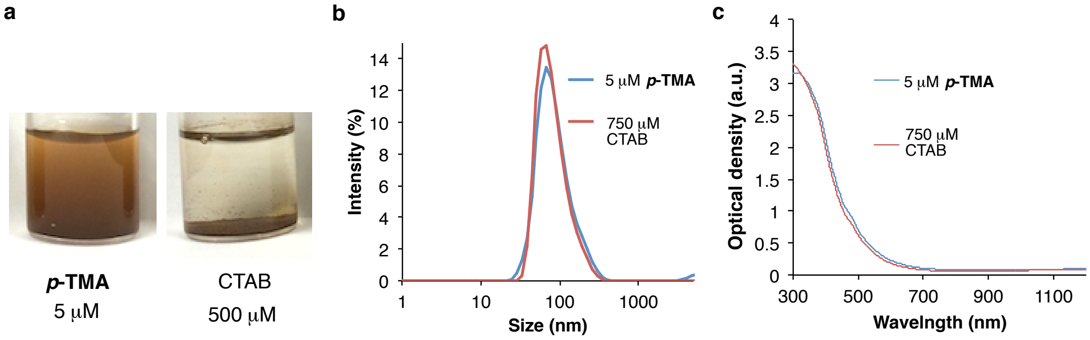

Figure 4-9. Dipsersibility of MNPs in ***p*-TMA** and CTAB solutions in water at low concentrations. (a) Pictures of the samples 24 h after sonication. (b) Size distribution of MNPs dispersed with 5 μM ***p*-TMA** and 7.5 x 10^2 μM CTAB. (c) Absorption spectra of the MNP dispersions.

Figure 4-10 summarizes the correlation between the amounts of the surfactant and MNP dispersed in water determined from optical density recorded at 500 nm. The optical density of MNP dispersions was converted into weight concentration by measuring the weight of the MNPs after condensation of the dispersions. The ionic CFAs disperse MNP at <10 μM concentration, while nonionic CFA, ***p*-HEO** is ineffective, which suggests necessity of charges for interaction with the iron oxide surface.[28] The positive ion of cationic CFAs attracts anionic surface of Fe_3O_4, and carboxylate of anionic CFA, ***p*-CA**, coordinates to iron atoms. The concentration of MNPs in CFA solutions decreases at c ≥ 20 μM due to flocculation caused by bridging of MNPs by excess amount of surfactant molecules.[29]

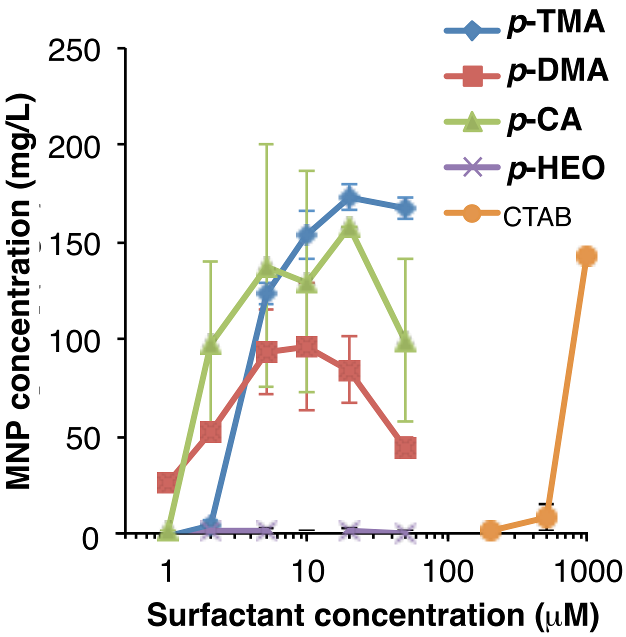

Figure 4-10. Dispersion of MNPs in CFAs and CTAB at low concentrations of surfactants.

4.9. Dispersion of carbon nanotubes

The ionic CFAs also effectively disperse bundled single-walled carbon nanotubes (CNTs). Generally sonication followed by centrifugation is the process for dispersion of CNTs with surfactants, and SDS is the most widely used.[30] A 3-mL aqueous mixture of the CFA (5-50 μM) and bundled CNT powder (1.0 mg, CoMoCAT, Grade S-P95-02-Dry, SouthWest Nanotechnologies)[31] were sonicated with a probe sonicator at an energy level of ~20 W for 5 min at 0 °C, and centrifuged to obtain CNT dispersion as dark liquid (Figure 4-11a). As shown in Figure 4-10b, the ionic CFAs are more effective in dispersing CNT than the others, ***p*-HEO** and SDS, requiring ≥ 20 μM and ≥ 50 μM for effective dispersion. In this case, ***p*-HEO** showed dispersibility unlike for the MNPs because the fullerene core can directly adsorb on the CNT surface via hydrophobic effect,[32] regardless of the charges of the hydrophilic groups. This suggests that adsorption by hydrophobic fullerene moiety and micellization on the solid surface is the driving force for CNTs, unlike MNPs that interact with the hydrophilic groups of CFA hemimicelles formed on the surface.[33] The saturation of dispersibility can be explained by partial precipitation of CNTs in the centrifugation process by flocculation, as reported previously.[34] They dissolve 39 mg/L to 56 mg/L of CNT at a concentration of

50 μM, whereas SDS dissolves only 2.6 mg/L at the same concentration. The lack of fluorescence indicates that the dispersed CNTs are still largely bundled, as TEM only showed bundled CNTs (Figure 4-11c, d).

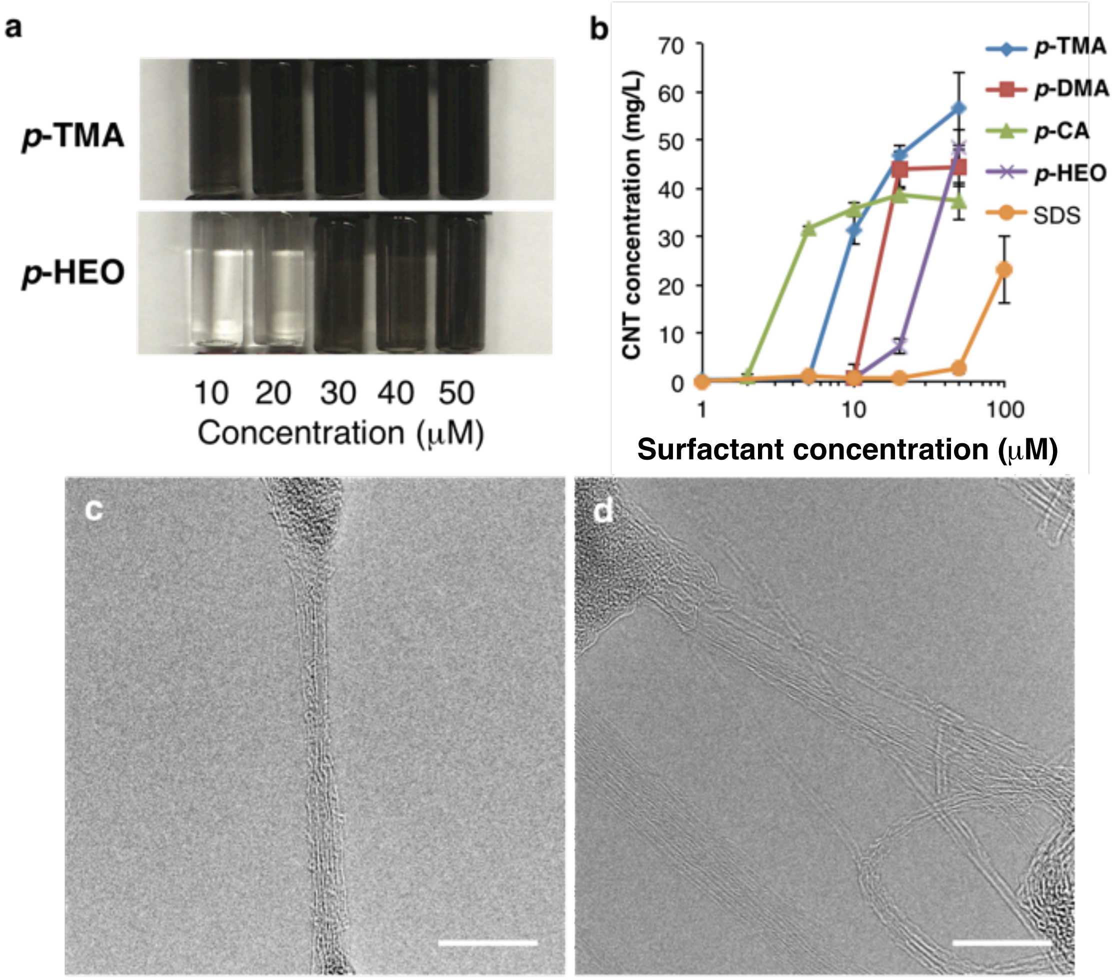

Figure 4-11. Dispersion of nanocarbons with CFAs. (a) Picture of CNT dispersions prepared with ***p*-TMA** and ***p*-HEO**. (b) Concentration of CNT dispersed in aqueous solutions of surfactants. The concentration of dispersed CNT was determined by quantification of the characteristic absorption of CNT at 800 nm. (c, d) TEM images of CNTs dispersed by ***p*-CA**. Scale bars are 10 nm.

4.10. AFM observation of CFA hemimicelles on CNTs

Formation of CFA hemimicelles on CNTs is confirmed by AFM (Figure 4-12). Prolonged sonication time for 2 h under ambient temperature enabled partial dissociation of CNT bundles and subsequent observation of a single tube. Dispersion of

CNTs in ***p*-TMA** solution (5 μM) in water was deposited on a mica substrate followed by removal of excess amount of the solution for AFM observation. The non-uniform adsorption of CFA molecules as shown by the height of 3.1 ± 1.9 nm on CNT (with the thickness of 1.0 ± 0.2 nm) suggest that the CFA molecules, bearing the1-nm sized fullerene core, formed micelles on CNTs.[35] As has been studied in the previous study on adsorption of surfactants on CNTs, the fullerene is expected to be in contact with the CNT surface (Figure 4-12e). The micellization ability of CFAs as well as the interaction between fullerene and CNT contributed to the effective dispersion.

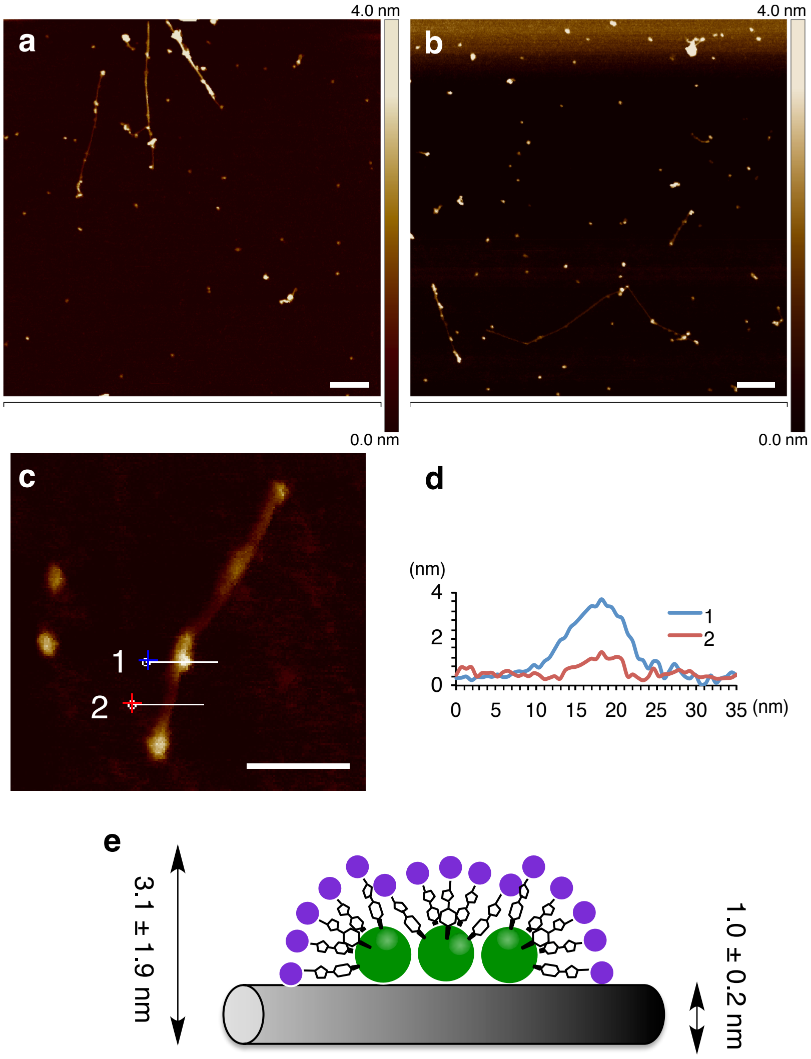

Figure 4-12. AFM image of ***p*-TMA**/CNT. (a, b) CFA-modified CNTs dispersed on mica. (c) Magnified image with (d) height profile. The globular particles in the image are micelles. (e) Illustration of a CNT with a CFA micelle on it. Scale bars are 100 nm (a, b) and 50 nm (c), respectively.

4.11. SEM observation of carbon nanohorns dispersed by ionic CFAs

The ionic CFAs also effectively disperses a 50- to 150-nm sized aggregate of carbon nanohorns (CNHs), a radial aggregate of tapered CNTs.[36] Dispersion of CNHs has also been done using surfactants,[37] in addition to chemical modification.[38] Sonication of CNH powder (3 mg) with CFA (0.1 mM in 3 mL water) at 0 °C for 5 min gave a homogeneous dark dispersion. DLS analysis showed an average diameter of 83 ± 11 nm for the dispersion obtained by every CFA, which fits well with the SEM data. Comparison of the low-landing-voltage SEM images of CFA-dispersed CNHs (Figure 4-13a-c) with the starting CNH sample dispersed in 2-propanol (Figure 4-13d-f) indicates that the surface is covered by clusterized CFA molecules, as shown by the interconnected edges of nanohorns. The size distributions obtained by DLS and SEM matches with each other well, indicating good dispersibility of the modified CNH particles.

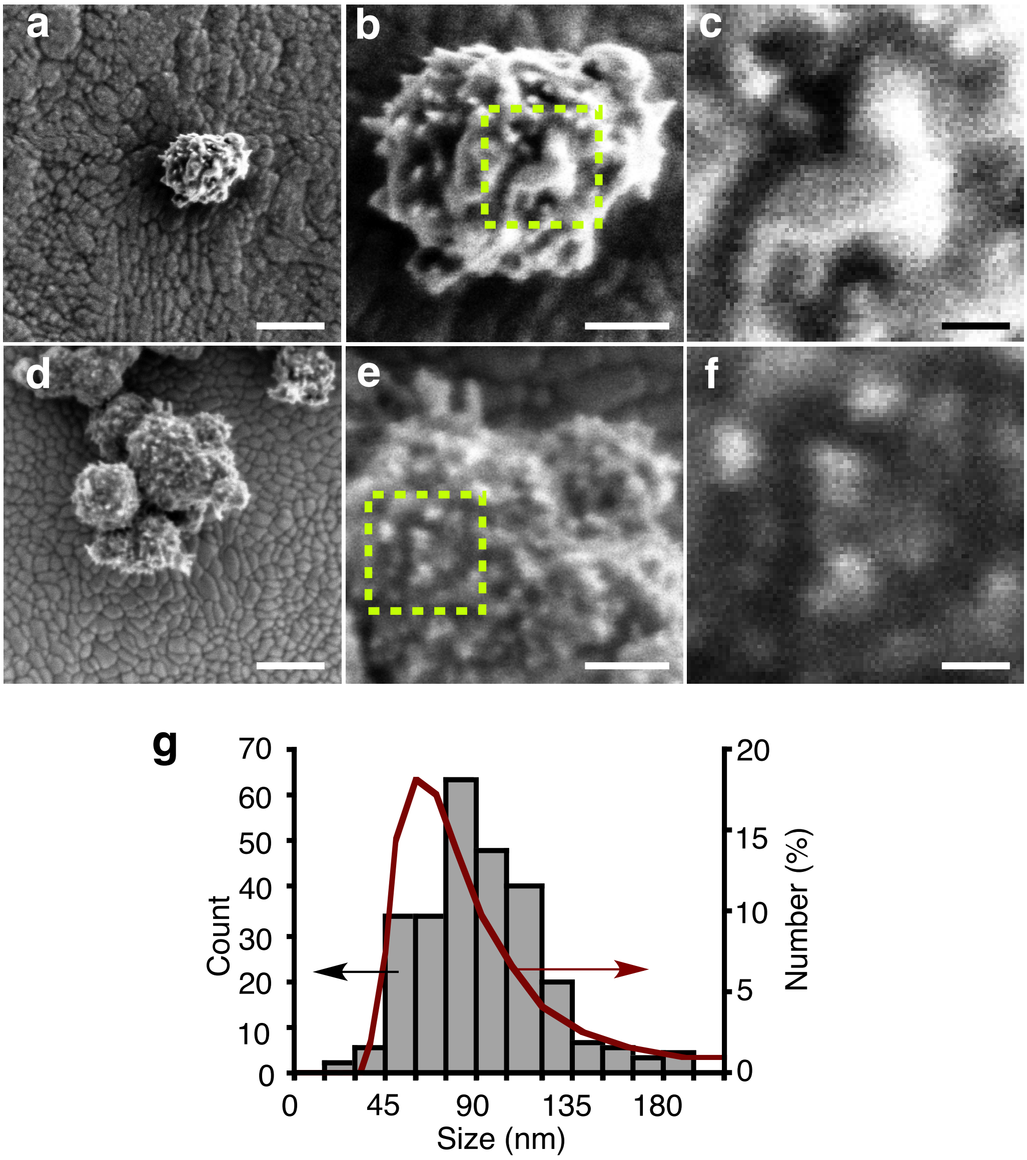

Figure 4-13. (a-c) SEM images of CNH particles coated with ***p*-TMA** prepared from aqueous dispersion. Low-landing-voltage SEM analysis on indium-tin oxide (ITO)/glass) prevents sample charging to allow us achieve < 1 nm resolution.[39] (d-f) CNH particles prepared from dispersion in 2-propanol by deposition onto ITO/glass. Scale bars are 500 nm in c and f, 50 nm in d and g, and 10 nm in e and g, respectively. (g) Comparison between size distributions of CNH particles dispersed with ***p*-TMA** obtained from SEM experiments and DLS experiments.

When the dispersion results and the CMC values are compared, the concentration vs. CNT dispersion ability profile is the same as for MNP, the efficacy suddenly increasing near the CMC value (5-10 μM), and then saturates (without re-precipitation unlike MNP, see above). This profile supports that the solubilization of CNTs by the hemimicelle formation of the fullerene molecules, as shown by the AFM image in Figure 4-13.

4.12. Conclusion

In summary, I have developed ionic CFAs that totally lack interfacial activity at air-water and oil-water interfaces. The suppressed adsorption to the interface enabled to inhibit deterioration of bulk concentration, and thus lead to improved efficiency of micelle and hemimicelle formation. The low CMC values for the CFAs were proved by solubilization of NR molecules in the micelles, which were at ≤ 10 μM, the range of concentration where dispersibility of the solid nanomaterials dramatically increased. Suppression of Gibbs monolayer formation was proved by interfacial tension measurement and SFG spectroscopy. The adsorption to air-water and oil-water interfaces is suppressed by the large surface energy of fullerene and the large electrostatic repulsion with mirror charge owing to the multiple charged groups. The ionic CFAs dispersed MNPs and CNTs in water at low concentration of the surfactants at ≤ 10 μM, which is ~100 times better than CTAB and SDS. Formation of hemimicelles on the surfaces was shown by microscopic analysis. The results demonstrate effectiveness of the strategy to suppress adsorption to air-water interface to selectively enhance functions of surfactants in water. The new surfactant will be useful for solubilization of MNP and other nano-scale solid materials under physiological conditions for in bioimaging, hyperthermia and drug delivery.[40,41,42,43]

4.13. Experimental section

General

All the reactions dealing with air- or moisture-sensitive compounds were carried out in a dry reaction vessel under a positive pressure of nitrogen or argon. The water content of the solvent was confirmed with a Karl-Fischer Moisture Titrator (MKC-210, Kyoto Electronics Company) to be less than 100 ppm. Analysis with high-pressure liquid chromatography (HPLC) was performed on a Shimadzu HPLC system equipped with Buckyprep column (Nakalai Tesque Inc., 4.6 mm ID x 250 mm). Melting points of solid materials were determined on a Mel-Temp capillary melting-point apparatus and were uncorrected. Infrared (IR) spectra were recorded on a JASCO FT/IR-6100 with an attenuated total reflection (ATR) instrument. NMR spectra were measured on JEOL ECX-400 and ECA-500 spectrometers and reported in parts per million from tetramethylsilane. ^{1}H NMR spectra in $CDCl_3$ were referenced internally to tetramethylsilane as a standard. ^{1}H NMR and ^{13}C NMR spectra in other solvents were referenced internally to the solvent resonance. High-resolution mass spectra were acquired by atmospheric pressure chemical ionization (APCI) using a time-of-flight mass analyzer on a JEOL MS-T100LC spectrometer with a calibration standard of polyethylene glycol (M_W 2000) or by electrospray ionization (ESI) using a time-of-flight mass analyser on a Micromass LCT Premier XE mass spectrometer. Water was deionized with Millipore Milli-Q. Dynamic laser light scattering (DLS) study was carried out on a Malvern Zetasizer Nano ZS machine. Atomic force microscopy measurement was performed on a JEOL JSPM-4200 with a silicon cantilever (NSC-35, resonant frequency 120-190 kHz) or Bruker Multimode 8 with a silicon nitride cantilever (SCANASIST-AIR, resonant frequency 70 kHz). Scanning transmission electron microscopy (STEM) observations were performed on a JEOL JEM-2100. Scanning electron microscopy (SEM) was carried out using a FEI Magellan 400L. The UV-Vis-NIR spectra were recorded on a JASCO V-570UV/VIS/NIR Spectrophotometer. Fluorescence spectra were recorded on a HITACHI F-4500 Fluorescence Spectrophotometer.

Materials

Unless otherwise noted, materials were purchased from Tokyo Kasei Co., Aldrich Inc. and other commercial suppliers, and used after appropriate purification before use. Anhydrous ethereal solvents (stabilizer-free) were purchased from WAKO Pure Chemical and purified by a solvent purification system (Glass Contour) equipped with columns of activated alumina and supported copper catalyst (Q-5) prior to use. All other solvents were purified by distillation and stored over 4 Å molecular sieves. The following compounds were synthesized as described in literature: 1-methyl-6,9,12,15,18-pentakis(4-trimethylsilylethynylphenyl)-1,6,9,12,15,18-hexahydro(C_{60}-I_h)[5,6]fullerene[44], 3-azidopropyl-*N*,*N*,*N*-trimethylammonium iodide[45], 3-azidopropyl-

N,*N*-dimethylamine[46], and 4-azidobutyric acid.[47] [60]Fullerene was purchased from Frontier Carbon Co. CoMoCAT® Single-Walled Carbon Nanotubes (SouthWest NanoTechnology, grade S-P95-02-DRY) were purchased from Aldrich Inc. Carbon nanohorn particles were purchased from NEC corporation.

General procedure for the synthesis of CFAs

An organic azide (484 μmol) was added to a mixture of **6** (100 mg, 80.5 μmol), CuBr•SMe$_2$ (16.5 mg, 80.5 μmol), and PMDETA (17.0 μL, 80.5 μmol) in DMF (16 mL) at 40 °C and stirred for 24 h. ***p*-TMA** and compound **9** were reprecipitated by addition of chloroform and ether to the reaction mixture (50 mL) followed by filtration and washing of the precipitates with acetonitrile (1 mL). Compound **8** was purified by the addition of dichloromethane and successive washing of the organic layer with 10% aq. NH$_4$OH, followed by drying on magnesium sulfate and concentration *in vacuo*. All compounds were obtained as red solid. Compounds **8** and **9** were converted to corresponding salts, compounds ***p*-DMA** and ***p*-CA**, for further experiments by dissolving in excess amount of 1 M aq. HCl and 10% aq. NH$_4$OH respectively, followed by removal of the solvents *in vacuo*.

Scheme 4-1. Synthesis of ionic CFAs.

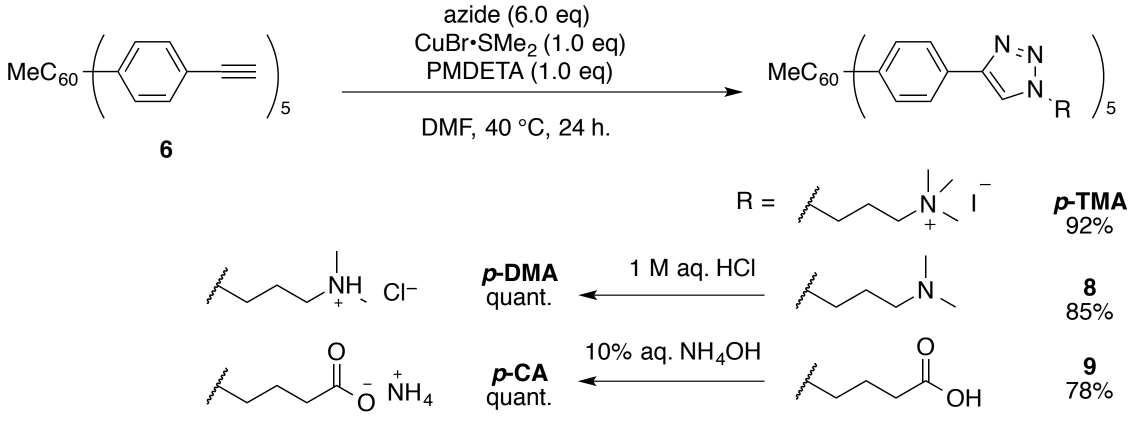

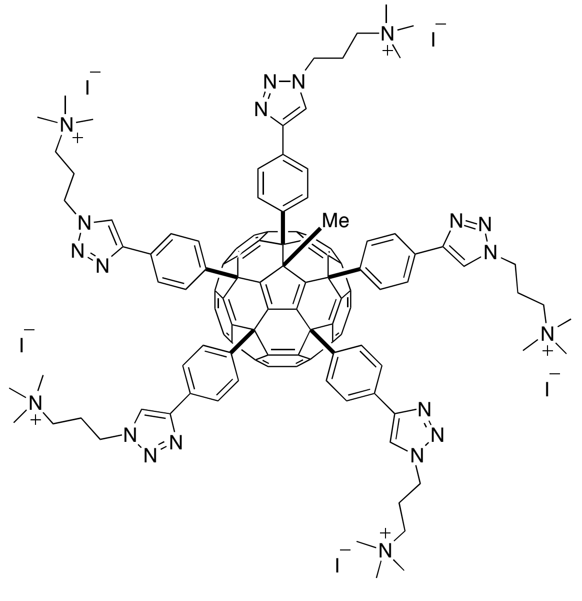

1-Methyl-6,9,12,15,18-Pentakis(4-[1-{3-(*N*,*N*,*N*-trimethylammonio)propyl}-1,2,3-triazoyl]phenyl)-1,6,9,12,15,18-hexahydro(C_{60}-I_h)[5,6]fullerene pentaiodide (*p*-TMA). Purified by addition of acetonitrile (ca. 1 mL) followed by the addition of dichloromethane. 92% yield (192 mg). mp 350 °C dec; IR (powder): 3018, 2948, 1662, 1489, 1227, 1045, 975, 801 cm^{-1}; ^{1}H NMR (500 MHz, DMSO-d_6): δ 1.69 (s, 3H), 2.26–2.31 (m, 2H), 2.36–2.38 (m, 8H), 3.02 (s, 9H), 3.07 (s, 18H), 3.07 (s, 18H), 3.26–3.40 (m, 10H), 4.41 (t, *J* = 6.9 Hz, 2H), 4.49–4.52 (m, 8H), 7.32 (d, *J* = 8.1 Hz, 2H), 7.60 (d, *J* = 8.0 Hz, 2H), 7.90 (d, *J* = 7.8 Hz, 4H), 7.93 (d, *J* = 8.1 Hz, 4H), 8.01–8.05 (m, 8H), 8.59 (s, 1H), 8.74 (s, 2H), 8.77 (s, 2H); ^{13}C NMR (100 MHz, DMSO-d_6): δ 23.19, 23.32, 34.36, 46.78, 52.40, 57.38, 60.56, 61.94, 62.08, 62.58, 122.09, 122.25, 124.95, 125.79, 125.93, 128.45, 128.64, 129.80, 129.98, 130.35, 130.59, 136.51, 138.01, 141.49, 141.72, 142.28, 143.55, 143.64, 143.74, 143.89, 144.17, 144.32, 145.28, 145.36, 145.52, 145.65, 145.68, 146.55, 146.77, 147.30, 147.65, 147.82, 147.93, 148.04, 148.22, 151.82, 148.22, 151.82, 152.63, 156.55, 160.49; HRMS (ESI^{+}) calcd for $C_{131}H_{103}N_{20}^{5+}$ [M]$^{5+}$ 391.3741, found 391.3728.

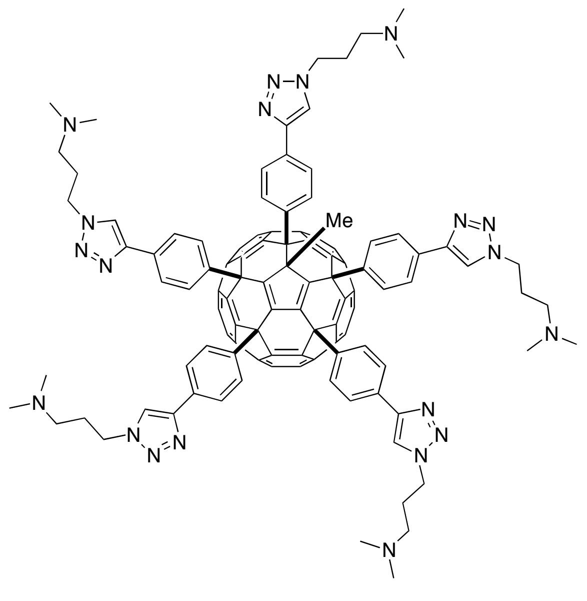

1-Methyl-6,9,12,15,18-Pentakis[4-{1-(3-dimethylaminopropyl)-1,2,3-triazoyl}phenyl]-1,6,9,12,15,18-hexahydro(C_{60}-I_h)[5,6]fullerene (8). Purified by the addition of dichloromethane and successive washing of the organic layer with 10% aq. NH_4OH, followed by drying on magnesium sulfate and concentration *in vacuo*. 85% yield (129 mg). Compound **8** was converted to ***p*-DMA** by addition of 1 M aq. HCl, followed by condensation *in vacuo*. mp 350 °C dec; IR (powder): 3132, 2940, 1663, 1460, 1226,1183, 1042, 974, 844 cm^{-1}; ^{1}H NMR (400 MHz, CD_2Cl_2): δ 1.62 (s, 3H), 1.97 (tt, *J* = 6.7, 7.6 Hz, 2H), 2.06 (tt, *J* = 6.7, 7.6 Hz, 4H), 2.08 (tt, *J* = 6.7, 7.6 Hz, 4H), 2.13 (s, 6H), 2.18 (t, *J* = 7.6 Hz, 2H), 2.19 (s, 12H), 2.20 (s, 12H), 2.27 (t, *J* = 7.6 Hz, 4H), 2.29 (t, *J* = 7.6 Hz, 4H), 4.35 (t, *J* = 6.9 Hz, 2H), 4.45 (t, *J* = 6.7 Hz, 4H), 4.46 (t, *J* = 6.7 Hz, 4H), 7.34 (d, *J* = 8.2 Hz, 2H), 7.56 (d, *J* = 8.2 Hz, 2H), 7.69 (s, 1H) 7.84-7.89 (m, 16H), 7.95 (s, 2H), 7.97 (s, 2H); ^{13}C NMR (100 MHz, CD_2Cl_2): δ 28.45, 28.57, 34.72, 45.41, 45.48, 48.43, 48.54, 56.02, 56.11, 56.14, 58.44, 61.39, 62.80, 62.91, 120.61, 120.86, 120.95, 125.63, 126.27, 126.57, 129.06, 129.51, 130.15, 130.78, 131.05, 131.18, 137.86, 139.54, 142.65, 142.97, 143.18, 144.21, 144.29, 144.43, 144.64, 144.72, 144.77, 145.20, 145.89, 146.15, 146.72, 147.02, 147.46, 147.68, 148.20, 148.48, 148.59, 148.72, 148.83, 148.97, 149.11, 152.20, 153.34, 157.47, 160.89; HRMS (ESI$^+$) calcd for $C_{126}H_{88}N_{20}$ [M+2H]$^{2+}$ 941.3829, found 941.3811.

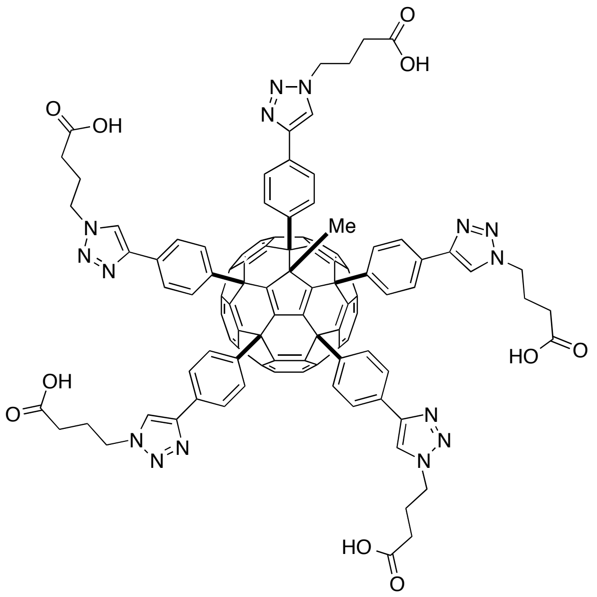

1-Methyl-6,9,12,15,18-Pentakis[4-{1-(3-carboxypropyl)-1,2,3-triazoyl}phenyl]-1,6,9,12,15,18-hexahydro(C_{60}-$\boldsymbol{I_h}$)[5,6]fullerene (9). Purified by addition of acetonitrile (ca. 1 mL) followed by the addition of diethyl ether. 78% yield (118 mg). Compound **9** was converted to ***p*-CA** by addition of 10% aq. NH_4OH, followed by condensation *in vacuo*. mp 350 °C dec; IR (powder): 3134, 3048, 2932, 2615, 1715, 1461, 1226, 1187, 800 cm^{-1}; ^1H NMR (500 MHz, DMSO-d_6): δ 1.61 (s, 3H), 1.97 (tt, J = 6.3, 7.2 ,2H), 2.07 (tt, J = 6.3, 7.2 Hz, 4H), 2.08 (tt, J = 6.3, 7.2 Hz, 4H), 2.16 (t, J = 7.2 Hz, 2H), 2.26 (t, J = 7.2 Hz, 4H), 2.28 (t, J = 7.2 Hz, 4H), 4.31 (t, J = 6.3 Hz, 2H), 4.40 (t, J = 6.3 Hz, 4H), 4.42 (t, J = 6.3 Hz, 4H), 7.26 (d, J = 8.0 Hz, 2H), 7.60 (d, J = 8.0 Hz, 2H), 7.87–7.94 (m, 16H), 8.51 (s, 1H), 8.62 (s, 2H), 8.65 (s, 2H), 12.18 (br s, 5H); ^{13}C NMR (100 MHz, DMSO-d_6): δ 25.07, 25.25, 30.31, 30.45, 30.51, 34.26, 48.95, 57.43, 60.53, 61.92, 62.04, 121.93, 125.02, 125.81, 126.01, 128.43, 128.65, 129.95, 130.55, 130.79, 136.55, 138.10, 141.41, 141.77, 142.23, 143.49, 143.68, 143.79, 143.84, 144.11, 144.26, 145.14, 145.34, 145.41, 145.71, 145.75, 146.39, 146.63, 147.17, 147.52, 147.72, 147.81, 147.90, 148.11, 151.72, 152.52, 156.46, 160.42, 173.61, 173.71, 173.73; HRMS (ESI^-) calcd for $C_{121}H_{62}O_{10}N_{15}^-$ $[M–H]^-$ 1884.4799, found 1884.4888.

DLS experiments

Dynamic light scattering (DLS) measurements were performed using a Malvern Zetasizer Nano ZS instrument equipped with a He-Ne laser operating at 4 mW power and 633 nm wavelength, and a computer-controlled correlator, at 173° accumulation angle. Measurements were carried out in a polystyrene or glass cuvette. Samples were equilibrated for 2 min at the set temperature each time. The data were processed using Dispersion Technology software version 5.10 to give the particle size distribution and average particle sizes. Data were obtained as average of triplicated experiments.

SFG spectroscopy

In the SFG experiments an infrared and visible laser beam are overlapped on the sample. The laser pulses originate from an amplified Ti:sapphire laser system (Spitfire Ace, Spectra-Physics) giving 5 W at 800 nm with a repetition rate of 1 kHz and a pulse duration of ~ 40 fs. Part of the laser output is converted into IR light in an optical parametric generation/amplification stage (TOPAS, Light Conversion), resulting in pulses centered at 2800 cm^{-1} with a full width half maximum (FWHM) of 450 cm^{-1}. Another part of the amplifier output was passed through an etalon to obtain visible pulses with a bandwidth of 15 cm^{-1}. The visible and IR beam have a power of 23 and 6 μJ and an angle of incidence with respect to the surface normal around 35 and 40°, respectively. All experiments were performed in a rotating trough to avoid laser induced displacement of the molecules out of the laser focus especially at low concentrations due to heating (*J. Phys. Chem. B* **2012**, *116*, 2703−2712). The fluorescence has been subtracted by collecting data with the IR light blocked. The SFG spectra were measured under SSP (S: SFG, S: vis, P:IR) polarization and normalized to an SFG spectrum taken from z-cut quartz to account for the frequency-dependent IR power. All samples were dissolved in D_2O instead of H_2O, as more IR power can be obtained in the D_2O frequency range allowing a better signal to noise.

The SFG experiments were performed with an amplified Ti:sapphire laser system (Spitfire Ace, Spectra-Physics) delivering pulses of ~40 fs at 800 nm with a repetition rate of 1 kHz and a pulse energy of 5 mJ. Roughly 1.7 W from the laser output was frequency converted in an optical parametric generation/amplification

(TOPAS, Light Conversion), resulting in tunable infrared (IR) pulses with a full width at half-maximum bandwidth of around 450 cm^{-1} and a power of ~2 and 6 μJ at a wavelength of 6 and 3.3 μm, respectively. To provide the spectral resolution of the experiment, a narrow-band visible (VIS) upconversion pulse was created by passing 1 mJ of the 800 nm laser output through an etalon, resulting in pulses with a bandwidth of 15 cm^{-1} and an energy of 20 μJ. The reflected SFG light was frequency dispersed in a spectrograph (Acton Instruments) and detected with an electron-multiplied charge coupled device (EMCCD, Andor Technologies). To account for the frequency-dependent IR power, all SFG spectra were normalized to a reference spectrum taken from z-cut quartz. The incident angles with respect to the surface normal of the IR and vis beams were 38° and 32°, respectively. Peak amplitudes and frequencies were obtained.

STEM experiment

STEM measurement was conducted on a JEOL JEM-2100F at 294 K with a spherical aberration coefficient Cs = 1.0 mm at an acceleration voltage of 200 kV under reduced pressure of 1.0×10^{-5} Pa in the sample column. The current density was ca. 0.5 pA cm^{-2}. The imaging instrument used was an ultrascan charge-coupled device (CCD) camera (512 x 512 pixels). Aqueous solutions of CFAs (0.1 mM, 2 μL) were deposited on a transmission electron microscopy (TEM) copper mesh coated with carbon film (Super Ultra High Resolution Carbon film, thickness < 6 nm, Oken Shoji Co., Ltd.), then dried under reduced pressure at room temperature for 1 h.

Determination of CMC by Nile red assay

Nile red assay was conducted following the procedure reported in ref 48. 1 μL of Nile red solution in ethanol (2.5 mM) was added to 1 mL of CFA solutions in pure water or PBS buffer at various concentrations. The CFA solutions were prepared by dilution of aliquots of the stock solution in water. The fluorescence emission was measured using an excitation wavelength of 550 nm. Maximum emission wavelengths were determined by curve fitting with quadratic functions. CMC values were determined from equilibrium points.

Dispersion of MNPs

One milligram of MNP (diameter 50-100 nm) was suspended in 3 mL of CFA solutions at varying CFA concentrations with horn sonicator at 20 W power for 5 min at 0 °C. The suspensions were left standing for 24 h before collection of supernatant. The amount of MNPs was estimated by optical density recorded at 500 nm with subtraction of absorption of CFAs as background. Note that the absorption of CFA at the wavelength is negligible. The absorbance was converted to weight using a calibration curve created by weighing residue after evaporation of the suspensions.

Dispersion and analyses of CNTs

CoMoCAT SWNT was used as received. 1 mg of CNT was suspended in 3 mL of aqueous solutions of CFAs at various concentrations by sonication with a probe sonicator at 20W amplitude for 5 min at 0 °C. The dispersion was centrifuged at 200*g* for 5 min to remove undispersed nanotubes. The top ~50 vol% of supernatants were collected for measurements. The nanotube concentration was determined from absorption of the dispersed nanotubes at 800 nm, using a standard curve created for CNT suspension in 2 wt% SDS solutions. AFM measurement was performed by using Multimode 8 with a silicon nitride probe (SCANASIST-AIR, resonant frequency 70 kHz). The suspension of SWCNT in 5 μM aqueous solution of **1** was sonicated for additional 2 h. 2 mL of the dispersion was deposited on mica. After drying the sample by blowing air and then under reduced pressure (5×10^{-2} Pa) for 10 min, the AFM image was obtained by PeakForce Tapping mode measurement.

TEM imaging of CNTs dispersed with CFA

2 μL of the supernatant of CNT dispersion in an aqueous solution of ***p*-CA** (20 μM) was deposited on a copper grid. Excess solution was blotted, and the substrate was dried *in vacuo* for 1 h. TEM images were taken by JEOL JEM-ARM200F at acceleration voltage of 120 kV.

Dispersion and analyses of CNH particles

Three milligrams of CNHs in powder state were dispersed into 3 mL of 0.1 mM solutions of CFAs by bath sonication for 6 h followed by probe sonication (1 W) for 30 min. The solutions were diluted 10 times with pure water for DLS experiments. The size distributions were obtained as average of triplicated experiments. SEM measurement was conducted on a Magellan 400L. An aqueous dispersions of CNH particles (0.1 mL) was placed on an indium-tin oxide (ITO) /glass substrate cleaned by UV/ozone treatment before use, and was spin-coated at 1500 rpm for 30 s. After drying under reduced pressure (5 x 10^{-2} Pa) for 10 min, the ITO substrate was subjected to the SEM observation under a vacuum of 1 x 10^{-5} Pa without any conductive coatings.

4.14. References

[1] Lu, A.-H.; Salabas, E. L.; Schüth, F. *Angew. Chem., Int. Ed.* **2007***, 46*, 1222–1244.

[2] Kam, N. W. S.; O'connell, M.; Wisdom, J. A.; Dai, H. *Proc. Natl. Acad. Sci. U.S.A.* **2005**, *102*, 11600–11605.

[3] Ryu, Y.; Jin, Z.; Lee, J.-J.; Noh, S.-H.; Shin, T.-H.; Jo, S.-M.; Choi, J.; Park, H.; Cheon, J.; Kim, H.-S. *Angew. Chem., Int. Ed. in press*, doi:10.1002/anie.201408593

[4] Park, H.; Afzali, A.; Han, S.-J.; Tulevski, G. S.; Franklin, A. D.; Tersoff, J.; Hannon, J. B.; Haensch, W. *Nat. Nanotech*. **2012**, *7*, 787–791.

[5] Biscay, F.; Ghoufi, A.; Goujon, F.; Lachet, V.; Malfreyt, P. *J. Phys. Chem. B* **2008**, *112*, 13885–13897.

[6] Rosen, M. J.; Chapter 3. Micelle Formation by Surfactants ; *Surfactant and Interfacial Phenomena*, 3rd ed.; 2004, pp 105–177.

[7] Jackson, J. D. Classical Electrodynamics, 3rd ed. Chapter 4. Multipoles, Electrostatics of Macroscopic Media, Dielectrics. John Wiley & Sons, Inc., New York, 1999, pp111-112.

[8] a) Ghosh, A.; Yusa, S.-I.; Matsuoka, H.; Saruwatari, Y. *Langmuir* **2011**, *27*, 9237–9244. b) Matsuoka, H.; Maeda, S.; Kaewsaiha, P.; Matsumoto, K. *Langmuir* **2004**, *20*, 7412–7421. c) Matsuoka, H.; Chen, H.; Matsumoto, K. *Soft Matter* **2012**, *8*, 9140–9146.

[9] Nitta, H.; Harano, K.; Nakamura, E. *Chem. Lett.* in press.

[10] Labille, J.; Masion, A.; Ziarelli, F.; Rose, J.; Brant, J.; Villiéras, F.; Pelletier, Borschneck, D.; Wiesner, M.R.; Bottero, J. –Y. *Langmuir* **2009**, *25*, 11232–11235.

[11] Isobe, H.; Homma, T.; Nakamura, E. *Proc. Natl. Acad. Sci. U.S.A.* **2007**, *104*, 14895–14898.

[12] a) Isobe, H.; Cho, K.; Solin, N.; Wertz, D. B.; Seeberger, P. H. Nakamura, E. *Org. Lett.* **2007**, *9*, 4611-4614. b) Alvaro, M.; Atienzar, P.; de la Cruz, P.; Delgado, J. L.; Troiani, V.; Garcia, H.; Langa, F.; Palkar, A.; Echegoyen, L. *J. Am. Chem. Soc.* **2006**, *128*, 6626–6635.

[13] Guldi, D. M.; Hungerbühler, H.; Asmus, K. D. *J. Phys. Chem.* **1995**, *99*, 13487–13493.

[14] Li, C.-Z.; Matsuo, Y.; Nakamura, E. *J. Am. Chem. Soc.* **2010**, *132*, 15514-15515.

[15] Stuart, M. C. A.; van de Pas, J. C.; Engberts, J. B. F. N. *J. Phys. Org. Chem.* **2005**, *18*, 929–934.

[16] Binks, B. P.; Clint, J. H. *Langmuir* **2002**, *18*, 1270–1273.

[17] Ma, X.; Wigington, B.; Bouchard, D. *Langmuir* **2010**, *26*, 11886–11893.

[18] Guldi, D. M.; Rahman, G. M. A.; Marczak, R.; Matsuo, Y.; Yamanaka, M.; Nakamura, E. *J. Am. Chem. Soc*. **2006**, *128*, 9420–9427.

[19] Jacob N. Israelachivili, Intermolecular nad Surface Forces, 3rd ed. Elsevier, Burlington, MA, 2011.

[20] Eastoe, J.; Dalton, J. S. *Adv. Colloid Interface Sci.* **2000**, *85*, 103–144.

[21] Nihonyanagi, S.; Yamaguchi, S.; Tahara, T. *J. Am. Chem. Soc.* **2014**, *136*, 6155–6158.

[22] Sen, A. D.; Anicich, V. G.; Arakelian, T. *J. Phys. D: Appl. Phys.* **1992**, *25*, 516–521.

[23] Pevzner, B.; Hebard, A. F.; Dresselhaus, A. S. *Phys. Rev. B* **1997**, *55*, 16439–16449.

[24] Stigter, D. *J. Phys. Chem.* **1974**, *78*, 2480–2485.

[25] Li, Y.; Reeve, J.; Wang, Y.; Thomas, R. K.; Wang, J.; Yan, H. *J. Phys. Chem. B* **2005**, *109*, 16070–16074.

[26] Shen, L.; Laibinis, P. E.; Hatton, T. A.; *Langmuir* **1999**, *15*, 447–453.

[27] Zhao, X.; Shi, Y.; Cai, Y.; Mou, S. *Environ. Sci. Technol*. **2008**, *42*, 1201–1206.

[28] Laurent, S.; Forge, D.; Port, M.; Roch, A.; Robic, C.; Vander Elst, L.; Muller, R. N. *Chem. Rev.* **2008**, *108*, 2064–2110.

[29] Rosen, M. J.; Chapter 9. Dispersion of Solids and Liquids in Liquid Media by Surfactants; *Surfactant and Interfacial Phenomena*, 3rd ed.; 2004, pp 332–352.

[30] Liu, H.; Nishide, D.; Tanaka, T.; Kataura, H. *Nat. Commun*. **2011**, *2*, doi: 10.1038/ncomms1313.

[31] Resasco, D. E.; Alvarez, W. E.; Pompeo, F.; Balzano, L.; Herrera, J. E.; Kitiyanan, B.; Borgna, A. *J. Nanopart. Res.* **2002**, *4*, 131–136.

[32] Matarredona, O.; Rhoads, H.; Li, Z.; Harwell, J. H.; Balzano, L.; Resasco, D. E. *J. Phys. Chem. B* **2003**, *107*, 13357–13367.

[33] Harano, K.; Takenaga, S.; Okada, S.; Niimi, Y. *J. Am. Chem. Soc.* **2014***, 136, 466–473.*

[34] Rastogi, R.; Kaushal, R.; Tripathi, S. K.; Sharma, A. L.; Kaur, I.; Bharadwaj, L. M. *J. Colloid Interf. Sci.* **2008**, *328*, 421–428.

[35] Carilli, C. L. *Science* **2003**, *300*, 773–775.

[36] a) Iijima, S.; Yudasaka, M.; Yamada, R.; Bandow, S.; Suenaga, K.; Kokai, F.; Takahashi, K. *Chemical Physics Letters* **1999**, *309*, 165. b) Richard, C.; Balavoine, F.; Schultz, P.; Ebbesen, T. W.; Mioskowski, C. *Science* **2003**, *300*, 775–778. c) Isobe, H.; Tanaka, T.; Maeda, R.; Noiri, E.; Solin, N.; Yudasaka, M.; Iijima, S.; Nakamura, E. *Angew. Chem., Int. Ed.* **2006**, *45*, 6676.

[37] Xu, J.; Iijima, S.; Yudasaka, M. *Appl. Phys. A* **2010**, *99*, 15–21.

[38] a) Harano, K.; Homma, T.; Niimi, Y.; Koshino, M.; Suenaga, K.; Leibler, L.; Nakamura, E. *Nat. Mater.* **2012**, *11*, 877–881. b) Nakamura, E.; Koshino, M.; Tanaka, T.; Niimi, Y.; Harano, K.; Nakamura, Y.; Isobe, H. *J. Am. Chem. Soc.* **2008**, *130*, 7808–7809.

[39] Harano, K.; Minami, K.; Noiri, E.; Okamoto, E.; Nakamura, E. *Chem. Commun*. **2013**, *49*, 3525–3527.

[40] Rosen, B. M.; Wilson, C. J.; Wilson, D. A.; Peterca, M.; Imam, M. R.; Percec, V. *Chem. Rev*. **2009**, *109*, 6275–6540.

[41] Schade, B.; Ludwig, K.; Böttcher, C.; Hartnagel, U.; Hirsch, A. *Angew. Chem., Int. Ed*. **2007**, *46*, 4393–4396.

[42] Zhang, G.; Liu, Y.; Liang, D.; Gan, L.; Li, Y. *Angew. Chem., Int. Ed*. **2010**, *49*, 5293–5295.

[43] a) Maeda-Mamiya, R.; Noiri, E.; Isobe, H.; Nakanishi, W.; Okamoto, K.; Doi, K.; Sugaya, T.; Homma, T.; Nakamura, E. *Prac. Natl. Acad. Sci. U.S.A.* **2010**, *107*, 5339–5344. b) Isobe, H.; Nakanishi, W.; Tomita, N.; Jinno, S.; Okayama, H.; Nakamura, E. *Chem. Asian J.* **2006**, *1*, 167–175. c) Minami, K.; Okamoto, K.; Doi, K.; Harano, K.; Noiri, E.; Nakamura, E. *Sci. Rep*. **2014**, *4*, 4916.

[44] Zhong, Y. –W.; Matsuo, Y.; Nakamura, E. *J. Am. Chem. Soc.* **2007**, *129*, 3052–3053.

[45] Engler, A. C.; Shukla, A.; Puranam, S.; Buss, H. G.; Jreige, N.; Hammond, P. T.; *Biomacromolecules* **2011**, *12*, 1666–1674.

[46] Engler, A. C.; Bonner, D. K.; Buss, H. G.; Cheung, E. Y. Hammond, P. T. *Soft Matter* **2011**, *7*, 5627–5637.

[47] Reux, B.; Weber, V.; Galmier, M. –J.; Borel, M. Madesclaire, M.; Madelmont, J. –C. Debiton, E.; Coudert, P. *Bioorg. Med. Chem.* **2008**, *16*, 5004–5020.

[48] Barnard, A.; Posocco, P.; Pricl, S.; Calderon, M.; Haag, R.; Hwang, M. E.; Shum, V. W. T.; Pack, D. W.; Smith, D. K. *J. Am. Chem. Soc*. **2011**, *133*, 20288–20300.

Chapter 5. Summary and outlook

In chapter 2, I have shown a synthesis of an ***p*-hex-DMA** by modular assembly of a pentaorganofullerene and an amine group via click cycloaddition chemistry, and found that ***p*-hex-DMA** forms a stable micelle in water and in a buffer at low CMC (Figure 5-1). The micelle of ***p*-hex-DMA** tolerates a considerably wide range of pH and forms a structurally defined stable complex with DNA in a buffer solution. The N/P ratio =1 needed for efficient DNA compaction is expected to render this new aminofullerene a transfection agent with minimum side effects.

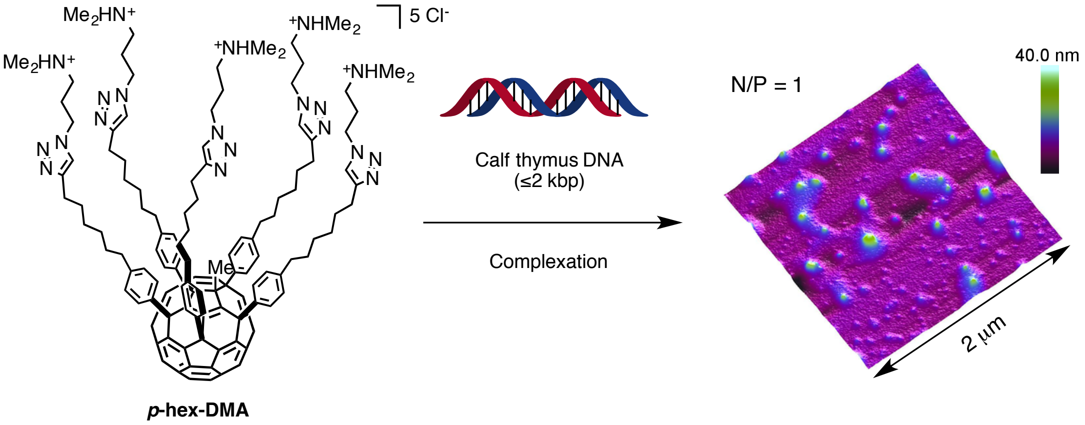

Figure 5-1. Complexation between ***p*-hex-DMA** and calf thymus DNA resulting in formation of spherical particles.

In chapter 3, I have shown that the framework structure of ***p*-HEO** enables suppression of interfacial activity at air-water interface and enhanced micelle formation ability compared with ***m*-HEO** (Figure 5-2). The expanded configuration with pseudo-C_5 symmetry for ***p*-HEO** prohibits of packing of the CFA framework at air-water interface, which made it possible to form micelles without reducing interfacial tension.

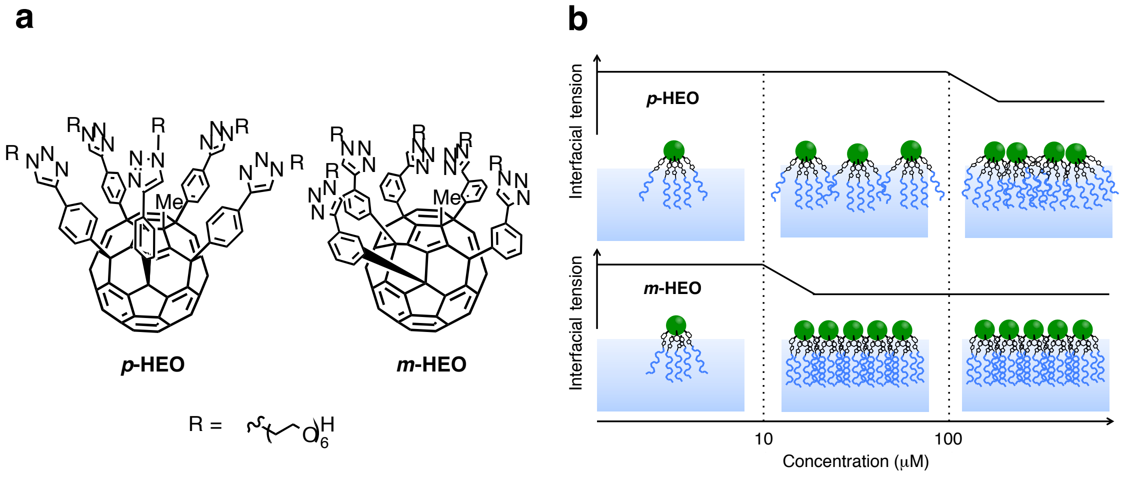
a
b
p-HEO
m-HEO
Me
R =
6
Interfacial tension
Interfacial tension
p-HEO
m-HEO
10
100
Concentration (μM)

Figure 5-2. Retarded interfacial activity of nonionic CFA at air-water interface. (a) chemical structures of ***p*-HEO** and ***m*-HEO**. (b) Change of Gibbs monolayer with increased bulk concentration.

In chapter 4, I have shown the development of ionic CFAs that totally lack interfacial activity at air-water interface, and their applicability as dispersion agents (Figure 5-3). The adsorption to the interface was suppressed owing to the existence of the fullerene moiety and the multiple charges. The low CMC at ≤ 10 μM was expected to contribute to effective dispersion of MNPs and CNTs in water at low concentration of the surfactants at ≤ 10 μM, which is ~100 times better than a conventional surfactant.

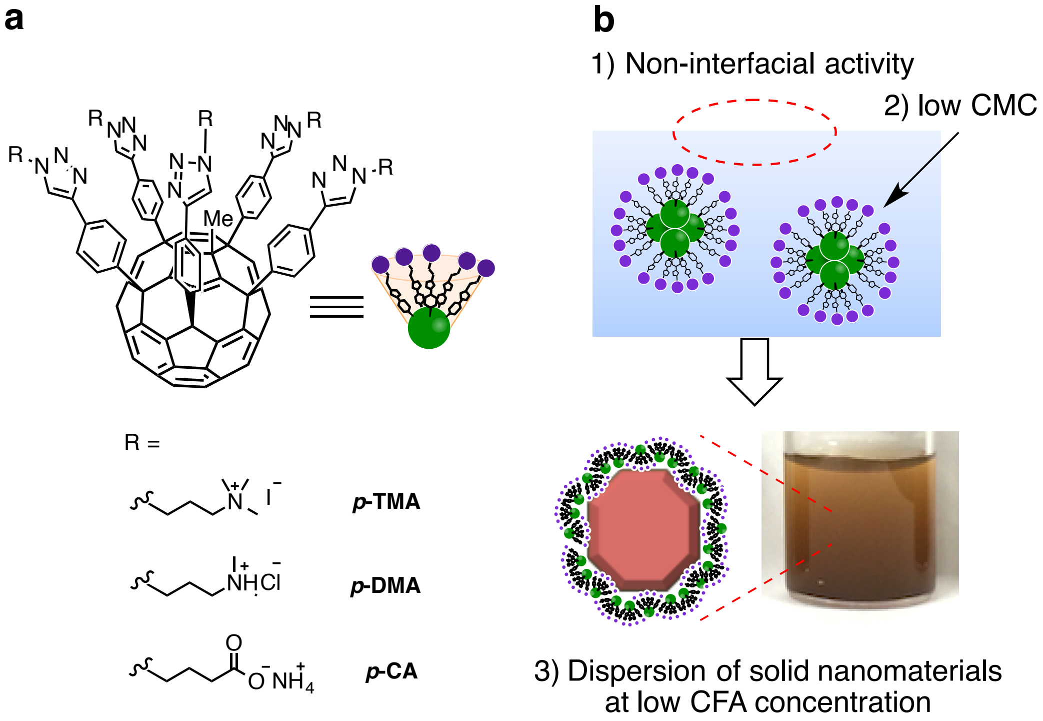
a
R
N
Me
R =
p-TMA
p-DMA
p-CA
b
1) Non-interfacial activity
2) low CMC
3) Dispersion of solid nanomaterials at low CFA concentration

Figure 5-3. Solid dispersion with non-surface active ionic CFAs. (a) Chemical structures of ionic CFAs. (b) Relationship between surfactant properties and effectivity of solid nanoparticle dispersion.

As shown above, I have demonstrated in this thesis that molecular geometry and interactions originating in the fullerene moiety in addition to the hydrophilic groups of CFAs are responsible for the functions. The systematic study on structure-activity relationship of the fullerene amphiphiles will enable us to expand the utility of fullerene amphiphile to practical use such as delivery of drug molecules including nucleic acids, or nanoparticles by use of minimal amount of surfactants, or as dispersants for formulation of cosmetics and pigments that show effectiveness without causing foaming.